SPALLATION PRODUCTS FORMED BY THE BOMBARDMENT OF COBALT
WITH PROTONS OF ENERGIES UP TO 100 MEV.

by

Natasha Hollbach, B.Sc.

Thesis submitted to the Faculty of Graduate
Studies and Research of McGill University
in partial fulfilment of the requirements
for the Degree of Doctor of Philosophy

From the Radiochemistry Laboratory,
Department of Chemistry, McGill University,
under the supervision of Dr. Leo Yaffe.

McGill University,   April, 1957.
Montreal, Canada.

ACKNOWLEDGMENTS

TABLE OF CONTENTS

1. INTRODUCTION

A. Preface

The nature of the nucleus: its constituents, the forces that bind them together, and the way in which these forces act on various groupings of nucleons is one of the most important problems of modern physics. The main method of investigation consists in bombarding a stationary target with a beam of energetic neutrons, protons, deuterons, alpha-particles or gamma-rays. The interaction of a target nucleus with a projectile may result in the emission of nucleons or groups of nucleons. At sufficiently high projectile energies, large sections of the nucleus may be torn away. The results of the collision are determined by observing the emitted nucleons in cloud chambers and photographic emulsions, or by determining the angular distribution of the emitted particles. Alternatively, the results of the collision may be determined by identifying the residual nucleus and so inferring the number of units of charge and of mass given off by the disrupted target nucleus. The latter is the radiochemical approach and was the method used for the research described in this thesis.

During the last twenty years, experiments have suggested theories of nuclear structure which,

when subjected to experimental tests, have had to be
modified or replaced by new theories. The first section
of this thesis traces the threads of theory and experiment
from the time of Rutherford to the present day. The two
threads are often interwined and difficult to separate,
but an attempt has been made to differentiate between
those experiments which suggested new theories and those
which were designed to test the concepts of the theoreticians.

B. Theory of Nuclear Reactions

The pioneer work of Rutherford (1) on art-
ificial nuclear transformations was the starting point
for the present universal interest in the nucleus.
In 1933, Chadwick (2) showed the effectiveness of
neutrons in producing nuclear transmutations and,
shortly after, Fermi et al. (3) found that neutron bom-
bardment may result in radiative capture, gamma-rays
being emitted by the nucleus. Fermi's results showed
that the characteristic gamma-ray spectra of radioactive
nuclides consisted of very sharp lines. This work led
directly to the compound nucleus theory, for from the
sharpness of the gamma-ray spectra, Bohr (4) deduced
that the lifetime of the excited nuclear stated was
longer than the periods of the lines in the spectrum, i.e.,
longer than 10^{-20} seconds. To account for Fermi's exper-
imental cross-sections for (n, γ) reactions, Bohr concluded
that the excited state must persist for a much longer
time than would be required for the neutron to pass
straight through the nuclear volume, i.e., longer than
10^{-21} seconds. (More recent estimates (5) place the life-
time of the excited state at about 10^{-15} seconds.) Bohr
proposed that, when the compound nucleus was formed, since
the mean free path of matter in the nucleus is very small,

the newly amalgamated projectile would quickly distribute
its energy among the other nucleons. The energy of the
compound system, E, is equal to the kinetic energy of
the projectile plus the binding energy of the system.
Collisions within the compound nucleus containing A
nucleons result in an average energy per nucleon of E/A.
The excited nucleus is thus analogous to a drop of liquid,
and E/A may be expressed in terms of an effective nuclear
temperature. The theory was further developed by Bohr
and Wheeler in 1939 (6).

The main feature of the Bohr mechanism is the
hypothesis that the lifetime of the compound is much
longer than the time required for the projectile to share
its energy among the nucleons of the target atom. The
result of such an existence in time of the compound
nucleus is that the reaction channel by which the nucleus
can lose its excitation energy is independent of the mode
of formation and depends only on the excitation energy
of the system. The effect of the many nucleon-nucleon
collisions within the highly excited compound nucleus is
that eventually sufficient energy is accumulated by one
nucleon to cause it to be ejected from the system. Using
the example of protons incident on cobalt,

$$p + Co^{59} \rightarrow Ni^{60*} \rightarrow Ni^{60} + \gamma$$
$$\rightarrow Ni^{59} + n$$
$$\rightarrow Co^{59} + p$$
$$\rightarrow Co^{58} + d$$
$$\rightarrow Fe^{56} + \alpha$$
$$\rightarrow Ni^{58} + n + n$$
$$\rightarrow Co^{58} + n + p$$
$$\rightarrow Fe^{58} + p + p$$
$$\rightarrow etc.$$
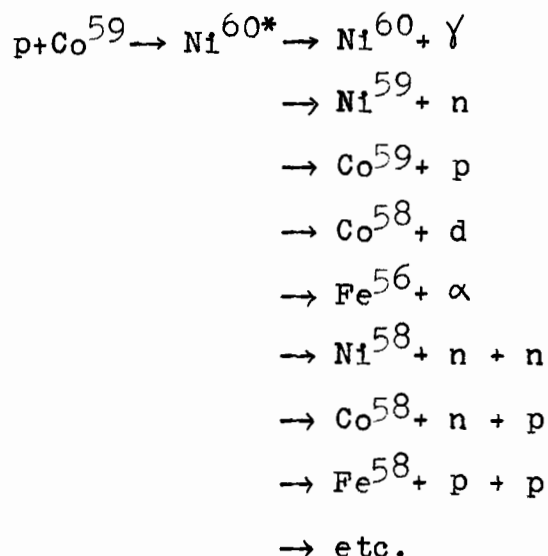
where Ni^{60*} represents the highly excited compound state.

Because of the Coulomb barrier, about 7 Mev. less energy is required for the ejection of a neutron than of a proton. The excitation function (graph of yield versus projectile energy) for a (p,n) reaction will show maximum yield about 7 Mev. lower than the maximum yield for a (p,p) reaction for the same target element. It follows from the Bohr theory that more excitation energy is required for the ejection of two neutrons from the nucleus than for the ejection of one neutron. Assuming an average binding energy of 8 Mev. per neucleon, a (p,n) excitation function will show maximum yield 8 Mev. lower than a (p,2n) reaction. The alternative modes of the composition are competitive: as the (p,2n) yield increases, the (p,n) yield shows a corresponding decrease.

Radiative capture, i.e. decomposition by the emission of gamma-rays is observed only with the lighter elements. The radiative capture process has a very low probability if it has to compete with a (p,n) reaction and is observed only when (p,n) is energetically impossible (7).

Bohr's theory of the compound nucleus has been extended by Konopinski and Bethe in 1938 (8) and by Weisskopf et. al. in 1940 (9) (10) (11) into a statistical theory of nuclear reactions. Their theories take into account the varying angular momenta given to the compound nucleus by the collision. Bohr's basic idea remains! the statistically independent formation and decay of a compound state with strong interaction between target and projectile.

Experimental data have been accumulated rapidly since Bohr proposed his theory of the compound nucleus, and many of them are in excellent agreement with the pred - ictions of the statistical theory.

In 1950, Ghoshal (12) published a direct exper- imental verification of the theory of the compound nucleus. The excited nucleus Zn^{64} was produced in two ways: by the irradiation of Ni^{60} with alpha-particles at energies up to 40 Mev. and by the irradiation of Cu^{63} with protons at energies up to 32 Mev.

$$_{28}\text{Ni}^{60} + {}_{2}\alpha^{4} \rightarrow {}_{30}\text{Zn}^{64*}$$

$$_{29}\text{Cu}^{63} - {}_{1}\text{p}^{1} \rightarrow {}_{30}\text{Zn}^{64*}$$
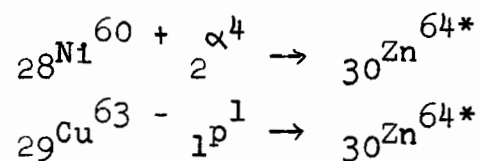
If it is true, as specified by the Bohr theory, that the mode of formation of the compound nucleus is immaterial then the mode of decomposition should be identical in each case. Ghoshal showed that the ratios of the cross-sections, σ, for the various reactions $\sigma(\alpha,n):\sigma(\alpha,2n):\sigma(\alpha,pn)$ for Ni^{60} agree with the ratios of the cross-sections $\sigma(p,n):\sigma(p,2n):\sigma(p,pn)$ for Cu^{63}, directly verifying the Bohr theory.

Measurements of energy spectra of emitted neutrons (13) (14) (15) (16) and protons (17) showed them to be approximately Maxwellian as required by the statistical theory.

Brolley, Fowler and Schlacks (18) measured the cross-section for (n,2n) reactions in C^{12}, Cu^{63} and Mo^{92} from threshold to 27 Mev. They found satisfactory agreement with the statistical theory of Weisskopf et al. from threshold to the onset of tertiary reactions.

Weisskopf and Ewing (9) use a Fermi gas model to obtain an estimate of the energy dependence of the energy level density. They consider the nucleus as a gas of A particles confined in a volume $\frac{4\pi R^{3}}{3}$ and, assuming an equation for the average energy of the system as a function of the nuclear temperature, obtain the relation

$$W = C \exp\left[2(aE)^{1/2}\right] \qquad \qquad \text{... (1)}$$

where w is the energy level spacing in the nucleus,
E is the excitation energy and C and a are adjustable
parameters. Nabholtz, Stoll and Waffler (19) deter-
mined the energy distribution of alpha-particles emitted
in (γ,α) reactions on Li^6,O^{16} and $Br^{79,81}$. They cal-
culated the theoretical energy distribution of the
emitted alpha-particles from equation (1), and found that
the use of a value of $a = 2.7$ Mev.$^{-1}$ gave an energy distri-
bution in satisfactory agreement with the experimental
results.

A similar study by Toms and Stephens (20) of
the energy distribution of photoprotons from cobalt
was carried out using bremsstrahlung X-rays from a 24 Mev.
betatron. They found that the energy distribution could be
accounted for mainly by evaporation from a compound nucleus,
although 5% or 10% could have been from a direct process
(see below for the discussion of such a process).

Shapiro (21) has applied the statistical theory
as extended by Feshbach and Weisskopf (22) to a calcul-
ation of cross-sections for the formation of the
compound nucleus by protons, deuterons and alpha-part-
icles. Shapiro's calculated excitation functions have
the same shape as the experimental curves, although he

found that in many cases the cross-sections of different isotopes of the same element differ from each other, and hence from the calculated cross-sections, by a factor of two.

Several other authors (23) (20) (24) have also found qualitative agreement between experimentally determined cross-sections and the predictions of the statistical theory.

With the advent of synchro-cyclotrons capable of accelerating nuclear projectiles to energies in the hundred Mev. range experimental studies gave the following unexpected results:

(1) On the basis of the Bohr theory it had been expected that at energies of about 100 Mev. the yields of nuclides of Z near that of the target nucleus would be low, while yields of nuclides far removed from the target would be high. Experimental results (25) showed exactly the opposite: yields of nuclides near the target were larger by several powers of 10 than yields of nuclides further removed.

(2) Instead of peaking sharply and then falling off to very small yields eg. Figure 1A, the excitation functions of reactions in the hundred Mev. range exhibited broad maxima and decreased very little at higher projectile energies (26) (27) eg. Figure 1B.

Figure 1

Typical Excitation Functions

(a) For Proton Energies Below 100 Mev.

(b) For Proton Energies in the Hundred Mev. Range

FIG. 1A

RELATIVE CROSS-SECTION

1.0

0.5

0   50   100

PROTON ENERGY (Mev.)

FIG. 1B

RELATIVE CROSS-SECTION

1.0

0.5

100   200   300
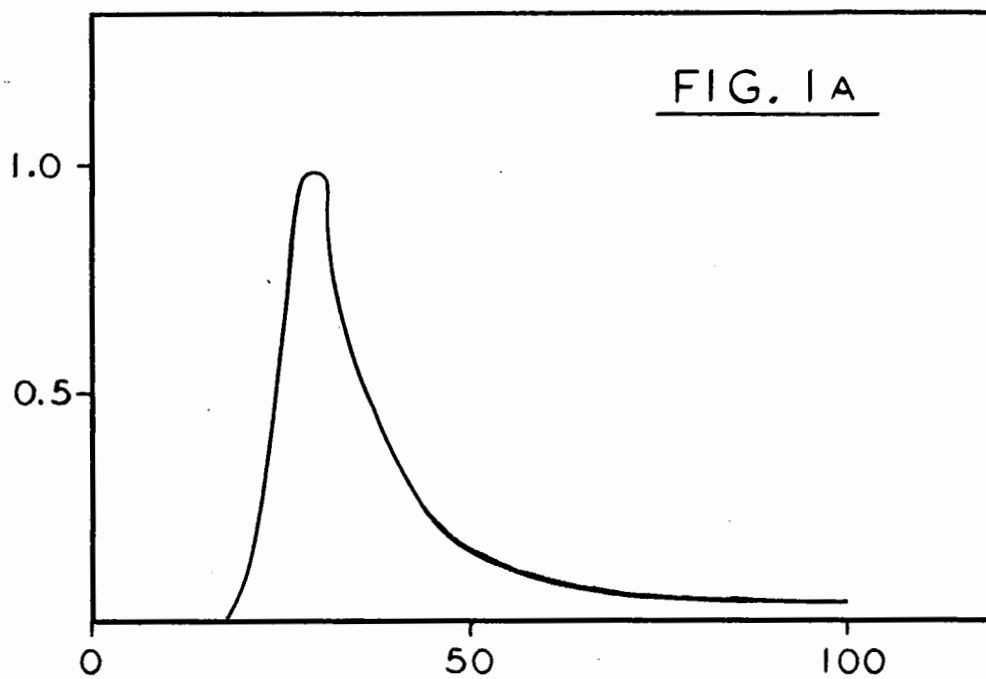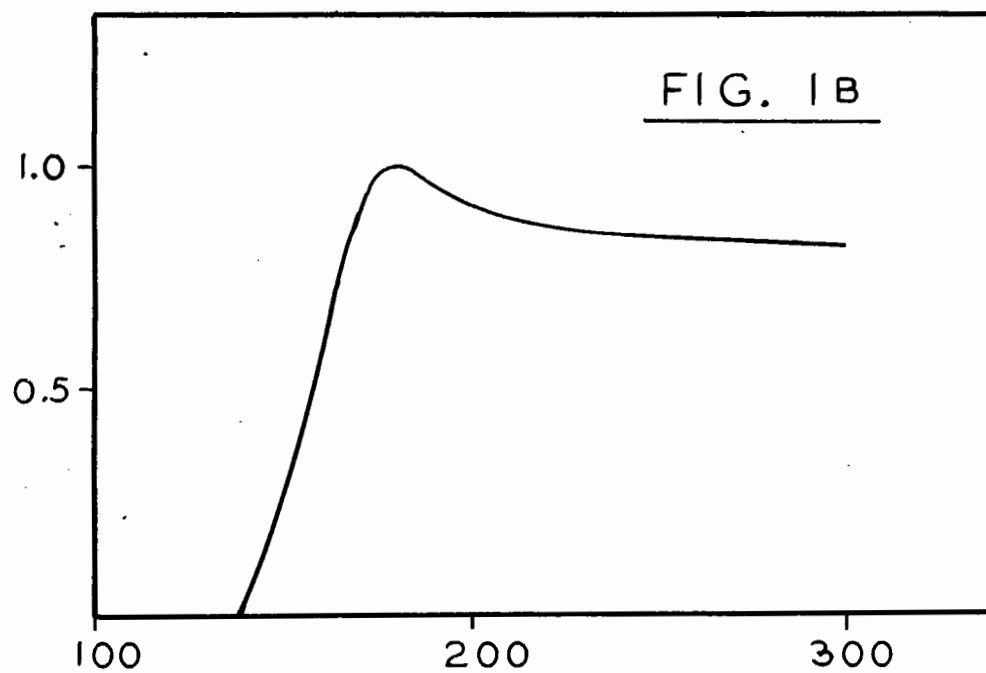
PROTON ENERGY (Mev.)

(3) Measurements by Cork et al. (28) showed that the total cross-section for absorption or scattering by 100 Mev. neutrons was much smaller for light elements than for heavy elements.

The Bohr theory could not explain the above experimental results, and in 1947 a mechanism for high-energy reactions was proposed by Serber (14).

Serber explained the inadequacy of the statistical model at high energies as due to the fact that the mean free path of nucleons in the nucleus increases with energy. Serber suggested the figure 4×10^{-13} cm. for a 100 Mev. proton or neutron. Such a distance is comparable to nuclear radii. Thus the lifetime of the compound state is of the same order of magnitude as the time required for the nucleon to pass through the nucleus. Under such conditions, the reaction proceeds by individual collisions between target and projectile nucleons.

Serber pointed out that his theory adequately explained the three experimental points in the previous section:

(1) The wide distribution of residual nuclei can be explained by the wide distribution of energies of the struck nucleus, depending on how near the edge of the target nucleus the impact occurred.

(2) A reaction can occur when the incident particle leaves the nucleus approximately the right excitation energy for the reaction in question. The probability of leaving a given excitation energy depends only on the mean free path. Since the latter varies only slowly with energy, the excitation function will vary only slowly with energy.

(3) The unexpectedly low total cross-section was explained by Serber in terms of the transparency of nuclear matter i.e., a highly energetic projectile would pass straight on through a target nucleus. For elements of low atomic number the transparency would be expected to increase because of the looser packing of nuclear matter.

In 1948, Serber's theory was extended by Goldberger (29) who applied Monte Carlo calculations to the nucleus. Following Serber, he assumed that at high projectile energies a large number of particles suffer only one collision before escaping from the nucleus. The residual nucleus then de-excites by the emission of nucleons or photons, and Goldberger assumed that the second process may be described by the statistical model. The interaction of a proton, p, with a target nucleus, e.g. cobalt, will take place by one or more of the following processes (30):

$$p + Co^{59} \rightarrow Co^{59*} + p; \qquad Co^{59*} \rightarrow Co^{58} + n$$
$$Co^{59*} \rightarrow Fe^{58} + p$$

$$p + Co^{59} \rightarrow Ni^{59*} + n; \qquad Ni^{59*} \rightarrow Ni^{58} + n$$
$$Ni^{59*} \rightarrow Co^{58} + p$$
$$Ni^{59*} \rightarrow Ni^{59} + \gamma$$

$$p + Co^{59} \rightarrow Fe^{58*} + 2p; \qquad Fe^{58*} \rightarrow Fe^{58} + \gamma$$

$$p + Co^{59} \rightarrow Ni^{58*} + 2n; \qquad Ni^{58*} \rightarrow Ni^{58} + \gamma$$

$$p + Co^{59} \rightarrow Co^{58*} + p + n; \qquad Co^{58*} \rightarrow Co^{58} + \gamma$$
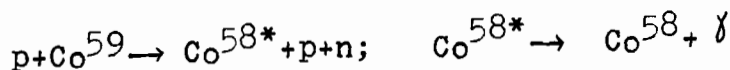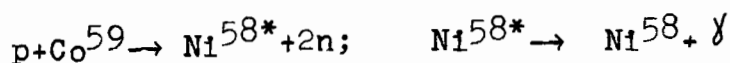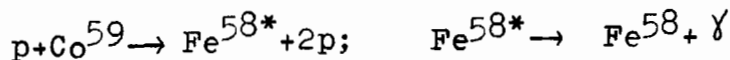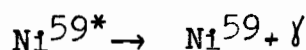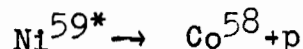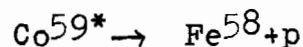
Early experimental studies in the hundred Mev. range (31) (32) (33) showed that one of the main features of nuclear reaction at such energies was the multiplicity of products formed. Reaction products were identified all the way from the target of mass A down to about (A-20). A new term was coined to refer to such reactions where the excited nucleus loses energy by the emission of nucleons or groups of nucleons -- "spallation" (34). Gamma-rays, neutrons and charged particles have been observed to cause spallation, and the experimental spall-ation studies carried out include the following:

Target	Reference
aluminum	(35)
chlorine	(36)(37)
vanadium	(38)(39)
manganese	(38)
iron	(40)
cobalt	(41)(42)(38)(20)(43)(44)(45)
copper	(25)(33)(46)(47)(48)(49)(10)(50)(51)
zinc	(52)
arsenic	(53)
yttrium	(54)
silver	(55)
antimony	(34) iodine (55a)
cesium	(56)
tantalum	(57)
lead	(58)(59)(60)
bismuth	(58)(61)(62)(51)(63)(64)
uranium	(10)
plutonium	(65)

All the experiments listed above support the Serber
"knock-on" model.

Perkins (66) found that in nuclear disintegrations
initiated by cosmic rays heavy fragments are emitted with
an energy much greater than that expected from Coulomb
repulsion, indicating that fragments were ejected before

the excitation energy could be distributed.

The broad plateau and gradual decrease with energy of excitation functions first observed in 1947 (26) (27) and incorporated by Serber in his proposed mechanism have been found repeatedly in later studies (67) (68) (69) (70) (71).

Bernardini, Booth and Lindenbaum (72) (73) (74) carried out an investigation of the interactions of 300 to 400 Mev. protons with AgBr emulsions. The experimental results were compared with the Serber-Goldberger theory, assuming a nuclear gas with maximum kinetic energy 22 Mev. in a nuclear barrier including the Coulomb barrier of 35 Mev. They found satisfactory agreement between the experimental results and the predictions of the theory.

As pointed out by Green (75) the upper and lower limit of the intermediate energy range in which nuclear collisions begin to take on a nucleon-nucleon character have not yet been established. A few estimates have appeared in the literature, but the energy range suggested varies widely.

Fung and Pearlman (76) measured the recoil losses of Na^{24} formed in thin aluminum foils by the irradiation of 60 to 340 Mev. protons and 60 to 380 Mev. alpha-particles. They found that the experimental results could be explained by the Bohr picture for proton energies up to 70 Mev. and for alpha-particles energies up to 80 Mev. Calculations

were also made assuming constant nuclear excitation with
the degraded particle leaving in the forward direction.
Such calculations agreed with the experimental results
over the whole energy range i.e. from 60 to 380 Mev. It
appears from their results that the region of overlap of
the two mechanisms is from 60 Mev. or less than 60 Mev.
to 80 Mev.

According to Meadows (30), the statistical model
alone should account for all reactions at proton energies
of 25 Mev.

Segre (77) gives the intermediate energy range
where the statistical model and knock-on model merge as
between 40- 10 Mev. and several hundred Mev.

Eisberg and Igo (78) measured angular distributions
and energy distributions from inelastic scattering of
32 Mev. protons by various heavy elements. They found
evidence for direct interactions, indicating the presence
of a Serber-Goldberger mechanism even as low as 32 Mev.

Cohen (79) measured angular distribution of neutrons
emitted in (p,n) reactions for 23 Mev. protons on thick
targets of Mg,Al,Cu,Mo,Ag,Ta,Au,Th and U. He found that
all angular distributions showed peaks in the forward
direction, and concluded that direct interaction process-
es were very important at 23 Mev.

One explanation of the discrepancies in suggested energy limits of the intermediate range is the presence of a third reaction mechanism in addition to particle emission and spallation, namely fission. Batzel and Seaborg (80) have determined the proton-induced thresholds for the formation of several nuclides. They define spallation as a process in which alpha-particles are the largest groups of nucleons to be emitted. The spallation reaction occurring at the lowest energy will be that in which the maximum number of alpha-particles is given off. The spallation threshold includes

(i) the mass difference between reactants and products and,

(ii) the effect of the Coulomb barrier.

Some of the results of Batzel and Seaborg are shown in Table I.

Table I

Proton Induced Spallation Thresholds

Reaction	Spallation threshold (Mev.)	Observed threshold (Mev.)
Cl^{38} from $Cu^{63,65}$	110	65
Na^{24} from $Cu^{63,65}$	170	50
Na^{24} from Sn^{118}	425	50

Since the emission of large fragments is energetically more economical than the emission of small fragments, Batzel and Seaborg (80) conclude that the observed nuclides are formed by fission processes e.g.

$$Cu^{63} + p \longrightarrow Cl^{38} + Al^{25}.$$
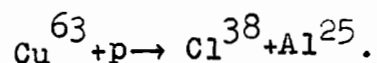
Since 1952, several papers have been published which have raised some doubts as to the validity of the statistical model even at energies as low as 30 Mev.

The equation developed by Weisskopf and Ewing (9) which gives the energy dependence of the energy level density

$$W = C \ exp\left[2(aE)^{1/2}\right] \qquad \qquad \ldots (1)$$

is in a form suitable for experimental verification. Widely differing values of the parameters C and a are obtained depending on the experimental method: slow neutron resonance measurement of level spacing (81), energy spectra of emitted particles, or excitation function measurements (18) (82).

Porges (83) obtained excitation functions for (α,n) $(\alpha,2n)$ (α,pn) $(\alpha,3n)$ on silver and copper for alpha energies up to 40 Mev. He found

(i) (α,pn) reactions were in good agreement with statistical theory,

(ii) For reactions other than (α,pn), Porges interprets his experimental results as due to direct interaction i.e. a greater number of high-energy particles

are emitted than can be accounted for by statistical theory.

Wolfgang et. al. (59) have suggested a mode of nuclear de-excitation in addition to spallation and fission, namely fragmentation. Fragmentation was suggested in order to account for the yields of nuclides of low Z observed in the Bev. region. Fragmentation is thought to occur at bombarding energies above the threshold for meson production i.e., above 0.4 Bev. Wolfgang et al. suggest that the essential characteristic distinguishing the postulated mechanism from spallation and fission processes is its rapidity. The short mean free path of pions in nuclear matter are considered as resulting in local heating and concomitant rapid dissociation of the nucleus.

C. Decay Characteristics of Product Nuclides

From a consideration of Z and A of the target nucleus, $_{27}Co^{59}$, the radioactive nuclides possibly formed as primary spallation products will be:

$Ni^{59,57,56,55,54}, Co^{58m,58,57,56,55,54}, Fe^{55,53,52},$

$Mn^{57,56,54,53,52m,52,51,50,49}, Cr^{55,53m,51,49,48,47,46},$

$V^{53,52m,52,49,48,47,46}, Ti^{51,45,44,43},$

$Sc^{50,49,48,47,46m,46,44m,44,43,41,40}, Ca^{49,47,45,41,39},$

$K^{45,44,43,42,40,38,37}.$ Three other groups of spallation products have not been included in the above list. They are:

(1) stable nuclides

(2) radioactive nuclides not yet reported in the literature

(3) nuclides with Z less than 18, e.g. $_{17}Cl^{39}$. Yields of reaction products in this region are very low at 100 Mev. (the maximum proton energy available to us) and cross-sections were not determined for nuclides lower than $_{19}K$.

Of the 64 radioactive spallation products listed above the following 24 have half-lives such that we were unable to measure their yields:

$Ni^{59}(8\times10^{4}y)$, $Co^{54}(0.18s)$, $Mn^{57}(1.7m)$,

$Mn^{54m}(2.1m)$, $Mn^{53}(140y)$, $Mn^{50}(0.27s)$,

$Mn^{49}(0.4s?)$, $Cr^{55}(3m)$, $Cr^{47}(0.4s?)$, $Cr^{46}(1.1s)$,

$V^{52m}(3.74m)$, $V^{52}(2.6m)$, $V^{49}(600d)$, $V^{46}(0.4s)$,

$Ti^{43}(0.58s)$, $Sc^{50}(1.74m)$, $Sc^{46m}(20s)$, $Sc^{42}(0.62s)$,

$Sc^{41}(0.87s)$, $Sc^{40}(0.22s)$, $Ca^{41}(1.2\times10^{5}y)$,

$Ca^{39}(1.1s)$, $K^{40}(1.2\times10^{9}y)$, $K^{37}(1.2s)$.

The limit of half-lives measurable was approx. 5 min.
to 100 days depending on the formation cross-section.
The decay chains of the remaining 40 nuclides are given
in Table II.

Table II

Decay Chains of Spallation Products

$Ni^{57} \xrightarrow[\text{36 h}]{\beta^+, \text{E.C.}} Co^{57} \xrightarrow[\text{70 d}]{\beta^+} Fe^{57}(\text{stable})$

$Ni^{56} \xrightarrow[\text{6.4 d}]{\text{E.C.}} Co^{56} \xrightarrow[\text{77 d}]{\text{E.C.} \beta^+} Fe^{56}(\text{stable})$

$Ni^{55} \xrightarrow[\text{<5 m}]{} Co^{55} \xrightarrow[\text{18.0 h}]{} Fe^{55} \xrightarrow[\text{2.94 y}]{\text{E.C.}} Mn^{55}(\text{stable}).$

$Ni^{54} \xrightarrow[\text{<5 m}]{} Co^{54} \xrightarrow[\text{0.18 s}]{} Fe^{54}(\text{stable}).$

$Co^{58m} \xrightarrow[\text{9.2 h}]{\text{I.T.}} Co^{58} \xrightarrow[\text{72 d}]{\text{E.C., } \beta^+} Fe^{58}(\text{stable}).$

$Co^{58} \xrightarrow[\text{72 d}]{\text{E.C., } \beta^+} Fe^{58}(\text{stable}).$

$Co^{57} \xrightarrow[\text{270 d}]{\beta^+} Fe^{57}(\text{stable}).$

$Co^{56} \xrightarrow[\text{77 d}]{\text{E.C., } \beta^+} Fe^{56}(\text{stable}).$

$Co^{55} \xrightarrow[\text{18.0 h}]{\beta^+, \text{E.C.}} Fe^{55} \xrightarrow[\text{2.94 y}]{\text{E.C.}} Mn^{55}(\text{stable}).$

$Fe^{55} \xrightarrow[\text{2.94 y}]{\text{E.C.}} Mn^{55}(\text{stable}).$

$Fe^{53} \xrightarrow[\text{8.9 m}]{\beta^+} Mn^{53} \xrightarrow[\text{140 y}]{\text{E.C.}} Cr^{53}(\text{stable}).$

Table II (contd.)

$Fe^{52} \xrightarrow[8.3\ h]{E.C.,\ \beta^+} \quad Mn^{52m} \xrightarrow[21.3\ m]{\beta^+,\ I.T.} \quad Mn^{52} \xrightarrow[5.72\ d]{\beta^+,\ E.C.} \quad Cr^{52}(\text{stable}).$

$Mn^{56} \xrightarrow[2.58\ h]{\beta^-} \quad Fe^{56}(\text{stable}).$

$Mn^{54} \xrightarrow[291\ d]{E.C.} \quad Cr^{54}(\text{stable}).$

$Mn^{52m} \xrightarrow[21.3\ m]{\beta^+,\ I.T.} \quad Mn^{52} \xrightarrow[5.72\ d]{\beta^+,\ E.C.} \quad Cr^{52}(\text{stable}).$

$Mn^{52} \xrightarrow[5.72\ d]{\beta^+,\ E.C.} \quad Cr^{52}(\text{stable}).$

$Mn^{51} \xrightarrow[44.3\ m]{\beta^+} \quad Cr^{51} \xrightarrow[27.8\ d]{E.C.} \quad V^{51}(\text{stable}).$

$Cr^{55} \xrightarrow[3.6\ m]{\beta^+} \quad V^{55}(\text{unknown})$

$Cr^{53m} \xrightarrow[1.8\ h]{I.T.} \quad Cr^{53}(\text{stable}).$

$Cr^{51} \xrightarrow[27.8\ d]{E.C.} \quad V^{51}(\text{stable}).$

$Cr^{49} \xrightarrow[41.9\ m]{\beta^+} \quad V^{49} \xrightarrow[330\ d]{E.C.} \quad Ti^{49}(\text{stable}).$

$Cr^{48} \xrightarrow[23.5\ h]{E.C.} \quad V^{48} \xrightarrow[16.0\ d]{\beta^+,\ E.C.} \quad Ti^{48}(\text{stable}).$

Table II (contd.)

$V^{53} \xrightarrow[\text{23 h}]{\beta^-}$ Cr^{53}(stable).

$V^{48} \xrightarrow[\text{16.0 d}]{\beta^+, \text{ E.C.}}$ Ti^{48}(stable).

$V^{47} \xrightarrow[\text{31 m}]{\beta^+}$ Ti^{47}(stable).

$Ti^{51} \xrightarrow[\text{6 m}]{\beta^-}$ V^{51}(stable).

$Ti^{45} \xrightarrow[\text{3.05 h}]{\beta^+}$ Sc^{45}(stable).

$Ti^{44} \xrightarrow[\text{23 y}]{\beta^+ \text{and/or EC}}$ $Sc^{44} \xrightarrow[\text{3.92 h}]{\beta^+, \text{ E.C.}}$ Ca^{44}(stable).

$Sc^{49} \xrightarrow[\text{57 m}]{\beta^-}$ Ti^{49}(stable).

$Sc^{48} \xrightarrow[\text{43.9 h}]{\beta^-}$ Ti^{48}(stable).

$Sc^{47} \xrightarrow[\text{3.43 d}]{\beta^-}$ Ti^{47}(stable).

$Sc^{46} \xrightarrow[\text{84 d}]{\beta^-}$ Ti^{46}(stable).

$Sc^{44m} \xrightarrow[\text{2.46 d}]{\text{I.T.}}$ $Sc^{44} \xrightarrow[\text{3.92 h}]{\beta^+, \text{ E.C.}}$ Ca^{44}(stable).

$Sc^{44} \xrightarrow[\text{3.92 h}]{\beta^+, \text{ E.C.}}$ Ca^{44}(stable).

Table II (contd.)
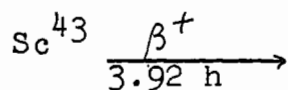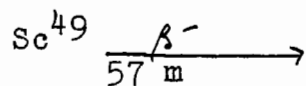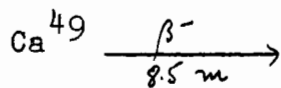
$Sc^{43} \xrightarrow[3.92 \text{ h}]{\beta^+} \qquad Ca^{43}(\text{stable}).$

$Ca^{49} \xrightarrow[8.5 \text{ m}]{\beta^-} \qquad Sc^{49} \xrightarrow[57 \text{ m}]{\beta^-} \qquad Ti^{49}(\text{stable}).$

$Ca^{47} \xrightarrow[4.8 \text{ d}]{\beta^-} \qquad Sc^{47} \xrightarrow[3.43 \text{ d}]{\beta^-} \qquad Ti^{47}(\text{stable}).$

$Ca^{45} \xrightarrow[152 \text{ d}]{\beta^-} \qquad Sc^{45}(\text{stable}).$

$K^{45} \xrightarrow[34 \text{ m} \quad ?]{\text{E.C.} \quad ?} \qquad (\text{unknown}).$

$K^{44} \xrightarrow[22.0 \text{ m}]{\beta^-} \qquad Ca^{44}(\text{stable}).$

$K^{43} \xrightarrow[22.2 \text{ h}]{\beta^-} \qquad Ca^{43}(\text{stable}).$

$K^{42} \xrightarrow[12.44 \text{ h}]{\beta^-} \qquad Ca^{42}(\text{stable}).$
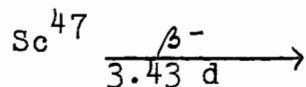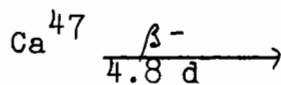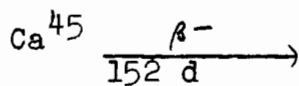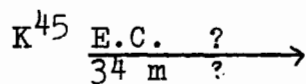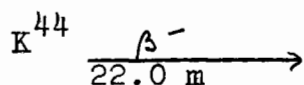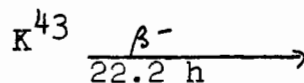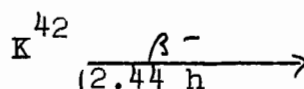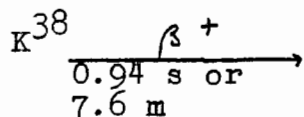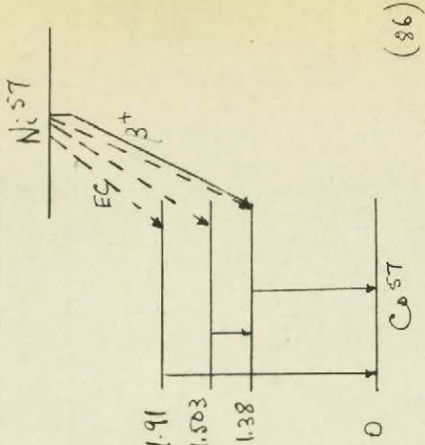
$K^{38} \xrightarrow[\substack{0.94 \text{ s or} \\ 7.6 \text{ m}}]{\beta^+} \qquad A^{38}(\text{stable}).$

The Data for Table III were compiled from
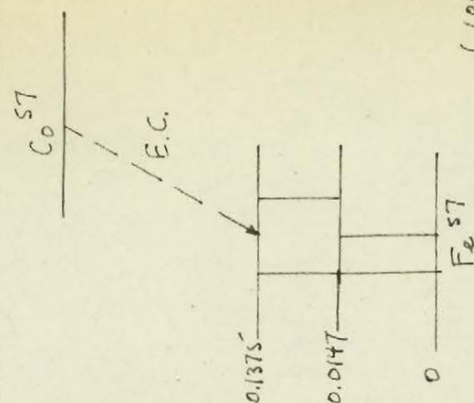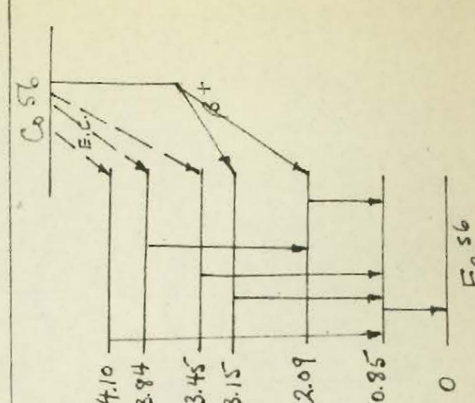
(1) Hollander J.M., Perlman I, and Seaborg G.T.,

Revs. Modern Phys. $\underline{25}$, 469 (1953).

(2) National Research Council Nuclear Data Cards up to

January 1957.

(3) "Nuclear Data" N.B.S. Circular 499 with supplements

I, II and III.

(4) A survey of more recent literature.

Table III

Decay Characteristics of Spallation Products
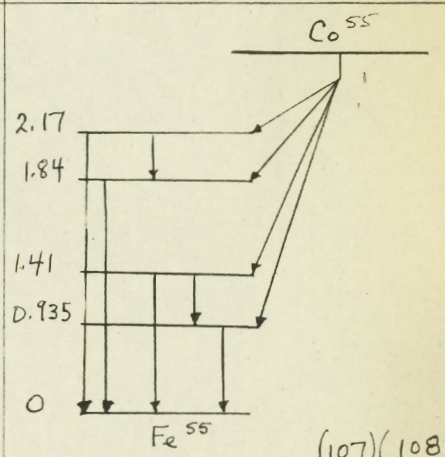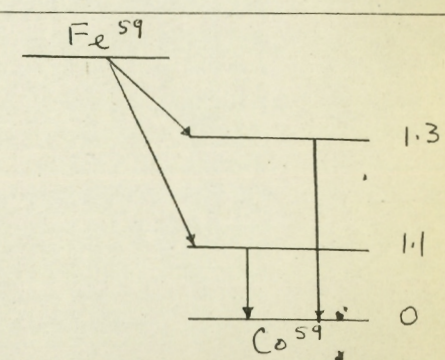
Nuclide	Half-life	Mode of Decay	Energy of Radiation in Mev.		Decay Scheme
			Particles	Gamma-transitions	
28Ni57	36 ± 1 h (94)(86)	50% β^+, 50% E.C. γ (85)	0.835 (85)	γ_1 1.91, γ_2 1.38 γ_3 0.13 84.5 ±1.2 % disint. through γ_2 (86)(87)	(86)
28Ni56	6.4 ± 0.1 d (87)	100% E.C., γ (87)		γ_1 0.17, γ_2 0.29, γ_3 0.48 γ_4 0.81, γ_5 0.76, γ_6 1.33 γ_7 1.58, γ_8 1.75 ($\gamma_1/\gamma_2/\gamma_3/\gamma_4/\gamma_5/\gamma_6/\gamma_7/\gamma_8$) = 1.0/0.3/0.4/0.8/0.1/ 0.05/0.15/0.02) (87)	

(qS)

Nuclide	Half-life	Mode of Decay	Energy of Radiation in Mev.		Decay Scheme
			Particles	Gamma-transitions	
28Ni65	<5 m (88)				
28Ni54	<5 m (88)				
27Co58m	9.2±0.2 h (89)	I.T. (90)		0.0249 (90)	Co58m → Co58, 1.810, 1.785
27Co58	72±1 d (91) (90)	14.5 % β+, 85.5% EC, γ (93)(94) 14% β+, 86% EC. (95)	0.472	γ_1 0.814, γ_2 0.500 (92) 100% of disintegrations through γ_1 (5) (92)(96) γ_1 0.81, γ_2 0.81 γ_3 1.62 ($\gamma_1/\gamma_2/\gamma_3$ = 97.9/ 1.57/0.49) i.e. 97.9% disint. through γ_1 (95)	Co58, 2% EC, 84% EC, 14% β+, 1.62, 0.81, 0, Fe58
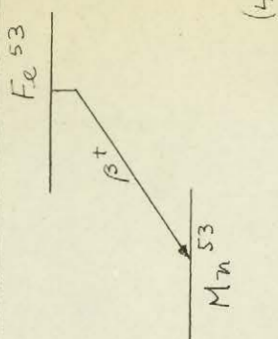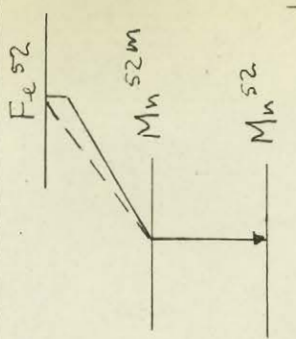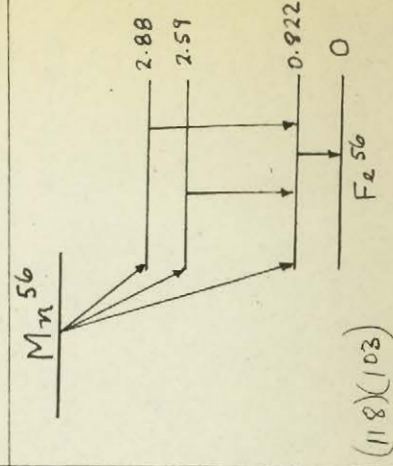
Nuclide	Half-life	Mode of Decay	Energy of Radiation in Mev.		Decay Scheme
			Particles	Gamma-transitions	
27Co57	270 ± 3 d (91)(92)	100% E.C., γ (97)		γ_1 0.1228 (92)(98) γ_2 0.1375 (92)(98) γ_3 0.0147 (92)(99) $(\gamma_1/\gamma_2/\gamma_3 = 93/7/93)$ (97)	Co57 — E.C. — 0.1375, 0.0147, 0, Fe57 (100)
27Co56	77 ± 3 d (101)(102)	25% (β^+, 75% E.C.), γ (103)(104)	β_1 1.50, β_2 0.44 $(\beta_1/\beta_2 = 96/4)$ (105)	γ_1 0.85, γ_2 1.24, γ_3 1.75, γ_4 2.30, γ_5 2.60, γ_6 3.25 $(\gamma_1/\gamma_2/\gamma_3/\gamma_4/\gamma_5/\gamma_6)$ $= 100/55/24/12/14/24$ 100% of disint. through γ_1 (105)	Co56 — E.C., β^+ — 4.10, 3.84, 3.45, 3.15, 2.09, 0.85, 0, Fe56 (105)

(105)
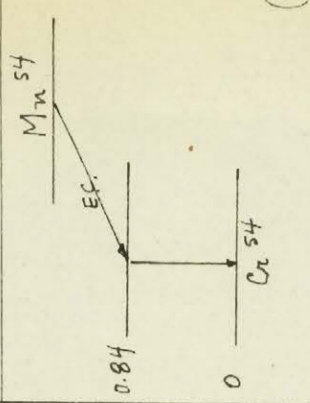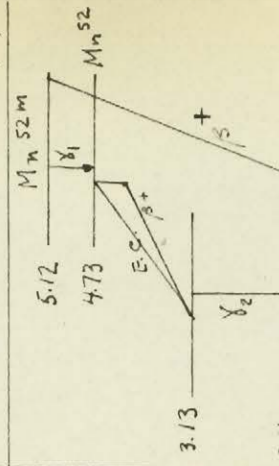
| Nuclide | Half-life | Mode of Decay | Energy of Radiation in Mev. | | Decay of Scheme |
			Particles	Gamma-transitions	
27Co55 (91)(106)	18.0±0.2 h (91)(106)	60 % β^+, 40 % E.C. γ (107)	β_1 0.26, β_2 0.53 β_3 1.03, β_4 1.50 (β_1 / β_2 / β_3 / β_4 = 2.3 / 4.9 / 39.5 / 53.3) (108) 6 % EC with β_3 34 % EC with β_4 (107)	γ_1 0.253, γ_2 0.477 γ_3 0.935, γ_4 1.41 γ_5 1.84, γ_6 2.17 (γ_1 / γ_2 / γ_3 / γ_4 / γ_5 / γ_6 = 2/ 28 /156 / 26 / 0.6 /4) (108)	Co^{55} 2.17 1.84 1.41 0.935 0 Fe^{55} (107)(108)
26Fe59 (109)	46.3±1.0 d (109)	β^-; γ	β_1 0.26, β_2 0.46 (β_1 / β_2 = 50/50) (110)	γ_1 1.1, γ_2 1.3 (γ_1 / γ_2 = 50/50) (110)	Fe^{59} 1.3 1.1 0 Co^{59}
26Fe55	2.94±0.03 y (111)(91)	100 % E.C. (112)(113)			

Nuclide	Half-life	Mode of Decay	Energy of Radiation in Mev		Decay Scheme
			Particles	Gamma-transitions	
$_{26}Fe^{53}$	3.0 ± 0.1 m (114)(41)	100% β^+ (45)	2.8 (41)		Fe53 β^+ → Mn53 (45)
$_{26}Fe^{52}$	8.3 ± 0.2 h (114)	38% β^+, 62% E.C. (116)	0.64 (116)	no γ's > 0.05 Mev. (116)	Fe52 → Mn52m, Mn52 (116)
$_{25}Mn^{56}$	$2.576\pm.002$ h (117)	100% β^- (45)	β_1 0.74, β_2 1.05, β_3 2.84 ($\beta_1/\beta_2/\beta_3 = 17/28/55$) (118)(103)	γ_1 0.822, γ_2 1.77, γ_3 2.06 ($\gamma_1/\gamma_2/\gamma_3 = 5/15/1$) (100% disintegration through γ_1) (118)(103)	Mn56 2.88, 2.59, 0.922, 0, Fe56 (118)(103)

Nuclide	Half-life	Mode of Decay	Energy of Radiation in Mev		Decay Scheme
			Particles	Gamma-transitions	
$_{25}Mn^{54}$	303±1 d (119)	100% E.C. γ, no β+ (96) < 0.1% β⁻ (120)		0.84 (121)	
$_{25}Mn^{52m}$	21.3 m (122)	0.05% I.T. 99.95% β+ (23)	2.66 (123)	0.39 (123)	
$_{25}Mn^{52}$	5.7±0.?? d (119)	35% β+, 65% E.C. γ (93)	0.582 (124)	γ₂ 0.734, γ₃ 0.94, γ₄ 1.46 (124)(125)	
$_{25}Mn^{51}$	44.3±0.5 m (127)	100% β+	2.16 (128)	no γ (128)	

Nuclide	Half-life	Mode of Decay	Energy of Radiation in Mev		Decay Scheme
			Particles	Gamma-transitions	
24Cr55 (129)(130)	3.6 m	100 % β^+	2.8 (130)		
24Cr53m (131)	1.8±0.5 h	I.T. (131)			
24Cr51 (132)	27.8±0.3 d	100 % E.C., γ (132)		8% of disintegrations through 0.32 Mev. γ (the only γ observed) (132)	
24Cr49 (133)	41.0±0.3 m	88.5 % β^+, γ (134)	β_1 0.73, β_2 1.39 β_3 1.54 ($\beta_1/\beta_2/\beta_3$ = 15/35/50) (134)	0.153 , 0.609 (134)	

Nuclide	Half-life	Mode of Decay	Energy of Radiation in Mev.		Decay Scheme
			Particles	Gamma-transitions	
$_{24}Cr^{48}$	23.5±0.5 h (135)(136)	100% E.C., γ (135)(136)		0.117, 0.306 (135)(136)	
$_{23}V^{?}$	23±1 h (137)	β⁻, γ (137)	0.56 (137)		
$_{23}V^{49}$	330±20 d (138)(130)	100% E.C., no γ, no conversion electrons (139)			
$_{23}V^{48}$	16.0±0.2 d (140)	58% β⁺, 2% E.C.₁, 40% E.C.₂, γ (93)	0.716 (124)	γ₁ 2.23, γ₂ 1.32, γ₃ 0.99 (141)	

Decay scheme for Cr^{48}: E.C. → 0.423, 0.117, 0, V^{48}

Decay scheme for V^{48}: EC₁, EC₂, β⁺ → 3.22, 2.31, 0.99, 0, Ti^{48}

Nuclide	Half-life	Mode of Decay	Energy of Radiation in Mev.		Decay Scheme
			Particles	Gamma-transitions	
23V47	31±1 m (142)	100% β+, possibly γ (142)(143)	1.90 (28)		
22Ti45	3.05±.04 h (144)	100% β+, γ (144)	β₁ 1.62 , β₂ 0.57 (β₁/β₂ = 96/4) (144)	0.45 (144) possibly 0.80 (145)	$Ti\ 45$ β_2 β_1 0.45 0 (144)
22Ti44	<1 m or >100 y (146) ≥23 y (147)			0.16 (147)	
21Sc49	57.5±0.7 m (148)	β⁻, no γ (148)	2.00 (128)		$Sc\ 49$ → $Ti\ 49$ (148)

Nuclide	Half-life	Mode of Decay	Energy of Radiation in Mev.		Decay Scheme
			Particles	Gamma-transitions	
21Sc48	43.0±0.5 h (143)(150)	β^-, γ	0.40 (141)	1.24, 1.32, 0.99 (141)	Sc48 β^- 3.55 / 2.31 / 0.99 / 0 Ti48 (141)
21Sc47	3.43±0.03 d (143)	β^-, γ	β_1 0.60, β_2 0.44 (β_1/β_2 = 40/60) (151)	0.159 (151)	Sc47 β_1 β_2 0.159 / 0 Ti47 (151)
21Sc46	84±1 d (152)	β^-, γ, no β^+ no E.C. (153)	β_1 0.36, β_2 1.4 (153 a) (β_1/β_2 = 99.0/1.0) (154)(152)(155)	γ_1 1.12, γ_2 0.90 (153)	Sc46 β_1 β_2 2.01 / 1.12 / 0 Ti46 (155)

Nuclide	Half-life	Mode of Decay	Energy of Radiation in Mev.		Decay Scheme
			Particles	Gamma-transitions	
21Sc44m	2.46±0.02 d (150)(156)	I.T.		I.T. 0.270 (157)	
21Sc44	3.92±0.03 h (156)	93.2% β^+ 6.8% E.C., γ (158)	1.471 (158)	γ_1 1.38, γ_2 1.16 β_3 2.54 ($\gamma_1/\gamma_2/\gamma_3 = 0.5/99.4/$ 0.12 (158)	
21Sc43	3.92±02 h (156)	80% β^+, 20% E.C., γ (156)	β_1 0.39, β_2 0.82 β_3 1.20 ($\beta_1/\beta_2/\beta_3 = 4/17/79$) (159)	γ_1 0.25, γ_2 0.37, γ_3 0.51, γ_4 0.63, γ_5 0.84, γ_6 ($\gamma_1/\gamma_2/\gamma_3/\gamma_4/\gamma_5$ = 0.5/8/100/2/weak) (159)	

Nuclide	Half-life	Mode of Decay	Energy of Radiation in Mev.		Decay Scheme
			Particles	Gamma-transitions	
20Ca49	3.0-7.2 m (160)	β^-, γ (161)	β_1 1.0, β_2 1.95 (148)	γ_1 3.10, γ_2 4.05 γ_3 4.68 ($\gamma_1/\gamma_2/\gamma_3 = 90/10/0.34$) (148)	
20Ca47	4.8-7.4 d (161)	β^-, γ	β_1 0.67, β_2 2.0 ($\beta_1/\beta_2 = 82/18$) (162)(161)	0.48, 0.83, 1.31 (161)	
20Ca45	152 d (115)(162)				
19K45	24 m ? (159)	E.C. ? (051)			

Nuclide	Half-life	Mode of Decay	Energy of Radiation in Mev.		Decay Scheme
			Particles	Gamma-transitions	
19K44	22.0 m (166)	β^-, γ	1.5, 4.9 assume ($\beta_1/\beta_2 = 50/50$)	1.13, 2.07, 2.48 possibly 3.6 (166)	
19K43	22.2±0.2 h (167)(7)	β^-, γ	β_1 0.24, β_2 0.46 β_3 0.83, β_4 1.22 β_5 1.84 ($\beta_1/\beta_2/\beta_3/\beta_4/\beta_5$ = 4.5/5.4 83.1/ 5.4/1.6) (7)	γ_1 0.219, γ_2 0.369 γ_3 0.393, γ_4 0.627, γ_5 1.00 ($\gamma_1/\gamma_2/\gamma_3/\gamma_4/\gamma_5$ = 1/67/6/100/4) (7)	K^{43} β^- 1.608 1.389 0.996 0.627 0 (7) Ca^{43}
19K42	12.44 h (168)	β^-, γ	β_1 2.04, β_2 3.58 ($\beta_1/\beta_2 = 25/75$) (168)		K^{42} β^- 1.51 (168) Ca^{42} .0
19K38	7.6±0.1 m (170)(171)	100% β^+	2.6 (170)(171)	2.16 (172)(173)	
	0.94±0.1 s (174)(175)	100% β^+	4.6 (175)		

D. Formulae Used to Calculate Cross-Sections

The general equation (176) describing the decay of a radioactive parent into a radioactive daughter is

$$N = \frac{\lambda_2}{\lambda_2 - \lambda_1} N_1^O (e^{-\lambda_1 t} - e^{-\lambda_2 t}) + N_2^O e^{-\lambda_2 t} \qquad ...(2)$$

where N_1^O = number of parent atoms present at $t=o$

N_2 = number of daughter atoms present at time t

N_2^O = number of daughter atoms present at $t=o$

λ_1 = decay constant of parent

λ_2 = decay constant of daughter

The first group of terms in the above equation show the growth of the daughter from the parent and the decay of these daughter atoms. The last term gives the contribution at any time from the daughter atoms present initially.

In the production of a radioactive substance (daughter) from a steadily operating cyclotron, $N_2^O = 0$ at $t=o$, $\lambda_1 << \lambda_2$, and $e^{\lambda_1 t} = 1$. $\lambda_1 N_1^O$ may be replaced by R, the rate of production of the active atoms.

$$N_2 = \frac{R}{\lambda_2} (1 - e^{-\lambda_2 t}) \qquad ...(3)$$

As t becomes long compared to the half-life of the activity, N_2 approaches $\frac{R}{\lambda_2}$ and equation (3) becomes

$$N_2 = (N_2)_{max.} (1 - e^{-\lambda_2 t}) \qquad ...(4)$$

The maximum number of atoms of product nuclide formed during an irradiation is proportional to the intensity of the proton beam, the number of target atoms/cm^3. and the thickness of the target.

$$(N_2)_{max.} \propto Inx \qquad \ldots(5)$$

where N_2 = number of atoms of product nuclide

    I = number of particles striking the target

    n = number of target atoms/cm^3

    x = target thickness in cm.

Introducing a proportionality constant, σ ,

$$(N_2)_{max.} = \sigma Inx \qquad \ldots(6)$$

where σ has the units cm^2, and is called the cross-section. When the duration of bombardment is not long enough to give saturation yield of product N_2 is measured rather than $(N_2)_{max.}$ The equation used to calculate the cross-section is then obtained by substituting equation (4) in equation (6), giving

$$N_2 = \sigma Inx(1-e^{-\lambda_2 t}) \qquad \ldots(7)$$

The accuracy of measurement of the cross-section will depend on the accuracy of measurement of the incident beam of charged particles. The number of particles striking the target can be determined by measuring the charge collect-

ed in a Faraday cup. Different experimental arrangements have been employed. Some workers in this field (177) (156) (178) (179) prefer to place the target in direct contact with the Faraday cup, while others (180) (181) (182) (183) prefer to have the beam pass through the target foil before it impinges on the cup.

There is an alternative to making a direct measurement of the incident beam. It is possible to monitor the beam by making a simultaneous yield determination of a reaction for which the cross-section is known. Consider the simultaneous bombardment of a mixture of two elements, a and b. Then from equation (7)

$$N_a = \sigma_a I n_a \times (1-e^{-\lambda_a t}) \qquad \ldots(8)$$

and

$$N_b = \sigma_b I n_b \times (1-e^{-\lambda_b t}) \qquad \ldots(9)$$

Dividing equation (8) by equation (9) gives

$$\frac{N_a}{N_b} = \frac{\sigma_a I n_a \times (1-e^{-\lambda_a t})}{\sigma_b I n_b \times (1-e^{-\lambda_b t})} \qquad \ldots(10)$$

The target thickness and, more important, the beam intensity cancel leaving

$$\frac{N_a}{N_b} = \frac{\sigma_a n_a (1-e^{-\lambda_a t})}{\sigma_b n_b (1-e^{-\lambda_b t})} \qquad \ldots(11)$$

The ratio of the number of atoms of nuclide formed to the number of atoms of monitor formed, $\frac{N_2}{N_b}$, can be calculated from the decay schemes and observed disintegration rates. If only quantities which are proportional to the disintegration rate are used, the ratio of the disintegration rates may be replaced by the ratio of the counting rates.

The targets used in this work consisted of a mixture of two powders with a known atom ratio.

E. Previous Work on the Nuclear Reactions of Cobalt

1. Preface

Since 1949, several papers have appeared in the
literature on the nuclear reactions of cobalt: five (43)
(42) (184) (38) (45) on proton-induced spallation as well
as one (185) on deutron-induced spallation. To facilitate
comparison, the results of all these papers have been
grouped together in Table IV. The cross-sections in
Table IV are the values as originally published.

Perhaps the main cause of error in spallation
studies is the monitoring of the incident beam. In the
primary determination of absolute cross-sections, the beam
is caught in a Faraday Cup and the current measured. Faraday
Cup measurements are, however, difficult and subject to
large errors and most researchers prefer to report relative
spallation yields. Each of the values in Table IV was
published relative to a certain monitoring reaction, and in
some cases recent work has indicated that the previously
accepted cross-section for that reaction was incorrect. In
section I.E. we shall deal with each of the published papers
in turn, discussing any necessary corrections. At the end
of section I.E., Table VI is a compilation of the corrected
cross-sections.

Table IV

Existing Data on the Nuclear Reactions of Cobalt (UNCORRECTED)
All cross-sections in mb.

Mev. Particle Reference	60 p (45)	60 p (42)	100 p (45)	100 p (42)	170 p (42)	187 p (38)	190 d (185)	240 p (184)	240 p (42)	370 p (43)
28N157	9.7±2.8	--	1.7±.5	--	--	--	--	1.1±.2	--	.34±.08
56	43±.11	--	.21±.05	--	--	--	--	--	--	--
27Co58m	129±38	--	81±24	--	--	--	--	--	--	--
58	98±116	865±433	54±64	363±182	185±93	--	--	260±50	120±50	121±60
57	76±23	--	31±9	--	--	--	--	--	--	--
56	7.8±27	120±60	2.9±10	89±45	30±16	--	--	33±7	22±11	15.2±3.8
55	10.6±3.1	5.7±1.1	7.8±2.3	21±4	9.4±1.9	--	--	--	6.6±1.3	5.2±1.3
26Fe55	--	--	--	--	--	--	--	--	--	37±9
53	5.8±1.4	--	3.8±.9	--	--	--	--	--	--	1.7±.6
52	.053±.018	.0009±.0005	.31±.11	.56±.17	.65±.19	--	--	.9±.2	.63±.19	.28±.07
25Mn56	9.4±1.5	12±3	11.5±1.8	14±3	11.5±3	--	27	10±2	9.0±2.3	3.8±1.0
54	49±12	--	46±11	--	--	--	--	--	--	25.4±7.0
52m	1.37±.23	--	8.7±1.5	--	--	--	--	--	--	5.6±2.2
52	3.5±1.1	1.3±.4	12.7±4.1	36±9	31±8	--	48	25±5	23±6	14.1±3.5
51	0	--	4.2±1.1	6±3	5.8±2.0	--	--	--	8±3	4.1±1.4

Table IV (contd.)

Mev. Particle	60 p	60 p	100 p	100 p	170 p	187 p	190 d	240 p	240 p	370 p
24Cr51	0	--	40±13	--	--	--	--	--	--	27.5±2.0
49	--	--	--	--	--	--	--	6.6±1.3	--	4.1±1.0
48	0	--	.089±.018	--	--	--	--	--	--	--
23V 53	0	--	.04±.01	--	--	--	--	--	--	--
49	--	--	--	--	--	--	--	--	--	31.1±9.0
48	0	--	6.4±1.4	--	--	$1.2\pm.6/Cr^{49}$	--	--	--	10.6±2.8
47	--	--	--	--	--	--	--	--	--	2.1±1.0
22Ti45	--	--	--	--	--	$.45\pm.22/Cr^{49}$	--	--	--	3.5±.9
21Sc48	--	--	--	--	--	$.35\pm.17/Sc^{47}$	--	--	--	--
46	--	--	--	--	--	$4.1\pm2.0/Sc^{47}$	--	--	--	2.2±.3
44m	--	--	--	--	--	$1.7\pm.9/Sc^{47}$	--	6.6±1.3	--	3.5±1.4
43-44	--	--	--	--	--	$1.7\pm.9/Sc^{47}$	--	9.2±1.8	--	5.0±1.7

Table IV (contd.)

Mev. Particle	60 p	60 p	100 p	100 p	170 p	187 p	190 d	240 p	240 p	370 p
$20Ca^{47}$	--	--	--	--	--	--	--	--	--	$.06\pm.03$
45	--	--	--	--	--	--	--	--	--	$.66\pm.33$
$19K\ 43$	--	--	--	--	--	--	--	--	--	$.50\pm.23$
42	--	--	--	--	--	$.16\pm.08/Cr^{49}$	--	13 ± 3	--	$.85\pm.28$
38	--	--	--	--	--	--	--	--	--	$.31\pm.14$
$17Cl^{39}$	--	--	--	--	$.007\pm.005$	--	--	$.66\pm.13$	$.15\pm.10$	$.50\pm.40$
$38-34$	--	$.005\pm.003$	--	$.07\pm.04$	$.018\pm.009$	--	--	$1.3\pm.3$	$.19\pm.10$	2.8 ± 1.4
$15P\ 33$	--	--	--	--	--	--	--	--	--	$.03\pm.02$
32	--	--	--	--	--	$.025\pm.012/Cr^{49}$	--	--	--	$.30\pm.1$
$14Si^{31}$	--	--	--	--	--	$.01\pm.005/Cr^{49}$	--	--	--	--
$13Al^{29}$	--	--	--	--	--	--	--	--	--	$<.30$
$12Mg^{27}$	--	--	--	--	--	--	--	--	--	$<.30$
$11Na^{24}$	--	--	--	--	--	--	--	--	--	$.07\pm.03$
$9F\ 18$	--	--	--	--	--	--	--	--	--	$.07\pm.03$
$6C\ 11$	--	--	--	--	--	--	--	--	--	$.05$

2. Corrections to Belmont and Miller's Data

Belmont and Miller's data on proton-induced spallation at 370 Mev. (43) are given in Table IV. These cross-sections are all based on a value of 44mb. for the $C^{12}(p,pn)C^{11}$ reaction interpolated from the data of Warshaw, Swanson and Rosenfeld (186). Accepting the value of 44 mb., Belmont and Miller (43) determined the cross-section for $Al^{27}(p,3pn)Na^{24}$ relative to the $C^{12}(p,pn)C^{11}$ cross-section and then used the aluminum reaction to monitor the proton beam. They obtained a value of 15.5 mb. for the cross-section for production of Na^{24} at 370 Mev. in disagreement both with Marquez' (187) value of 10.8±0.5 mb. at 420 Mev. and Stevenson and Folger's (188) value of 10.5 0.5 mb. at 350 Mev. Table V lists values of the cross-section for the production of Na^{24} from aluminum at energies up to 420 Mev., and includes data published up to January 1, 1957.

Both the carbon and aluminum cross-sections have been redetermined very carefully by Crandall, Millburn, Pyle and Birnbaum (189). The corrected value for $C^{12}(p,pn)C^{11}$ at 350 Mev. is now 36.0±0.7 mb; the corrected value for $Al^{27}(p,3pn)$ Na^{24} at 350 Mev. is now 11.1±0.2 mb. The carbon excitation function was determined absolutely by Faraday-Cup monitoring of the proton beam, and the aluminum excitation function was determined relative to the carbon reaction.

Recalculation of the aluminum monitor of Belmont
and Miller (43) to the corrected carbon cross-section gives:

$$15.5 \text{ mb.} \times \frac{36.0 \text{ mb.}}{44 \quad \text{mb.}} = 12.7 \text{ mb.}$$

This corrected value is included in Table V for purposes
of comparison.

Table V

Cross-Section for the Production of Na^{24} from Aluminum

Mev.	Cross-Section (mb.)	Reference
100	15.2* as published 13.2 corrected to Crandall's $C^{12}(p,pn)C^{11}$	Hintz & Ramsey (190)
100	10*	Stevenson and Folger (188)
110	10.6*	Hicks, Stevenson and Nervik (69)
187	10.8*	Rudstam (38)
350	11.3*	Hicks, Stevenson and Nervik (69)
350	11.1±0.2	Crandall et al. (189)
350	10.5±0.5	Stevenson and Folger (188)
370	15.5* as published 12.7 corrected to Crandall's $C^{12}(p,pn)C^{11}$)	Belmont and Miller (43)
420	10.8±0.5	Marquez (187)

* No error quoted.

As can be seen from Table V, the excitation
function for $Al^{27}(p,3pn)Na^{24}$ is constant within experimental
error from 100 to 420 Mev. Even after the correction des-
cribed above, Belmont and Miller's value of 12.7 mb. is
definitely higher than the other determinations, and since
no limits of error are quoted by the authors, it appears
that at 370 Mev. the value 11.1 mb. is more valid than
12.7 mb. For this reason, all Belmont and Miller's spall-
ation data (given in Table IV) have been multiplied by the
factor $\frac{11.1}{15.5} = 0.716$.

Their corrected data are listed in Table VI.

Summary: All Belmont and Miller's cross-sections have been
multiplied by 0.716.

3. Corrections to Wagner and Wiig's 1952 Data

Table IV lists the spallation data of cobalt plus
240 Mev. protons published by Wagner and Wiig in 1952 (184).
These cross-sections were all reported relative to the
cross-section for the production of $Co^{55} = 6.6 \pm 1.3$ mb. They
need a different correction factor from Wagner and Wiig's
1954 data and will therefore be discussed separately to
avoid confusion.

The Co^{55} cross-section was calculated relative to
Hintz and Ramsey's (190) excitation function for the prod-
uction of Na^{24} from aluminum which in turn depends on the
monitoring reaction $C^{12}(p,pn)C^{11}$ as determined by Aamodt,

Peterson and Phillips (191). Crandall, Millburn, Pyle and Birnbaum (189) have recently remeasured the carbon excitation function and found the data of Aamodt et al. to be 13% too high at all energies. The lowered value for the carbon monitor lowers Hintz and Ramsey's Al^{27} $(p,3pn)Na^{24}$ cross-sections by 13% (see Table V), lowering the value of the cross-section of Co^{55} from 6.6 to 5.7 mb. Since Wagner and Wiig's 1952 data were reported relative to Co^{55}, their data have been multiplied by 5.5/6.6.

Summary: Wagner and Wiig's 1952 data have been multiplied by 5.5/6.6.

4. Corrections to Wagner and Wiig's 1954 Data

Wagner and Wiig (42) have carried out spallation studies on cobalt bombarded with protons at energies of 60, 100, 170 and 240 Mev. The published data are included in Table IV. As previously described redetermination of the carbon monitor by Crandall, Millburn, Pyle and Birnbaum (189) lowers Hintz and Ramsey's (190) values for the cross-sections of $Al^{27}(p,3pn)Na^{24}$ by 13%. Wagner and Wiig used Hintz and Ramsey's values of the aluminum monitor, so that all their reported cross-sections need to be lowered by 13%.

Seliger (192) has reported a difference in the back-scattering of positrons and negatrons, the back-scattering being greater for negative than for positive electrons. He

53.

found that this effect is independent of the energy of
the back-scattered particle over a wide energy range, but
is a function of the geometry of the counting arrangement.
For the conventional small-geometry Geiger-Mueller counter,
Seliger found that the back-scattering for negative electrons
is 8% greater than for positrons.

Wagner and Wiig (42) found that under their
counting conditions the difference between positron and
negatron back-scattering was of the order of 3% rather than
8% as reported by Seliger. This discrepancy is probably due
to the fact that back-scattering is highly dependent on the
counting geometry, and should be determined in the counting
system used.

While Wagner and Wiig did correct for the difference
in positron and negatron back-scattering in the spallation
products, they did not notice the omission of that correction
in Hintz and Ramsey's determination of the aluminum monitor
(190). Hintz and Ramsey had standardized the negatron-
emitting Na^{24} against the positron-emitting C^{11} in a small
geometry Geiger-Mueller counter without correcting for the
difference in back-scattering so that their published
$Al^{27}(p,3pn)Na^{24}$ excitation function is 8% too high. This
error cancels out when calculating absolute yields of positron
emitters relative to Hintz and Ramsey's published curve; but
for negatron emitters Wagner and Wiig's cross-sections must

be multiplied by 0.92. The necessity for such a correction was first pointed out by Sharp, Diamond and Wilkinson (45). Wagner and Wiig's cross-sections for nuclides decaying 100% by electron capture must be lowered by 8%; their cross-sections for positron emitters need not be altered. It follows that cross-sections for nuclides decaying by both electron capture and positron emission must be lowered by $(8\% \times \frac{E.C.}{\beta^+ + E.C.})$. The branching ratios for β^+ emission used in this thesis are compiled in Table IV, and the correction factors $\frac{E.C.}{\beta^+ + E.C.}$ were calculated from them. The corrected values of the cross-sections are given in Table VI, together with the earlier results obtained by Wagner and Wiig.

Summary: Cross-sections of pure positron emitters were multiplied by 0.87. Cross-sections of negatron emitters and of nuclides decaying 100% by electron capture were multiplied by $0.87 \times 0.92 = 0.80$. Cross-sections of nuclides decaying by both electron capture and positron emission were first multiplied by 0.87 and then lowered by $(8\% \times \frac{E.C.}{\beta^+ + E.C.})$.

5. Data of Bonner and Orr

Bonner and Orr (185) have determined the yields of Mn^{56} and Mn^{52} (not including Mn^{52m}) in the spallation of cobalt with 190 Mev. deutrons. Their results are shown in Table IV. No errors are quoted because no error was quoted

by the author for the Cu^{64} monitor. As yet, we have
considered only proton bombardments. The question now
arises: are different groups of spallation data of cobalt
numerically comparable when the bombarding particles are
of a different nature? The answer seems to be two-fold.

At particle energies sufficiently great so that
compound nucleus formation is negligible, e.g. 200 Mev.,
the main reaction mechanism is of a "hit and run" nature.
The nucleus is struck by a particle possessing sufficient
kinetic energy to tear away fragments of the nucleus before
sufficient time has elapsed for the energy of the bombarding
particle to be distributed throughout the nucleus. The im-
pinging particle, still possessing most of its original
kinetic energy, continues on through the nucleus. Under
such conditions, the nature of the impinging particles would
seem to be relatively unimportant. Thus at energies of
about 200 Mev. one would expect excitation functions caused
by nucleon (i.e. proton and neutron) bombardment to be rough-
ly comparable.

Results of deuteron bombardment are complicated
by the polarization of the deuteron. Crandall et al. (189)
have determined absolute excitation functions of $C^{12}(p,pn)C^{11}$
for protons from 105 to 350 Mev., and of $C^{12}(d,dn)C^{11}$ for
deuterons from 85 to 190 Mev. The proton excitation funct-

ion rises steeply from the threshold at 40 Mev. to a peak
of 89 mb. at 50 Mev., falls off gradually and levels off
to 37 mb. from 200 to 350 Mev. The deuteron excitation
function is completely different: it rises from a threshold
at 32 Mev. to a plateau of 60 mb. from 100 to 190 Mev.

Results of alpha-particle bombardment may, to a
rough approximation, be thought of as caused by four nucleons,
since there is no reason to believe that, after impact, the
alpha-particle will remain as an entity.

At particle energies sufficiently low so that
compound nucleus formation is the main mechanism, e.g. 30 Mev.,
the situation is quite different. The lifetime of the com-
pound nucleus is 10^{-15} second (5) while the transit time
across the nucleus of a 30 Mev. nucleon is 10^{-21} second
(193), so that the redistribution of incoming energy is com-
plete before the nucleus begins to emit nucleons. The nucleus
to consider is now not the target nucleus but rather the com-
pound nucleus formed by the target nucleus plus the impinging
particle. It thus appears that, at particle energies of
30 Mev., comparison between bombardment results obtained with
different particles is only valid when the compound nucleus
formed is the same in each case.

The compound nucleus under consideration in this thesis, Ni^{60*}, is formed by the action of

(1) protons on $_{27}Co^{59}$ stable, 100% abundant

(2) deuterons on $_{27}Co^{58}$ radioactive

(3) tritons on $_{27}Co^{57}$ radioactive

(4) neutrons on $_{28}Ni^{59}$ radioactive

(5) α-particles on $_{26}Fe^{56}$ stable, 91.6% abundant.

Since Co^{58}, Co^{57} and Ni^{59} are radioactive, the only experimentally feasible comparison to Co^{59} plus protons is number (5): Fe^{56} plus alpha-particles. We were unable to find any references in the literature describing the irradiation of iron with alpha-particles.

From the preceding arguments we conclude that numerical comparison of cobalt plus protons with cobalt plus neutrons would be valid at particle energies above about 50 to 100 Mev. Bonner and Orr's (185) data on the spallation of cobalt by 190 Mev. deuterons would be difficult to compare numerically with proton-induced spallation because of polarization of the deuteron, and no numerical comparison will be attempted in this thesis. For the sake of completeness,

Bonner and Orr's data are nevertheless included in Tables IV and VI. The values need no corrections.

6. Data of Rudstam

It was not found necessary to apply any corrections to the data of Rudstam (38) (see Tables IV and VI). Rudstam did not determine absolute cross-sections; some of his values are reported relative to Cr^{49}, some relative to Sc^{47}. He quotes an error $\pm 50\%$. Rudstam used the positron-negatron counting correction of Seliger (192), so that his data are still valid as published.

7. Data of Sharp, Diamond and Wilkinson

Sharp, Diamond and Wilkinson (45) have recently published a comprehensive paper on the nuclear reactions of cobalt with protons from 0 to 100 Mev. energy. Absolute excitation functions were measured for 18 radioactive products from $_{23}V$ to $_{28}Ni$.

The stacked-foil technique was used to bombard simultaneously from four to twenty cobalt foils. The proton flux was measured relative to the reaction $Al^{27}(p,3pn)Na^{24}$, using the excitation functions of Hintz and Ramsey (190) as corrected by Crandall, Millburn, Pyle and Birnbaum (189) (see above for detailed discussion). As well as using the corrected value of the aluminum monitor, Sharp, Diamond and Wilkinson used Seliger's (192)

positron-negatron counting corrections, so that their data need no corrections. The published cross-sections are shown in Tables IV and VI.

Table VI

Existing Data on the Nuclear Reactions of Cobalt (CORRECTED)
All cross-sections in mb.

Mev. Particle Reference	60 p (45)	60 p (42)	100 p (45)	100 p (42)	170 p (42)	187 p (38)	190 d (185)	240 p (184)	240 p (42)	370 p (43)
28Ni57	9.7±2.8	--	1.7±.5	--	--	--	--	.9±.2	--	.24±.06
56	.43±.11	--	.21±.05	--	--	--	--	--	--	--
27Co58m	129±38	--	81±24	--	--	--	--	--	--	--
58	98±116	700±350	54±64	290±150	150±75	--	--	217±42	96±48	87±43
57	76±23	--	31±9	--	--	--	--	--	--	--
56	7.8±27	98±50	2.9±10	72±37	24±13	--	--	28±6	18±9	10.9±2.7
55	10.6±3.1	4.8±1.0	7.8±2.3	17±3	7.9±1.7	--	--	--	5.5±1.1	3.7±.9
26Fe55	--	--	--	--	--	--	--	--	--	26±6
53	5.8±1.4	--	3.8±.9	--	--	--	--	--	--	1.2±.4
52	.053±.018	.0007±.0004	.31±.11	.47±.14	.54±.16	--	--	.8±.2	.52±.16	.20±.05
24Mn56	9.4±1.5	9.2±2.3	11.5±1.8	11±2	9.2±2.4	--	27	8±2	6.7±1.7	2.7±.7
54	49±12	--	46±11	--	--	--	--	--	--	18±5
52m	1.37±.23	--	8.7±1.5	--	--	--	--	--	--	4.0±1.6
52	3.5±1.1	1.0±.3	12.7±4.1	29±8	26±7	--	48	21±4	19±5	10.1±2.5
51	0	--	4.2±1.1	5.2±2.6	5.0±1.7	--	--	--	7.0±2.6	2.9±1.0

Table VI (contd.)

Mev. Particle	60 p	60 p	100 p	100 p	170 p	187 p	190 d	240 p	240 p	370 p
24Cr51	0	--	40±13	--	--	--	--	--	--	19.7±1.4
49	--	--	--	--	--	--	--	5.5±1.1	--	2.9±.7
48	0	--	.089±.018	--	--	--	--	·--	--	--
23V 53	0	--	.04±.01	--	--	--	--	--	--	--
49	--	--	--	--	--	--	--	--	--	22±6
48	0	--	6.4±1.4	--	--	$1.2±.6/Cr^{49}$	--	--	--	7.6±2.0
47	--	--	--	--	--	--	--	--	--	1.5±.7
22Ti45	--	--	--	--	--	$.45±.22/Cr^{49}$	--	--	--	2.5±.6
21Sc48	--	--	--	--	--	$.35±.17/Sc^{47}$	--	--	--	--
46	--	--	--	--	--	$4.1±2.0/Sc^{47}$	--	--	--	1.6±.2
44m	--	--	--	--	--	$1.7±.9/Sc^{47}$	--	5.5±1.1	--	2.5±1.0
43+44	--	--	--	--	--	$1.7±.9/Sc^{47}$	--	7.7±1.5	--	3.6±1.2

Table VI (contd.)

Mev. Particle	60 p	60 p	100 p	100 p	170 p	187 p	190 d	240 p	240 p	370 p
20Ca47	--	--	--	--	--	--	--	--	--	$.04 \pm .02$
45	--	--	--	--	--	--	--	--	--	$.47 \pm .24$
19K 43	--	--	--	--	--	--	--	--	--	$.36 \pm .16$
42	--	--	--	--	--	$.16 \pm .08/Cr^{49}$	--	11 ± 3	--	$.61 \pm .20$
38	--	--	--	--	--	--	--	--	--	$.27 \pm .10$
17C139	--	--	--	--	$.006 \pm .004$	--	--	$.55 \pm .11$	$.12 \pm .08$	$.36 \pm .29$
38+34	--	$.004 \pm .002$	--	$.06 \pm .03$	$.015 \pm .007$	--	--	$1.1 \pm .3$	$.16 \pm .08$	2.0 ± 1.0
15P 33	--	--	--	--	--	--	--	--	--	$.021 \pm .014$
32	--	--	--	--	--	$.025 \pm .012/Cr^{49}$	--	--	--	$.21 \pm .07$
14S131	--	--	--	--	--	$.01 \pm .005/Cr^{49}$	--	--	--	--
13A129	--	--	--	--	--	--	--	--	--	$< .21$
12Mg27	--	--	--	--	--	--	--	--	--	$< .21$
11Na24	--	--	--	--	--	--	--	--	--	$.05 \pm .02$
9F 18	--	--	--	--	--	--	--	--	--	$.05 \pm .02$
6C 11	--	--	--	--	--	--	--	--	--	$.036$

F. Choice of Monitors

1. Absolute Cross-Section for $C^{12}(p,pn)C^{11}$

The monitoring reaction used for irradiations at proton energies below 60 Mev. was $B^{11}(p,n)C^{11}$. Above 60 Mev., the reaction used to monitor the proton beam was $Al^{27}(p,3pn)Na^{24}$. The decay characteristics of C^{11} and Na^{24} are given in Table VII. The published excitation functions for both $B^{11}(p,pn)C^{11}$ and $Al^{27}(p,3pn)Na^{24}$ depend on the primary monitoring reaction $C^{12}(p,pn)C^{11}$. Because the work described in this thesis was done at proton energies below 100 Mev. and because published spallation studies of cobalt have been carried out only at proton energies below 370 Mev., we have included in our compilation of published cross-sections of the $C^{12}(p,pn)C^{11}$ reaction only those values for proton energies below 370 Mev.

Four such papers have appeared in the literature to date, those of Hintz and Ramsey (190), Aamodt, Peterson and Phillips (191), Burcham, Symonds and Young (201) and Crandall, Millburn, Pyle and Birnbaum (189). The published values are listed in Table VIII. Critical evaluations of these four papers have been made by several authors (202) (37) (189) and it is generally agreed that the results of Crandall, Millburn, Pyle and Birnbaum are the most reliable to date. According to Rosenfeld et al. (202), the values reported by Burcham, Symonds and Young (201) may possibly be too high because of the large neutron flux

Table VII

Decay Characteristics of the Nuclides
Used as Monitors of the Proton Beam

Nuclide	Half-life	Mode of Decay	Energy of Radiation in Mev.		Decay Scheme
			Particles	Gamma-transitions	
C^{11}	20.5±0.1 m (194)	β^+, no γ (195)	0.968 (196)		
Na^{24}	15.04±.06 h (197)	β^- γ (126)	1.390 100% of disint. (126)	γ_1 2.76, γ_2 1.38 (198)	

:64

around the Birmingham synchrotron. The data are, however, in excellent agreement with the data of Crandall et al.

The values of Aamodt, Peterson and Phillips (191) are now accepted as being about 15% too high (202) (37) (189) due to lack of correction for knock-on electrons from the Faraday cup housing foil. It is generally agreed that the data of Aamodt, Peterson and Phillips should be normalized to that of Crandall, Millburn, Pyle and Birnbaum (189). The energy range shared by the two sets of data is 170 to 340 Mev. Unfortunately, the two curves are of different shape, that of Crandall et al. being almost independent of energy in the range 170 to 340 Mev., while the curve of Aamodt et al. dips sharply at 340 Mev. (ss Figure 2). The problem is to decide at what point the two curves should be made to coincide. Jones (37) has chosen to normalize the two curves at 300 Mev., but it appears from the paper by Aamodt et al. that the value at 340 Mev. was an absolute value using the full energy of the proton beam. Following Crandall et al., we have chosen to normalize the two curves at 340 Mev. The normalized values are shown in Table VIII and Figure 2.

Figure 2

Published Determinations of the Cross-Section for
the Reaction $C^{12}(p,pn)C^{11}$

FIG. 2

● HINTZ and RAMSEY (NORMALIZED)
△ AAMODT ET AL.   (NORMALIZED)
○ CRANDALL ET AL.
▲ BURCHAM ET AL.

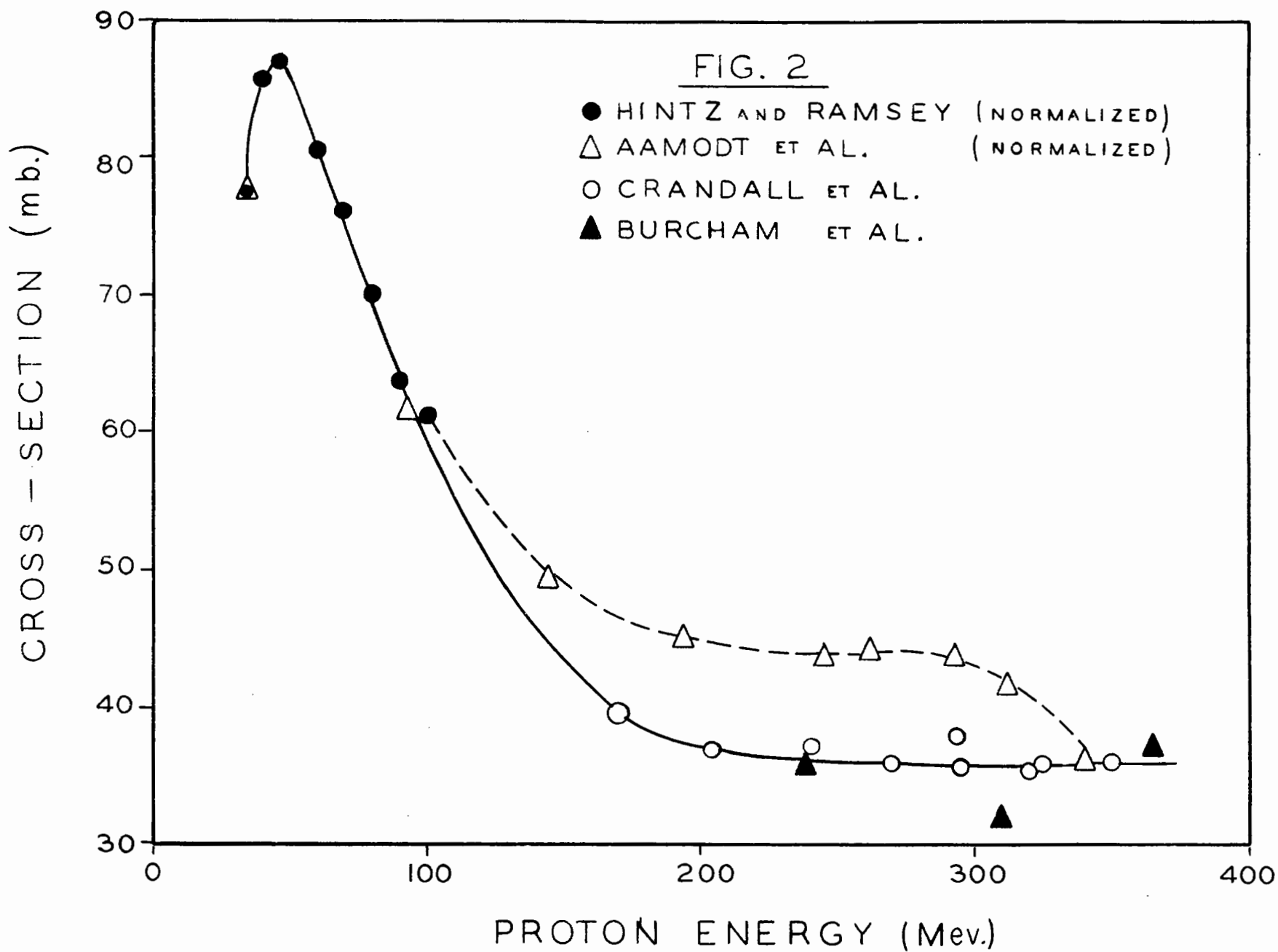## Table VIII

Published Determinations of the Cross-Section for the Reaction $C^{12}(p,pn)C^{11}$

Proton Energy (Mev.)	Cross-Section (mb.) Published	Normalized	Reference
32	89±10	78	
40	98±10	86	
46	99±10	86	
60	92± 9	80	Hintz and Ramsey
70	87± 9	76	
80	80± 8	70	
90	73± 7	64	
100	70± 7	61	
32	89± 4	77.7	
93	70.5±3.6	71.6	
144	56.5±1.5	49.4	
194	52.0±1.5	45.4	Aamodt, Peterson and
245	49.8±1.2	43.5	Phillips
263	50.5±2.6	44.1	
293	47.7±1.0	41.6	
313	47.6±2.1	41.6	
340	41.2±0.6	36.0	
170	39.7±0.9		
204	37.0±2.0		
240	37.2±1.8		
270	35.9±1.0		Crandall, Millburn,
295	37.9±0.4		Pyle and Birnbaum
320	35.5±0.7		
325	35.9±0.8		
350	36.0±0.7		
238	35.8±2.4		Burcham, Symonds,
310	31.9±2.4		and Young
365	37.4±3.1		

Hintz and Ramsey (190) did not determine the absolute cross-section for monitoring reaction $C^{12}(p,pn)C^{11}$, but obtained a relative excitation function and normalized it to the value obtained by Aamodt, Peterson and Phillips (191) of $89^{\pm}$ 4 mb. at 32 Mev. The corrected value of Aamodt et al. at 32 Mev. is now 77.7 mb., and we have normalized Hintz and Ramsey's data by the factor 77.7/89 to make their curve coincide with that of Aamodt et al. The corrected data are included in Table VIII and Figure 2.

The solid line in Figure 2 is the curve that will be used throughout this thesis. It may be mentioned that the solid line agrees with the values chosen by Hicks, Stevenson and Nervik (69) as most closely representing the presently known absolute excitation function for $C^{12}(p,pn)C^{11}$.

2. The Monitoring Reaction $B^{11}(p,n)C^{11}$

Hintz and Ramsey (190) have determined the excitation function for the reaction $B^{11}(p,pn)C^{11}$ relative to the monitoring reaction $C^{12}(p,pn)C^{11}$. Their published values are shown in Table IX. As discussed above, Hintz and Ramsey determined a relative excitation function for $C^{12}(p,pn)C^{11}$ and accepted the value of $89^{\pm}$ 4 mb. at 32 Mev. as published by Aamodt, Peterson and Phillips (191). In this thesis, we have used the value of 77.7 mb. at 32 Mev. for the carbon monitor because of the 15% correction discussed above. Hintz

and Ramsey's excitation function for the reaction $B^{11}(p,n)C^{11}$ depends on the excitation function $C^{12}(p,pn)C^{11}$. The revised values for the boron reaction used in the present work are shown in Table IX and Figure 3.

Table IX

Values of the Cross-Section* for B^{11} Used in this Thesis

Proton Energy (Mev.)	$\sigma B^{11}(p,n)C^{11}$ as published	$\sigma C^{12}(p,pn)C^{11}$ used by Hintz, Ramsey	Revised σ $C^{12}(p,pn)C^{11}$ from Fig. 2	Revised σ $B^{11}(p,n)C^{11}$
32	31.1	89	77.7	27.2
40	24.5	98	85.6	21.4
46	20.5	99	86.4	17.9
60	14.5	92	80.3	12.7
70	12.1	87	76.0	10.6
80	10.2	80	69.8	8.9
90	9.2	73	64.4	8.1
100	8.5	70	59.4	7.2

* All cross-sections in mb.

<u>Figure 3</u>

Values of the Cross-Section for
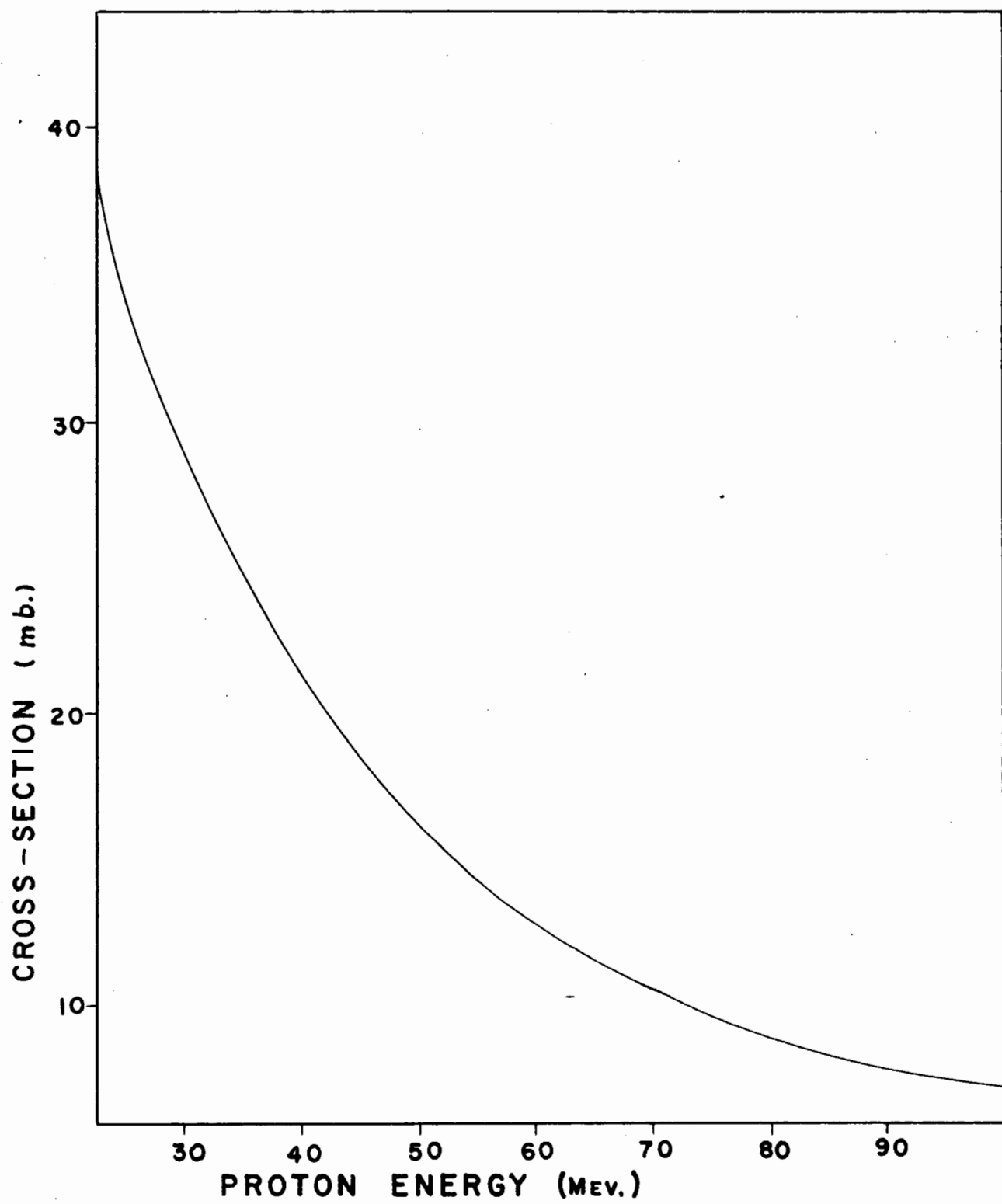$B^{11}(p,n)C^{11}$ Used in this Thesis

FIG.3

3. The Monitoring Reaction $Al^{27}(p,3pn)Na^{24}$

At energies above 60 Mev., we used the reaction $Al^{27}(p,3pn)Na^{24}$ to monitor the cobalt bombardments described in this thesis. Published determinations of the cross-section for the aluminum reaction, with the exception of one Faraday Cup measurement at 32 Mev. (206), have been reported relative to the reaction $C^{12}(p,pn)C^{11}$. The published ratios are given in Table X.

The ratios of Hintz and Ramsey (190) have been lowered by 8% because, as pointed out by Sharp, Diamond and Wilkinson (45), Hintz and Ramsey failed to correct their data for the 8% difference in back-scattering between positron and negatron emitters for small geometry Geiger-Mueller counters (192).

The cross-sections for the formation of Na^{24} were calculated from the published ratios and the corresponding value of the $C^{12}(p,pn)C^{11}$ cross-section taken from Figure 2. The calculated cross-sections are shown in Table X and Figure 4. The line drawn through the points in Figure 4 represents the values used by us to calculate the yields of the spallation products of cobalt.

Table X

Published Values of the Cross-Section for the Reaction
$Al^{27}(p,3pn)Na^{24}$ Relative to the Reaction $C^{12}(p,pn)C^{11}$

Proton Energy (Mev.)	Ratio $\sigma Na^{24}/\sigma C^{11}$	Lowered 8% (45)	σC^{11} from Fig. 2	σNa^{24}	Reference
40	0.0153	0.0141	85.6	1.21	
50	0.0817	0.0753	86.4	6.51	
60	0.152	0.0140	81.2	11.4	
70	0.184	0.0169	76.0	12.8	
80	0.200	0.0184	69.8	12.8	Hintz, Ramsey (190)
90	0.219	0.0202	64.2	13.0	
100	0.222	0.0204	59.2	12.1	
110	0.220	0.0202	54.8	11.1	
115	0.219	0.0202	52.8	10.7	
350	0.348		36.0	12.5	Turkevich (203)
350	0.362		36.0	13.0	Miller (204)
200	0.238		36.6	8.70	
230	0.263		36.3	9.55	Chackett et al. (205)
300	0.278		36.0	10.0	
320	0.286		36.0	10.3	
340	0.298		36.0	10.7	

Table X (contd.)

Proton Energy (Mev.)	Ratio $\sigma Na^{24}/\sigma C^{11}$	σC^{11} from Fig. 2	σNa^{24}	Reference
50	0.0175	86.4	1.52	
60	0.0668	81.2	5.4	
70	0.107	76.0	8.2	
80	0.146	69.8	10.3	
90	0.162	64.2	10.7	Hicks et al. (69)
110	0.185	54.8	10.6	
125	0.193	49.2	10.0	
125	0.201	49.2	10.4	
135	0.198	46.6	9.7	
150	0.209	43.2	9.3	
150	0.204	43.2	9.1	
175	0.230	39.0	8.9	
200	0.248	37.2	9.0	
200	0.256	37.2	9.3	
225	0.258	36.8	9.3	
250	0.275	36.4	9.9	
275	0.289	36.0	· 10.4	
300	0.311	36.0	11.2	
325	0.314	36.0	11.3	
340	0.319	36.0	11.5	
350	0.311	36.0	11.3	
32			0.005 (Faraday Cup)	Gilbert (206)

Figure 4

Published Values of the Cross-Section
for the Reaction $Al^{27}(p,3pn)Na^{24}$

△◯ Gilbert

◯ Hicks, Stevenson, and Nervik

△ Hintz and Ramsey

□ Chackett et al.

⊗ Turkevich

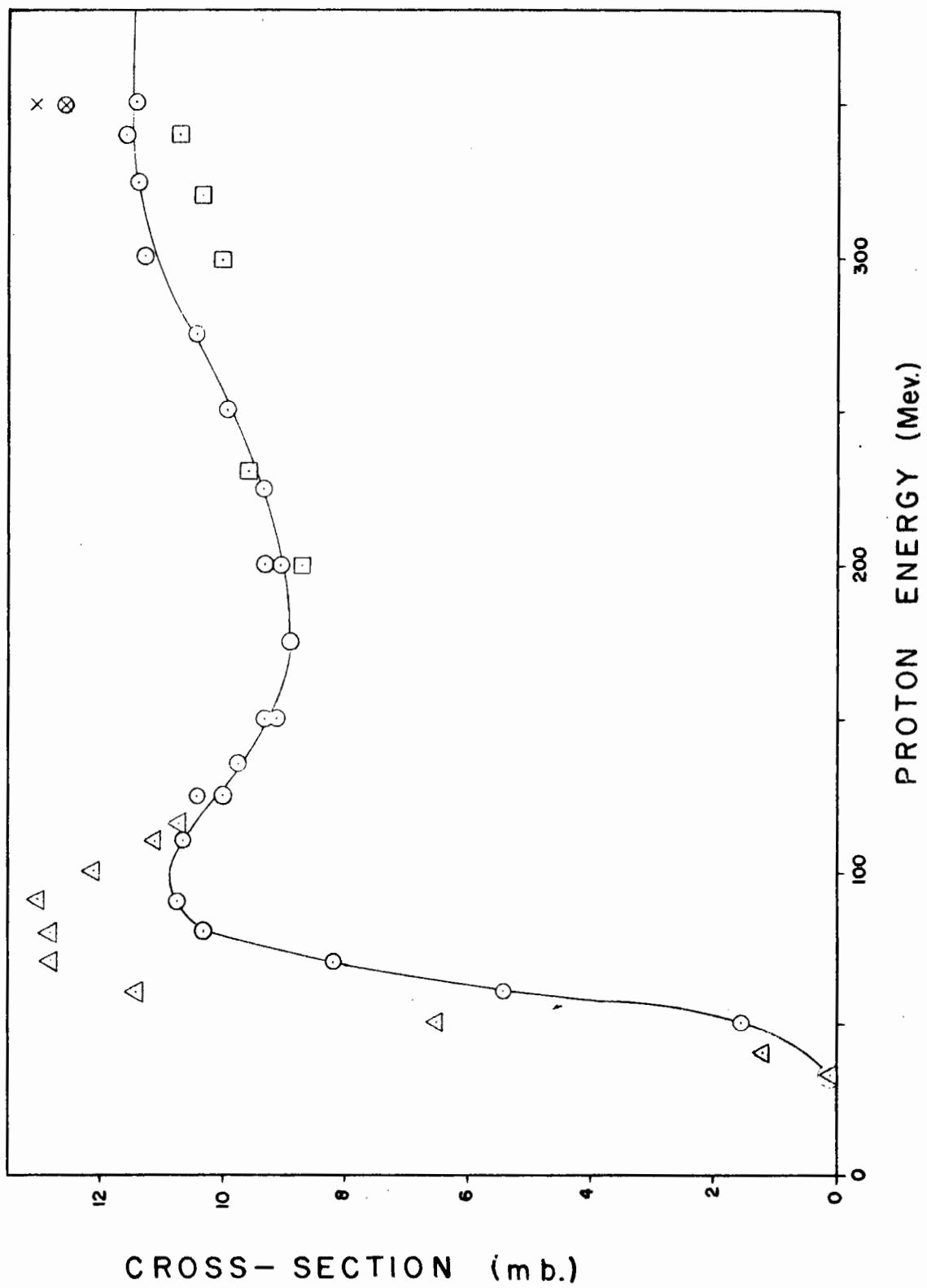X Miller

CROSS— SECTION (m b.)

PROTON ENERGY (Mev.)

FIG. 4

II EXPERIMENTAL

A. Preparation of Targets

The cobalt used was 'spec-pure' cobalt sponge obtained from Johnson, Matthey and Co. Ltd. The spectrographical analysis, as supplied by them, follows.

Spectrographical Analysis of Cobalt

Element	Estimate of Quantity Present
Si	0.002%
Mg	0.0005%
Al	0.0002%
Mn	0.0001%
Ca	less than 0.0001%
Fe	less than 0.001%
Ni	0.0005%

No lines of the following elements were observed: Ag,As,Au,Be,Bi,Cd,Cr,K,Li,Mo,Na,Pb,Rb,Sb,Sn,Ti,V,W,Zn,Zr.

At energies below 60 Mev., the monitoring reaction used was $B^{11}(p,n)C^{11}$. The boron used was electrolytic boron as supplied by the Fairmount Chemical Co. Inc. Spectrographical analysis of the boron showed 0.01% Cu, 0.05% Fe and 0.01% Pb.

Above 60 Mev., the spallation products of cobalt include nuclides with short half-lives (21 min. Mn^{52m}, 45 min. Mn^{54}) which obscure the decay of the C^{11} monitor. The monitoring reaction used for irradiations above 60 Mev. was $Al^{27}(p,3pn)Na^{24}$. The 'spec-pure' Al_2O_3 was supplied by Johnson, Matthey and Co. Ltd. Their analysis is given below.

Spectrographical Analysis of Al_2O_3

Element	Estimate of Quantity Present (ppm)
Mg	8
Pb	5
Si	5
Cu	3
Fe	2
K	
Na	
Li	< 1
Ag	
Mn	
Ca	

No lines of the following elements were observed:
As,Au,B,Ba,Be,Bi,Cd,Co,Cr,Ga,Ge,Hg,In,Ir,Mo,Nb,Ni,Os,P,
Pd,Pt,Rb,Re,Rh,Ru,Sb,Sn,Sr,Ta,Te,Ti,Tl,V,W,Zn,Zr.

When the reaction $B^{11}(p,n)C^{11}$ was used as a
monitor, the atom ratio of cobalt to boron was 2:1; when
the reaction $Al^{27}(p,3pn)Na^{24}$ was used as a monitor, the
atom ratio of cobalt to aluminum was 7.7:1.

The mixture of powdered boron and cobalt sponge,
or of powdered alumina and cobalt sponge was placed in
aluminum tubing supplied by the Precision Tube Company
Philadelphia, Pa. The dimensions of the tubing were as
follows:

outside diameter 0.0625" ± 0.005"

wall thickness   0.0015" ± 0.0005"

A 1 1/4" length of tubing was cut with scissors from the

main stock. This piece was pressed shut at one end with disecting forceps. About 20 mg. of the powdered mixture to be bombarded was weighed into the tubing and the open end of the tubing was pressed shut with forceps. The target was clamped into a U-shaped holder which was then screwed onto the end of the cyclotron probe. The area presented to the beam by the target was approximately 3/8" x 1/16". The targets were approximately 1/16" thick. The targets could be considered thin since the energy loss in the target was about 2 Mev. (42).

The target was irradiated by protons of energies varying from 24 to 95 Mev. in the circulating beam of the McGill 82" synchro-cyclotron. The duration of bombardment varied from 15 minutes to one hour, depending on the half-lives and yields of the nuclides under investigation.

After bombardment, the aluminum sheathing was split with a razor blade, the contents were removed, and the sheathing was then discarded. When a mixture of cobalt and boron was bombarded, no separation of monitor from radioactive sample was attempted since below 60 Mev. only one spallation product, 8.9 minute Fe^{53}, has a half-life shorter than nine hours. The decay of Fe^{53}, where present, was resolved from the decay of C^{11} by a combined analytical and graphical method (62) (55). The method is discussed in

detail in the section on Results. When a mixture of
cobalt and alumina was bombarded, the magnetic properties
of cobalt were used to effect a magnetic separation of the
two powders. The separation was carried out in the gloved
box using 6" squares of glass and a magnet having about
3" between its poles. The cobalt powder was transferred to
a beaker for chemical separation, while the alumina was coll-
ected with the sticky side of a piece of cellulose tape and
placed, sticky side down, on an aluminum planchet for measure-
ment of the radioactivity, i.e. counting.

B. Chemical Separations

1. Dissolution of Target and Oxidation-Reduction

Ion exchange separation procedures were used throughout; these procedures are quantitative even at concentrations below the 1 ppm. minimum for standard chemical analysis. The spallation products formed as a result of irradiation will be present in some or all of their stable valence states. For successful separation, all the atoms of a given element must be in the same oxidation state, so that oxidation-reduction procedures were necessary. Such procedures require the addition of inactive carrier.

The target was dissolved in hot concentrated nitric acid containing inactive carriers of those elements possessing more than one stable valence state, i.e., cobalt, iron, manganese, chromium, vanadium and titanium. Table XI lists the possible valence states of the spallation products measured. It can be seen from Table XI that, if any Co^{+3} is formed during the irradiation, a process involving oxidation by nitric acid followed by reduction by hydrochloric acid would fail to convert any Co^{+3} ions to Co^{+2} ions. Similarly, any Mn^{+7} or Cr^{+6} present in the target would result in a mixture of oxidation states.

Table XI

Possible Oxidation States of Spallation Products

Element	Possible Oxidation States	Oxidized by HNO_3 to	Reduced by HCl to
Ni	+2	+2	+2
Co	+2,+3	+2	+2
Fe	+2,+3	+3	+3
Mn	+2,+4,+7	+4	+2
Cr	+2,+3,+6	+3	+3
V	+2,+3,+4,+5	+5	+4
Ti	+2,+3,+4	+4	+4
Sc	+3	+3	+3
Ca	+2	+2	+2
K	+1	+1	+1

Rudstam (207) points out that investigations of the chemical form of spallation products formed in high energy bombardments are rare. He refers to the work of Chackett and Chackett (208) who found that phosphorous is formed mainly in the elementary or in a low oxidation state when aluminum is bombarded with 100 Mev. N^{14} ions.

The degree of formation of Co^{+3}, Mn^{+7}, and Cr^{+6} was determined in the following manner: a cobalt target was bombarded with protons, dissolved in nitric acid, and

diluted to a known volume. One aliquot of the target solution, aliquot A, was reduced with hydrochloric acid, the cobalt, manganese, and chromium were separated from each other by ion exchange (see Section II. B.3), and a decay curve was obtained for each separated fraction. A second aliquot of the target solution, aliquot B, was oxidized by the addition of solid sodium bismuthate and then treated in exactly the same way as aliquot A had been treated. Yields from aliquot A included Co^{+2}, Mn^{+2}, Mn^{+4}; Cr^{+2}, Cr^{+3}. Yields from aliquot B included Co^{+2}, Co^{+3}; Mn^{+2}, Mn^{+4}, Mn^{+7}; Cr^{+2}, Cr^{+3}, Cr^{+6}. Comparison of the decay curves of the separated fractions showed less than 2% of the manganese is formed as Mn^{+7}. On the other hand, Co^{+3} and Cr^{+6} are formed in significant amounts. The results are summarized in Table XII.

Table XII
Experimentally Determined Oxidation States
of Product Nuclides

% of total cobalt formed as Co^{+3}

at 92 Mev.	18%
at 81 Mev.	32%
	Average 25±7%

% of total maganese formed as Mn^{+7}

at 92 Mev.   Less than 2%

% of total chromium formed as Cr^{+6}

at 81 Mev.   15±5%

The use of the oxidizing agent sodium bismuthate is therefore necessary because of the presence of Co^{+3} and Cr^{+6}.

Procedure

The target was dissolved in hot conc. nitric acid containing Co,Fe,Mn,Cr,V and Ti carriers. MnO_2 precipitated. The solution was diluted to 3M. in nitric acid and chilled in an ice bath. $NaBiO_3$ in the solid state was added giving Ni^{+2}, Co^{+3}, Fe^{+3}, MnO_4^-, CrO_7^{-2}, V^{+5}, Ti^{+4}, Sc^{+3}, Ca^{+2}, and K^+. Conc. hydrochloric acid was added dropwise until reaction ceased. The target solution was then taken to dryness several times with conc. hydrochloric acid giving Ni^{+2}, Co^{+2}, Fe^{+3}, Mn^{+2}, Cr^{+3}, V^{+4}, Ti^{+4}, Sc^{+3}, Ca^{+2}, and K^+. Further procedures used depended on the bombarding energy and are outlined below.

2. Chemical Separations Used at Proton Energies Below 60 Mev.

Ion exchange techniques were employed throughout because of the great advantages of speed, simplicity and 100% separation. Nickel, manganese, cobalt and iron were separated from each other on Dowex-1 by the method of Kraus and Moore (209). Part of their published graph is reproduced in Figure 5. The separation method of Kraus and Moore is based on the fact that the stability of the singly charged negative chloride complexes increases in the order

$$NiCl_3^- \; < \; MnCl_3^- \; < \; CoCl_3^- \; < \; FeCl_4^- \quad .$$
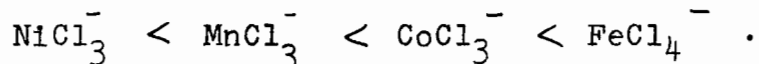
Figure 5

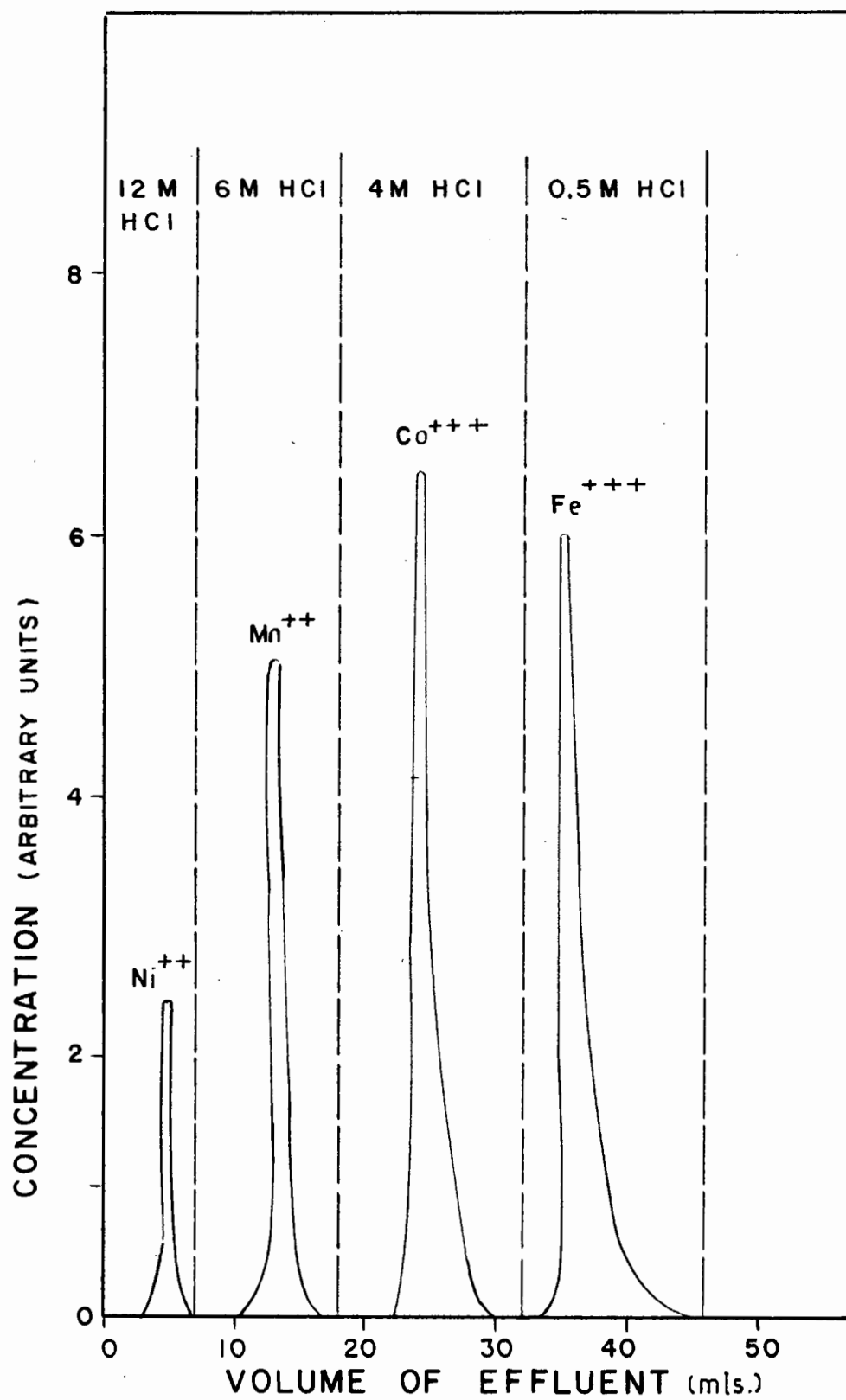Ion Exchange Separation of Ni, Mn, Co, and Fe
as published by Kraus and Moore

FIG.5

Nickel passes straight through the resin bed with negligible adsorption because of the instability of the nickel complex.

The target sheath was slit with a razor blade and the contents emptied into a small glass vial. The vial was then placed on a scintillation spectrometer and the 20.5 min. decay of the annihilation peak was followed until the activity of the C^{11} monitor had decayed into the long-lived background of the spallation products. The target was then dissolved in hot conc. HNO_3 and taken to dryness several times with conc. HCl to convert nitrates to chlorides.

A glass column had been filled with Dowex-1, supported at the bottom by a plug of glass wool. The Dowex-1, a styrene type, quaternary ammonium resin, was used in the 200-400 Mesh form. The target in conc. HCl solution was placed on the top of the column, and air pressure applied to increase the flow-rate. A dynamic equilibrium is established between anions and a positively charged anion exchange resin. The ions are adsorbed at the top of the column and desorb and adsorb many times as the solution moves down the column. Separation between ions increases with column length, decreased flow rate, increased temperature, decreased particle size, and exchange capacity of the resin. Completeness of separation increases with temperature and in order to separate certain ions, e.g. the rare earths,

it is necessary to work to elevated temperatures. The
ions under consideration are, however, easily separable
and all experiments were carried out at room temperature.
The column size must take into account ease of manipulation
inside a gloved box as well as total exchange capacity; the
size of the resin bed was held constant in all experiments
at 2.5 cm^2 x 7 cm. A flow rate of 5 drops/min. was found
to give the maximum rapidity consistent with sharp separation.
In the separation of Ni^{++}, Mn^{++}, Co^{++} and Fe^{+++} we always
obtained 100% separation as shown by the fact that neither
half-life determinations nor gamma-ray energy determinations
showed presence of a contaminating activity.

3. Chemical Separations Used at Proton Energies
    Above 60 Mev.

As the proton energy is increased, the situation
is complicated by the presence of chromium, vanadium, tit-
anium etc. The conc. HCl fraction now contains K^+, Ca^{++},
Ni^{++}, and Cr^{+++}. The 6 M. HCl fraction now contains Mn^{++},
Ti^{+4}, and V^{+4}. The 4 M. HCl fraction contains Co^{++} and
Sc^{+++}. The water fraction contains only Fe^{+++}.

Elution curves were obtained to enable the choice
of experimental conditions for the separation of mono-, di-,
and tri-valent cations on the cation-exchange resin, Dowex-50.
The experimental conditions desired were those giving maximum
rapidity consistent with 100% chemical separation.

(1). Using a constant flow rate, arbitrarily fixed at 39 drops/min., K^+ elution curves were obtained for differing molarities of the eluant, HCl. The results are shown in Figure 6. It can be seen from the figure that as the molarity of HCl increases, the sharpness of the potassium elution curve increases while the separation between potassium and nickel decreases.

(2) Using a constant eluant concentration of 0.90 M. HCl, K^+ elution curves were obtained for differing flow rates. The results are shown in Figure 7.

The data in Figures 6 and 7 may be shown graphically in a number of different ways. Figure 8 shows the width of the base of the potassium elution curve as a function of HCl concentration. It can be seen from Figure 8 that the sharpness of the potassium elution curve increases linearly up to acidities of about 0.9 M. HCl and then tails off, so that using an eluting agent much more acid than 0.9 M. HCl does not greatly affect the shape of the elution curve. 0.9 M. HCl was therefore selected as the eluent for monovalent cations on Dowex-50.

Figure 9 shows the separation in mls. between the monovalent and divalent cations as a function of HCl molarity. From Figure 9 it can be seen that the separation in mls. between K^+ and Ni^{++} is independent of flow rate from 36 to 76 drops/minute. In determining the yields of nuclides having

Figure 6

Separation of Mono - and Di-Valent Cations on
Dowex-50 for Various Eluant Concentrations

       (a)   Eluant 0.40 M. HCl

       (b)   Eluant 0.75 M. HCl

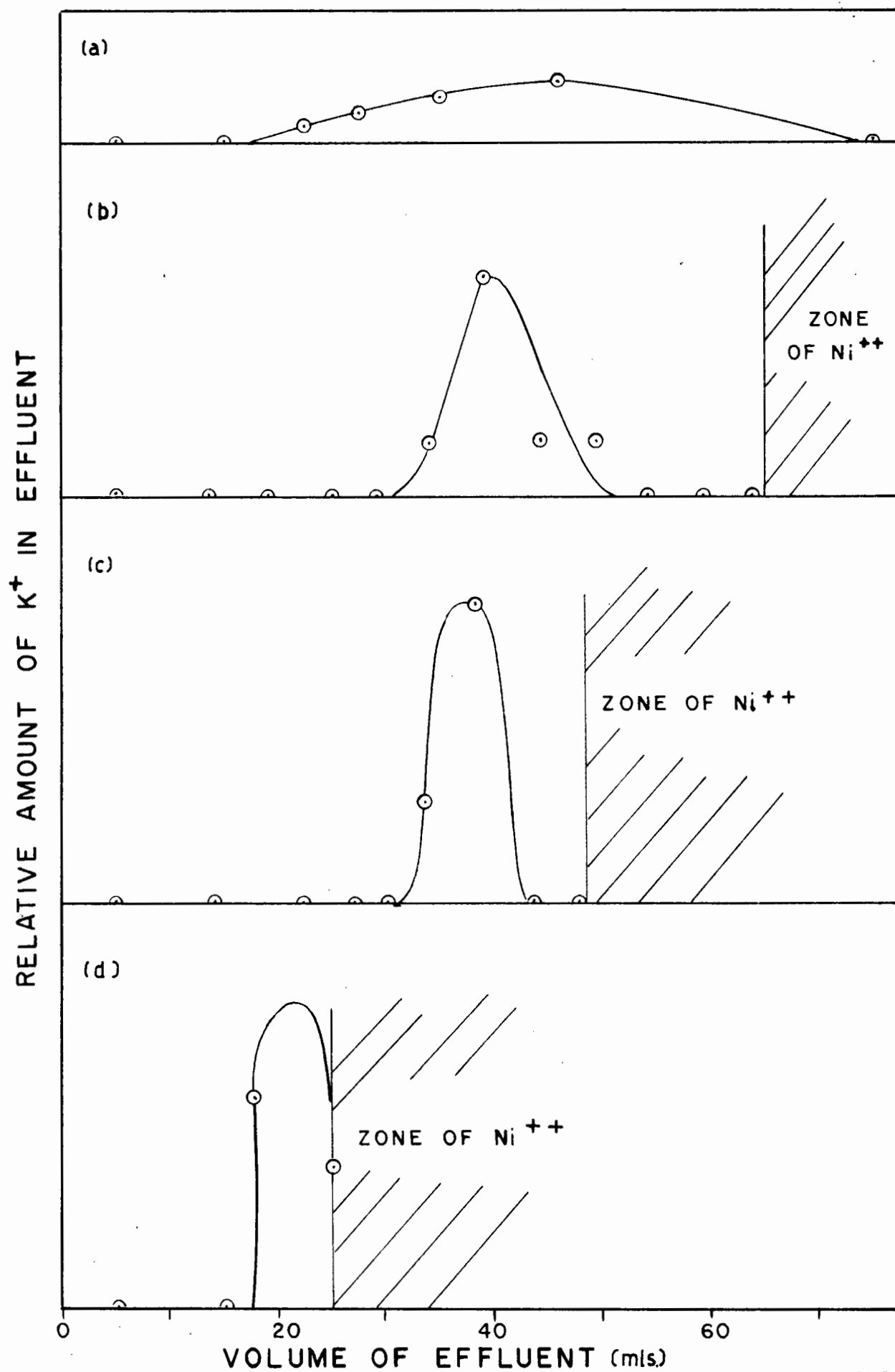   (c)   Eluant 0.90 M. HCl

       (d)   Eluant 1.10 M. HCl

FIG. 6

Figure 7

Separation of Mono - and Di-Valent Cations on
Dowex-50 for Various Flow Rates

        (a)   36-9 drops/minute

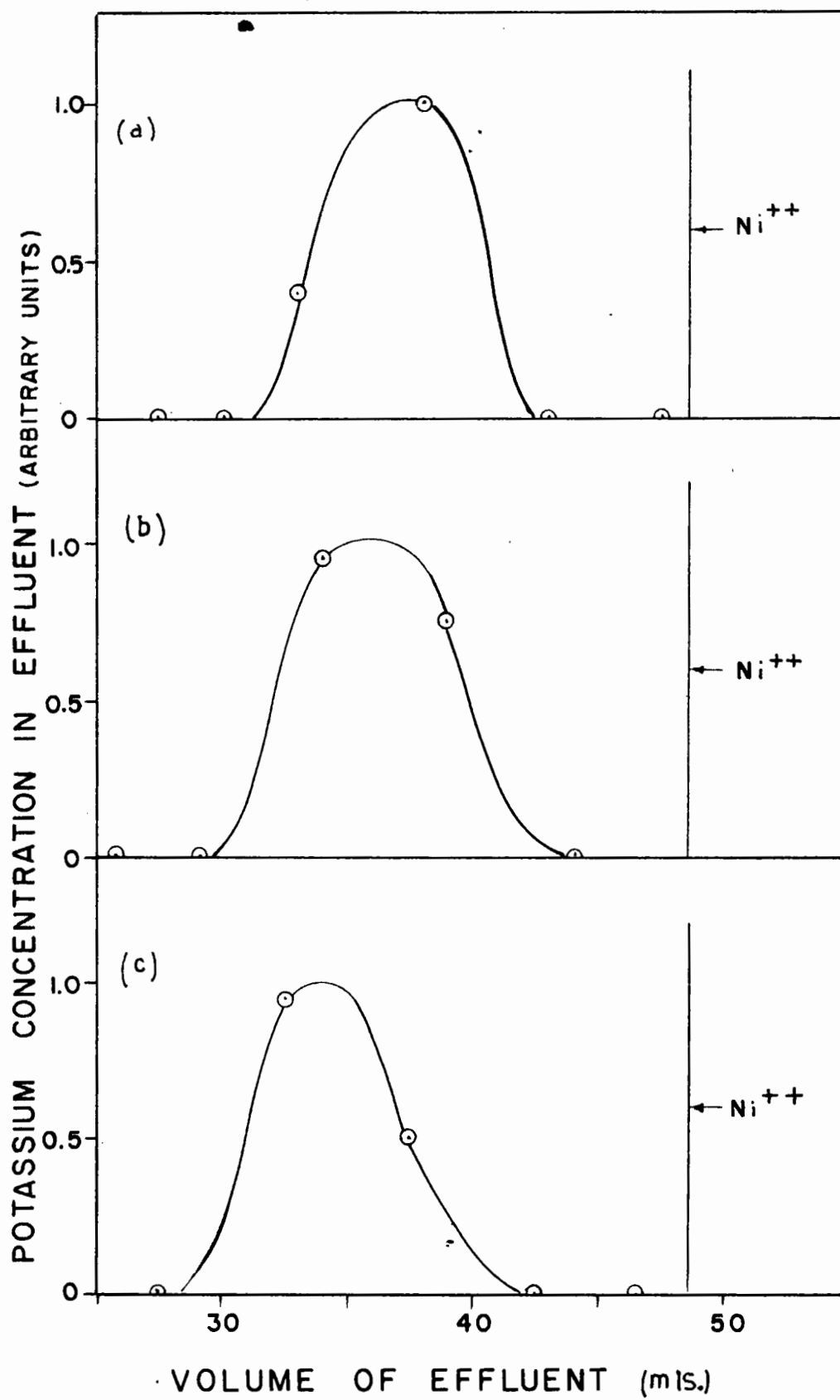   (b)   47-12 drops/minute

        (c)   76-20 drops/minute

FIG. 7

Figure 8

Width of the Base of the Potassium Elution Curve
Versus HCl Concentration

⊙   36±9 drops/minute

△   47±12 drops/minute

▫   76±20 drops/minute
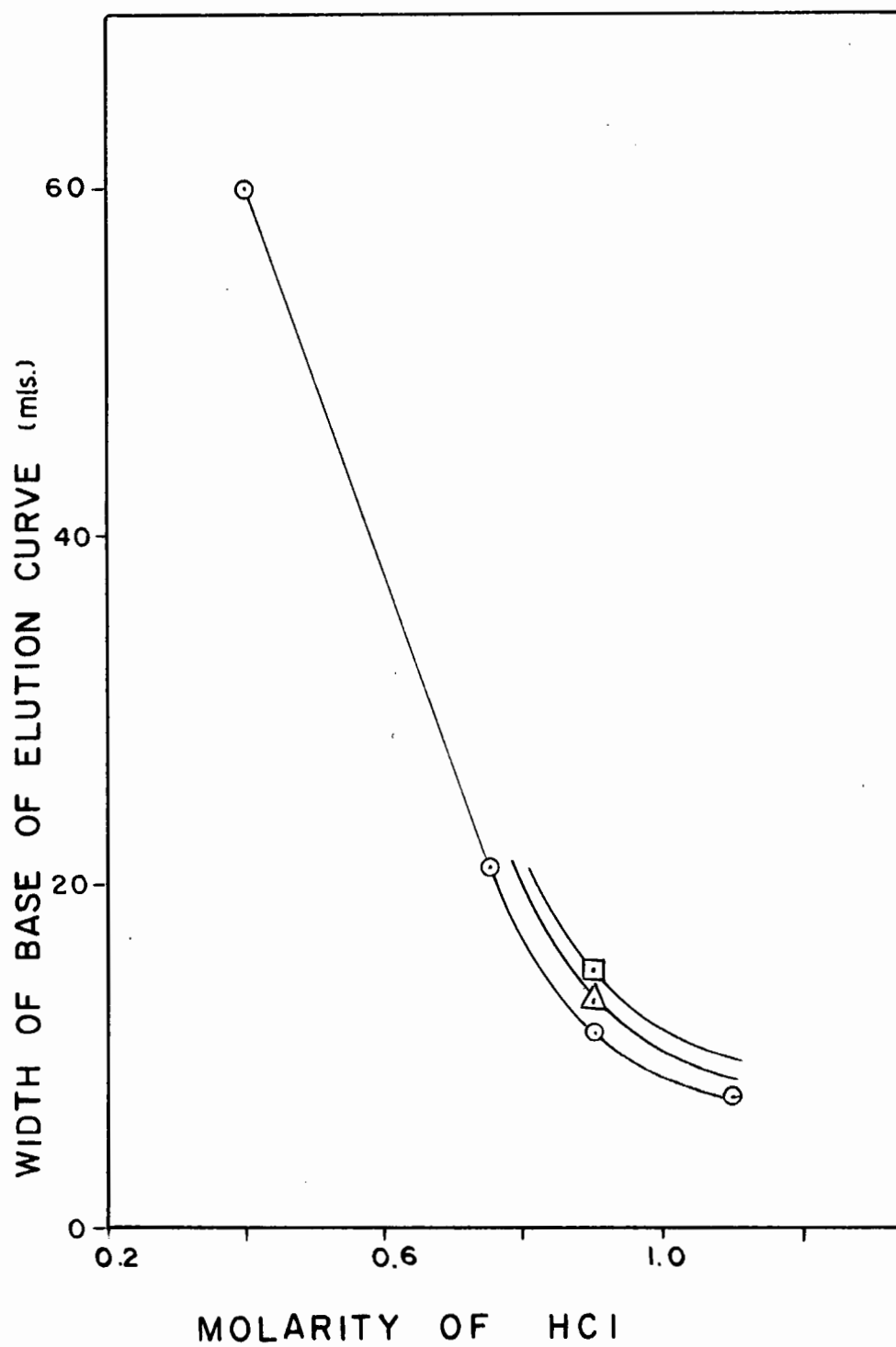
FIG.8

Figure 9

Separation Between Potassium and Nickel Versus
Molarity of the Eluant, HCl

Within the limits of error shown on the figure,
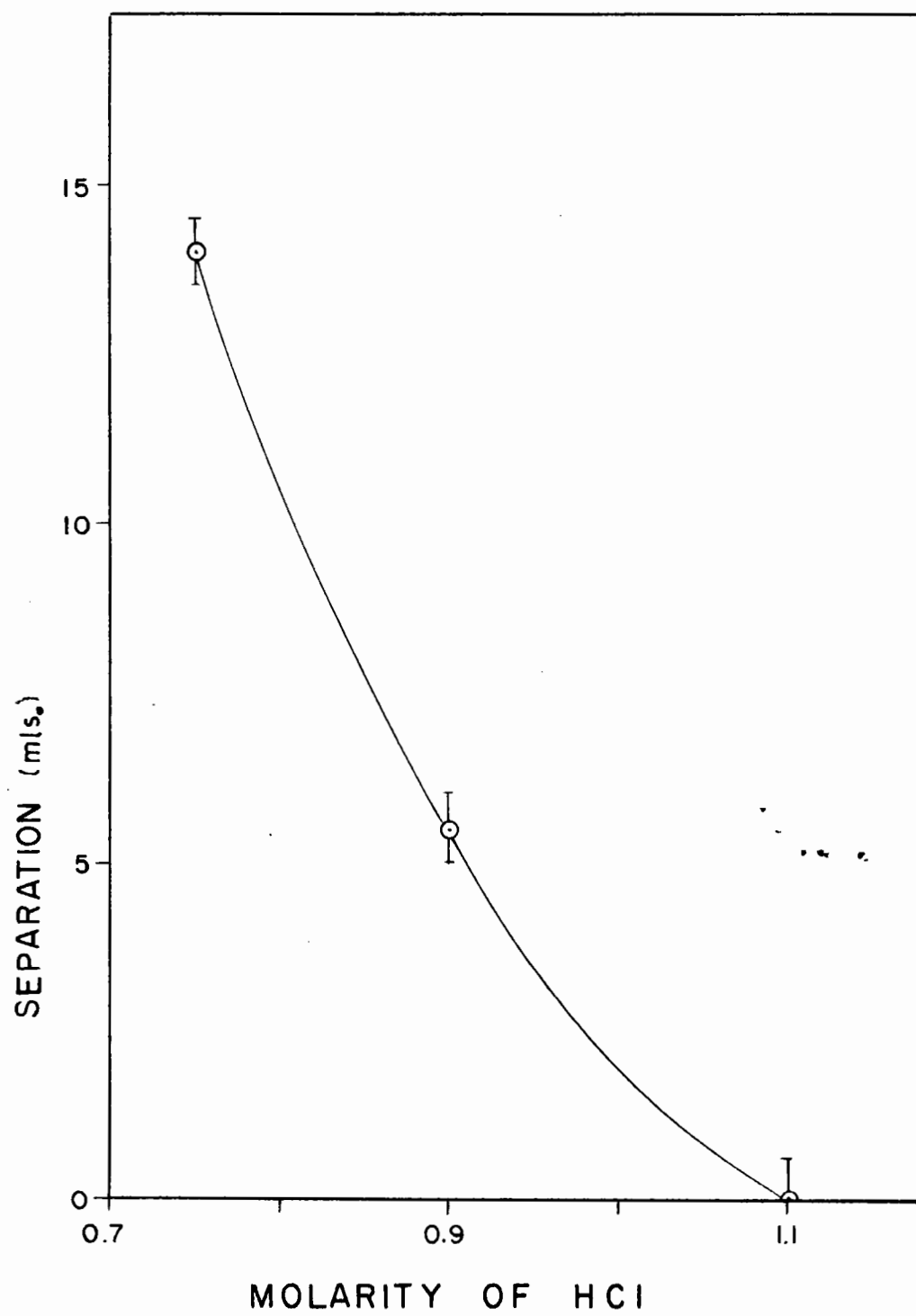the same results were obtained using flow rates
of 36, 47 and 76 drops/min.

FIG. 9

short half-lives, quick separations are of great importance.
For this reason, 76 drops/minute was chosen as the operating
flow rate. Any faster flow rate causes air bubbles to form
in the resin.

Procedure for the separation of Cr^{+3}, K^+ and Ni^{+2} on
Dowex-50: A column of Dowex-50 was prepared and washed with
water. The ions to be separated were in a chloride solution
of pH 7. The solution was adsorbed on the resin. The column
was eluted with 0.90 M. HCl, causing the chromium to appear
in the first 17 mls. of effluent. The next 3 mls. of effluent
were discarded. The next 20 mls. contained 100% of the K^+.
The column was then eluted with 2.2 M. HCl. The next 8.5 mls.
of effluent contained 100% of the Ni^{++}. The elution curves
are shown in Figure 10. The flow rate used was 76 ± 20
drops/minute. Total time of separation = 53 mls. x 20 drops/
ml. x 1 minute/76 drops = 14 minutes.

Nickel was separated from calcium by three dimethyl-
glyoxime precipitations after the addition of nickel and cal-
cium carriers. Duplicate chemical yield determinations were
made on 2 mls. of the 10 ml. nickel and calcium solutions,
and the nickel and calcium cross-sections were corrected for
chemical yield.

Vanadium in the +5 state is adsorbed by Dowex-1 at
high concentrations of HCl. Dowex-1 exerts a strong reducing

Figure 10

Separation of Chromium, Nickel and Potassium
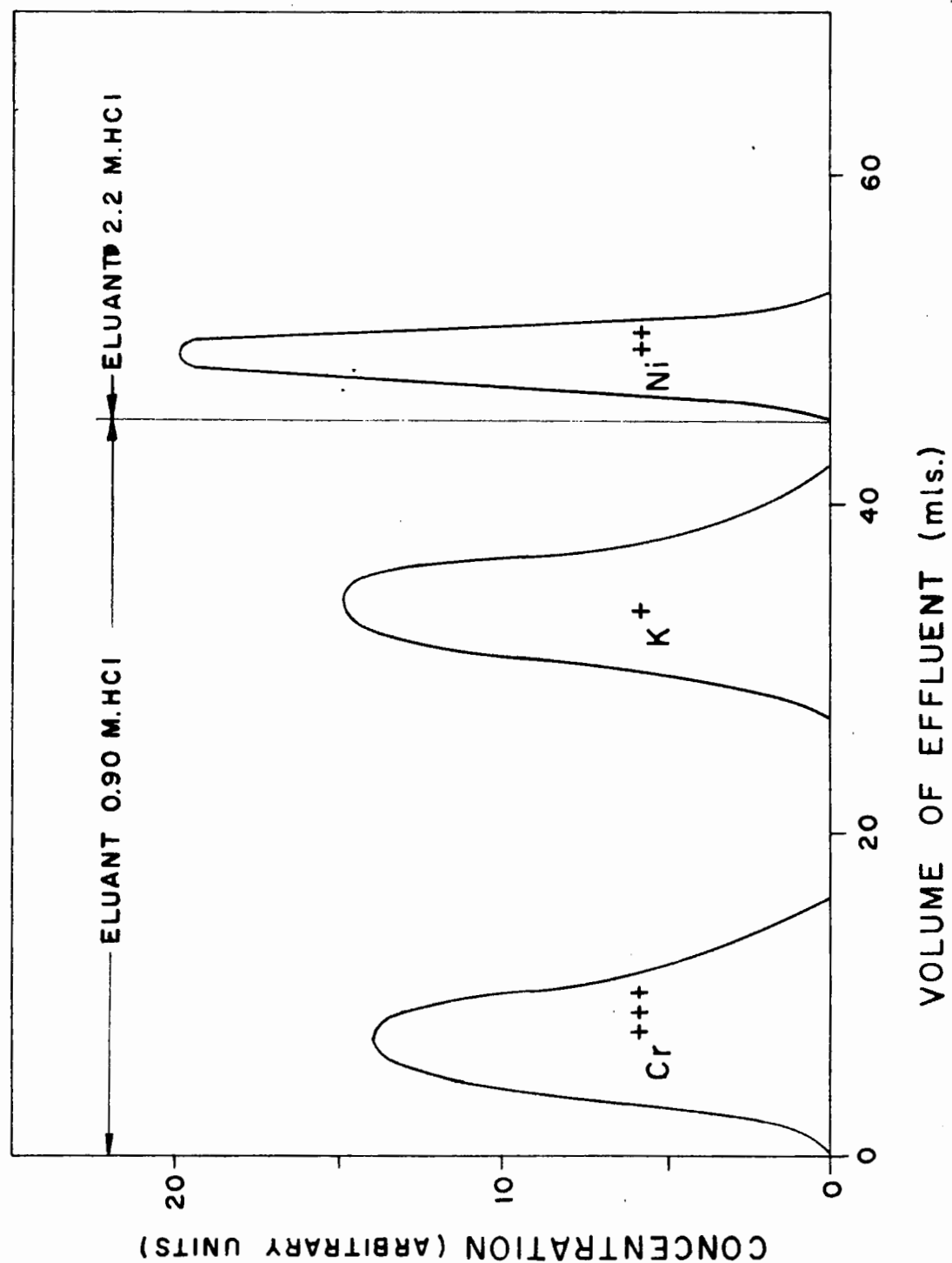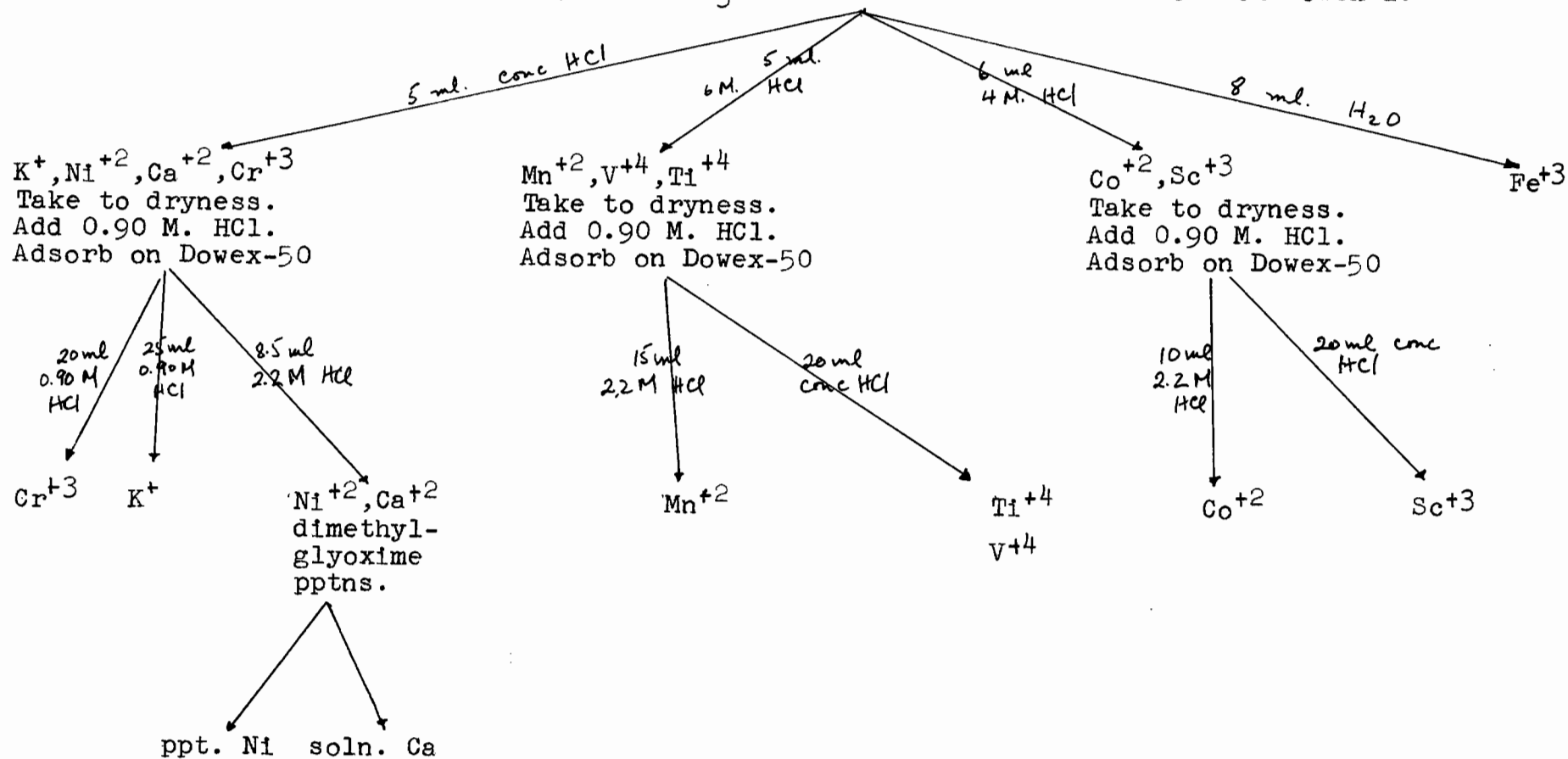on Dowex-50, using a Flow Rate of 76 drops/
minute

FIG.IO

action on V^{+5}, reducing it to V^{+4} which is not adsorbed at any concentration of hydrochloric acid (210). Under the experimental conditions, the V^{+4} appeared in the 6 M. HCl fraction together with Mn^{+2} and Ti^{+4}. Titanium and vanadium were not separated but were counted together.

The chemical procedures used are summarized in Table XIII.

Table XIII

Summary of Chemical Separations

Dissolve Target in HNO_3.   Oxidize and Reduce.   Adsorb on Dowex-1.

5 ml. conc HCl   5 ml. 6 M. HCl   6 ml. 4 M. HCl   8 ml. H_2O

$K^+, Ni^{+2}, Ca^{+2}, Cr^{+3}$
Take to dryness.
Add 0.90 M. HCl.
Adsorb on Dowex-50

Mn^{+2}, V^{+4}, Ti^{+4}
Take to dryness.
Add 0.90 M. HCl.
Adsorb on Dowex-50

Co^{+2}, Sc^{+3}
Take to dryness.
Add 0.90 M. HCl.
Adsorb on Dowex-50

Fe^{+3}

20 ml 0.90 M HCl   25 ml 0.90 M HCl   8.5 ml 2.2 M HCl

15 ml 2.2 M HCl   20 ml conc HCl

10 ml 2.2 M HCl   20 ml conc HCl

Cr^{+3} K^+ Ni^{+2}, Ca^{+2}
dimethyl-
glyoxime
pptns.

Mn^{+2} Ti^{+4}
V^{+4}

Co^{+2} Sc^{+3}

ppt. Ni   soln. Ca

The chemical fractions thus isolated were
diluted to a volume of 10 or 25 ml. Samples for gamma-
ray analysis in the scintillation spectrometer were prepared
by pipetting 2 ml. of the solution into a small glass bottle.
Samples to be counted in the Geiger-Mueller counter were
prepared by pipetting 200 microliters onto aluminum planchets
of sufficient thickness to give saturation back-scattering (211).
Since many of the solutions had a sufficiently high acid con-
centration to attack the aluminum, all the planchets were
pretreated by painting with VYNS solution (212) and drying
under an infrared lamp. When dry, the plastic coating rend-
ered the planchets inpervious to attack even by concentrated
hydrochloric acid. The difference in the back-scattering
of electrons from VYNS and from aluminum causes no error in
our results, since the Geiger counter was calibrated using
sources on VYNS films placed on aluminum planchets.

C. Counting Equipment

1. The Geiger-Mueller Counter

Samples emitting beta particles were counted with a conventional small-geometry Geiger-Mueller tube, filled with a mixture of 9.5 cm. argon and 0.5 cm. methanol. The counter had a mica window of thickness 1.6 mg./cm^2 rendered conducting by 0.1 mg./cm^2 of Aquadag. The tube was housed in a lead castle. An external quenching circuit had a nominal dead time of 600 microseconds.

The counting rates thus determined have to be transformed into disintegration rates.

The first correction to be applied to the raw counting data was addition of counting rate losses due to the dead time of the counter. This coincidence correction was obtained by the lamination of calibrated sources of Tl^{204} in the following manner: Ten sources of Tl^{204} were prepared on VYNS films (212) of thickness $10 \mu g/cm^2$, each source giving approximately 900 c/m in the Geiger tube, i.e. negligible coincidence correction. The counting rate of each of the sources was determined. The sources were then placed one on top of the other, forming a laminate. The counting rates of the laminates composed of sources A + B, sources A + B + C etc. were determined. The counting rate of the laminate at each stage was less than the calculated activity due to the sum of the component sources, the difference in counting rate

being the coincidence loss. The correction curve thus
obtained gave corrections for apparent counting rates up
to 9,000 counts/min. The curve was extended to higher
counting rates by the lamination of ten sources each giving
about 9,000 counts/min. in the Geiger tube.

A large discrepancy was obtained between the
experimentally determined coincidence correction and the
values calculated from

$$R^* = R + R^2 t \quad (167)$$

where $R =$ observed counting rate

$R^* =$ counting rate corrected for coincidence losses

$t =$ dead time of the counter

In this case t was the nominal dead time of the external
quenching circuit, set at 600 micro-seconds. The experimental
and calculated results are shown in Figure II.

The counting rates were then corrected for back-
ground activity due to cosmic rays and the presence of
radioactive sources in the laboratory.

All counts were bracketed by one minute counts of a
standard of approximately 10,000 c/m and the counting rates
were normalized to exactly 10,000 c/m for the standard, in
order to correct for small sensitivity fluctuations of the
Geiger tube.

The corrected c/m were plotted giving decay curves
which were extrapolated either to time of separation or to

Figure 11

Coincidence Correction Curve for the Geiger-
Mueller Counter

$\odot$ experimental values

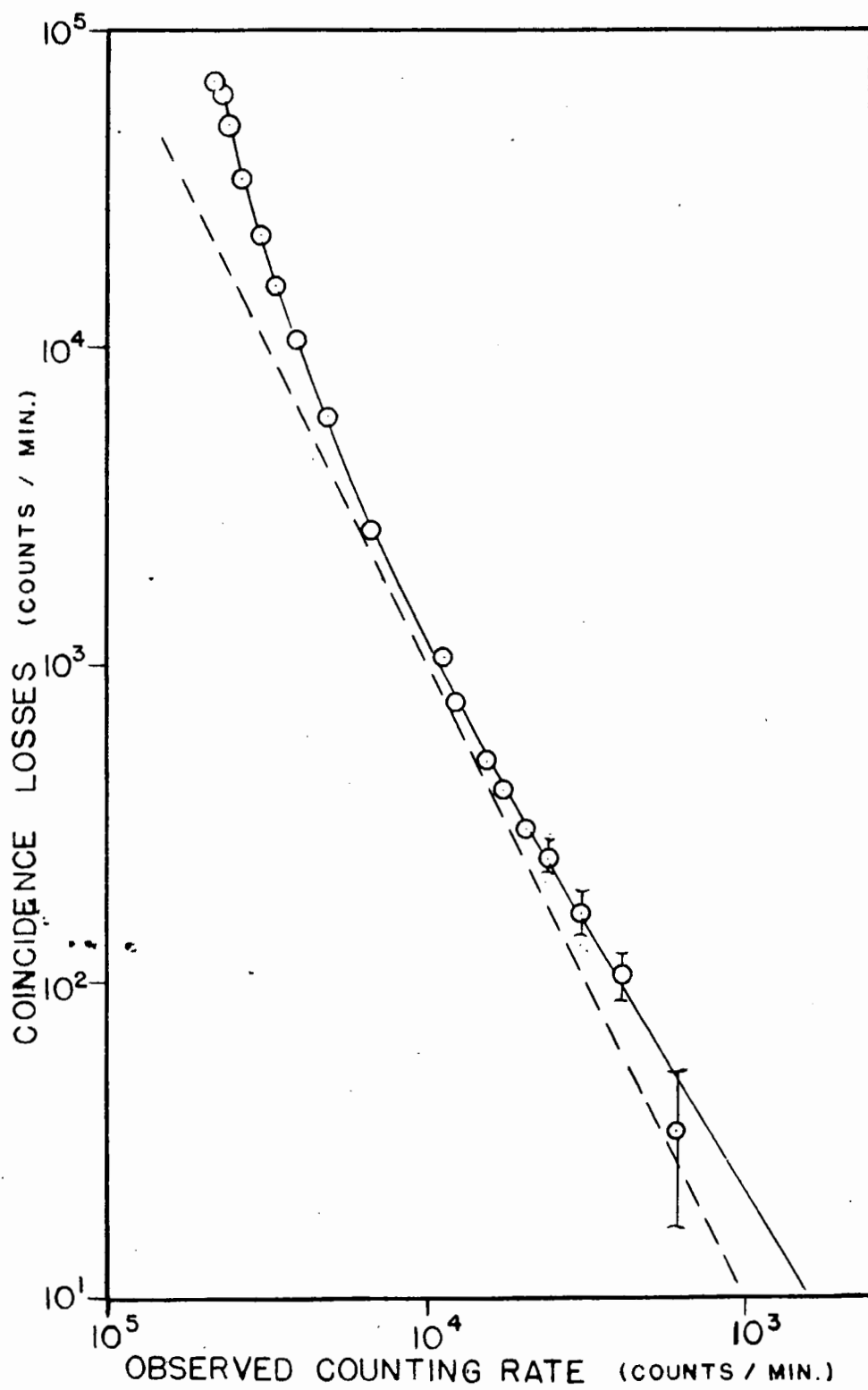---   calculated from $R^* = R + R^2 t$

FIG. II

end of bombardment. To convert counting rates at
zero time to disintegration rates at zero time it was
necessary to determine the efficiency for each shelf pos-
ition as a function of beta energy. The count rate
corrected for coincidence losses of a source in any part-
icular shelf of the Geiger tube divided by the disintegration
rate of that source gives the efficiency of the Geiger tube
for that shelf. Such experimentally determined shelf factors
include back-scattering from the aluminum planchet, wall
scattering, and adsorption due to air and window.

A VYNS film of thickness 10 $\mu g/cm^2$ was prepared
using the technique developed in this laboratory (212). The
film was mounted on a metal ring and gilded in a vacuum dist-
illation apparatus to render the plastic film conducting.
A drop of Ca^{45} (0.25 Mev.β^-) solution was placed on the
conducting film, evaporated to dryness under an infrared
lamp, and counted in a 4π counter. Correction for coinci-
dence losses in the 4π counter gave the absolute counting
rate in dis./min. of the source. The film was sufficiently
thin so that absorption in the film was negligible. The
Ca^{45} was of sufficiently high specific activity so that
self absorption was negligible.

This calibrated source was then transferred to an
aluminum planchet in the following manner: VYNS films split
when they come in contact with dry objects. To effect a

transfer, the object must either be wetted with water
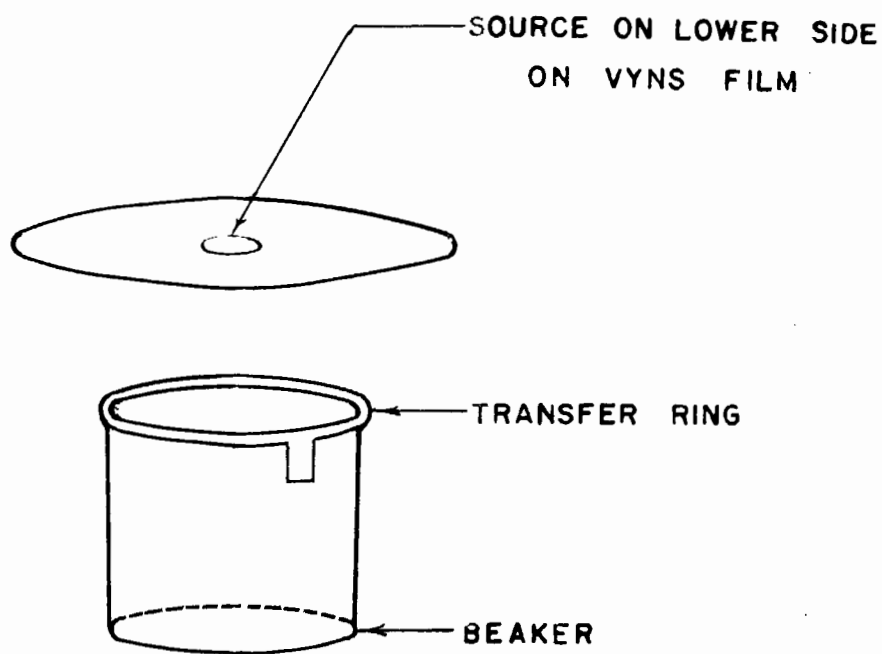or be lightly greased.

A transfer ring was cut out from metal foil in
the shape of a figure 6. The "tail" of the figure 6
was bent at right angles to the circular ring to serve as a
handle. This transfer ring was of such a size as to fit
snugly in the aluminum planchets used for counting samples
in the Geiger-Mueller counter. The transfer ring was wetted
with water and placed on a beaker for support. (See figure 12).
The VYNS film holding the calibrated source was then lowered
slowly over the transfer ring, transferring the film plus
source to the transfer ring. The transfer ring was removed
from the supporting beaker, inverted so that the source was
now on the upper side of the VYNS film and laid in an alum-
inum planchet which had been lightly greased with Vaseline.
All planchets used in this research were of thickness 0.025"
i.e., gave saturation back-scattering (211). The film
immediately adhered to the greased surface. After a nail or
other pointed object had been used to make a number of per-
forations around the edge of the film, the transfer ring
could be lifted off, leaving the source firmly adhering to
the aluminum planchet.

In calculating spallation cross-sections, all the
samples for beta counting were mounted on identical aluminum

Figure 12

Transfer of a Source Mounted on a VYNS film
to a Planchet

FIRST STEP

SOURCE ON LOWER SIDE
ON VYNS FILM

TRANSFER RING

BEAKER

SECOND STEP

SOURCE ON UPPER SIDE
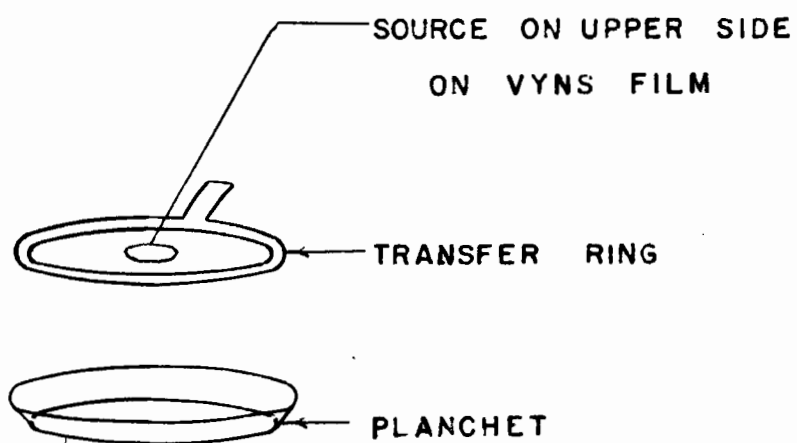ON VYNS FILM

TRANSFER RING

PLANCHET

FIG.12

planchets coated with VYNS solutions to provide an acid resistant surface. The calibration of the Geiger counter was therefore done similarly with the VYNS film between the source and the planchet. The effect observed by Yaffe and Justus (211) that the nature of the planchet surface affects the spectrum of backscattered radiation will not affect our results since the backscattering surface was identical at all times.

Calibrated sources of Tl^{204} (0.76 Mev. β^-) and P^{32} (1.71 Mev. β^-) were prepared in a similar manner. Each of the three sources was counted in all shelves of the Geiger. The results are shown in Figures 13 and 14.

The nuclides used for the Geiger-Mueller calibration do not all have the same spectrum shape (e.g. Tl^{204} first forbidden (64) P^{32} allowed (213) and the spallation products have a variety of orders of forbiddenness. The error introduced by this effect into the determination of the cross-sections will, however, be negligible in comparison with the other errors involved.

The three nuclides used for the Geiger-Mueller calibration were negatron emitters. In calculating cross-sections for position emitters, counting rates were corrected for the 8% difference in back-scattering of positions and negations as observed by Seliger (192).

Figure 13

Efficiency of Geiger Versus Distance from the
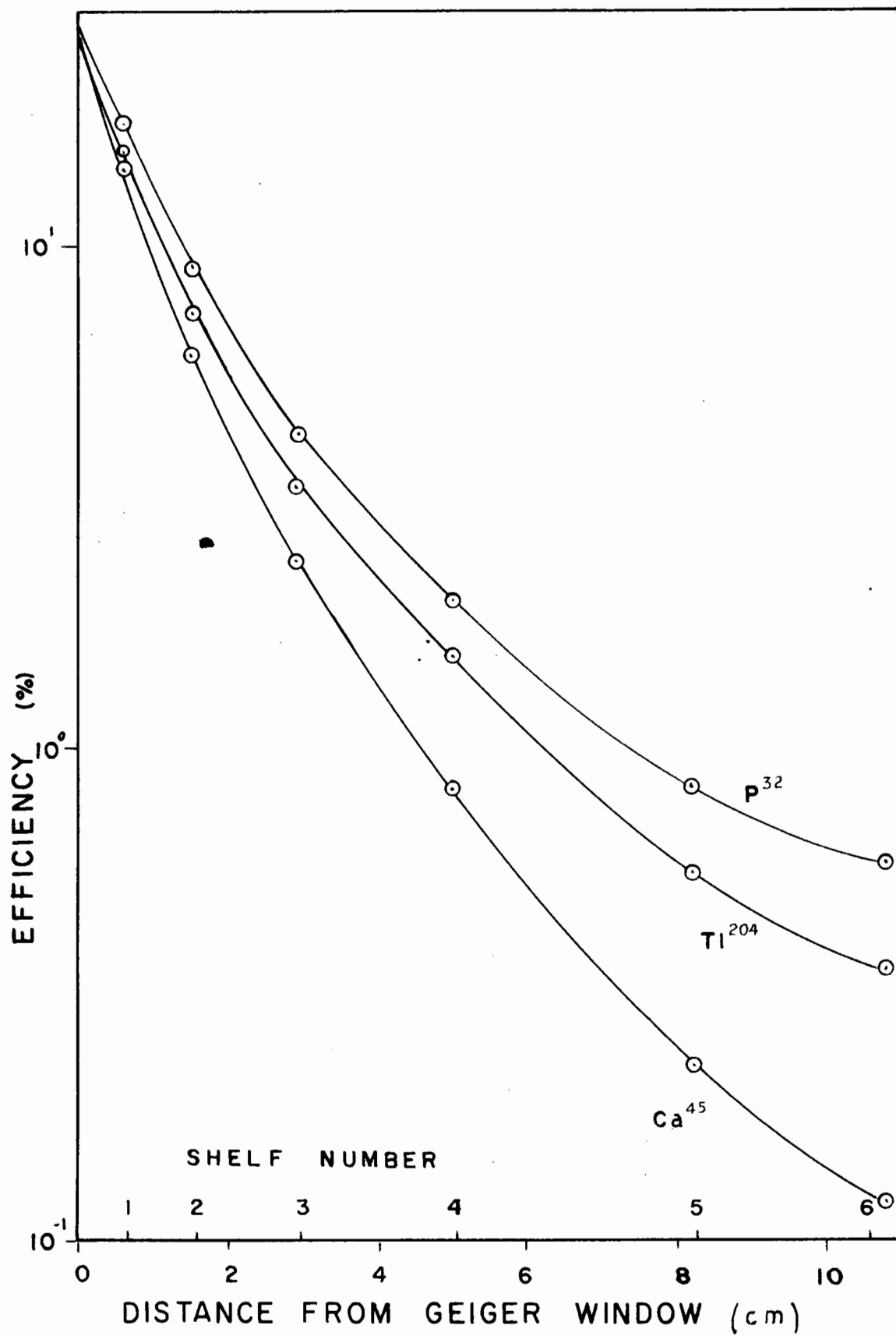Geiger Window for Ca^{45}, Tl^{204} and P^{32}

FIG.13

Figure 14

Efficiency of Geiger Versus $E_{max.}$ of Negatron
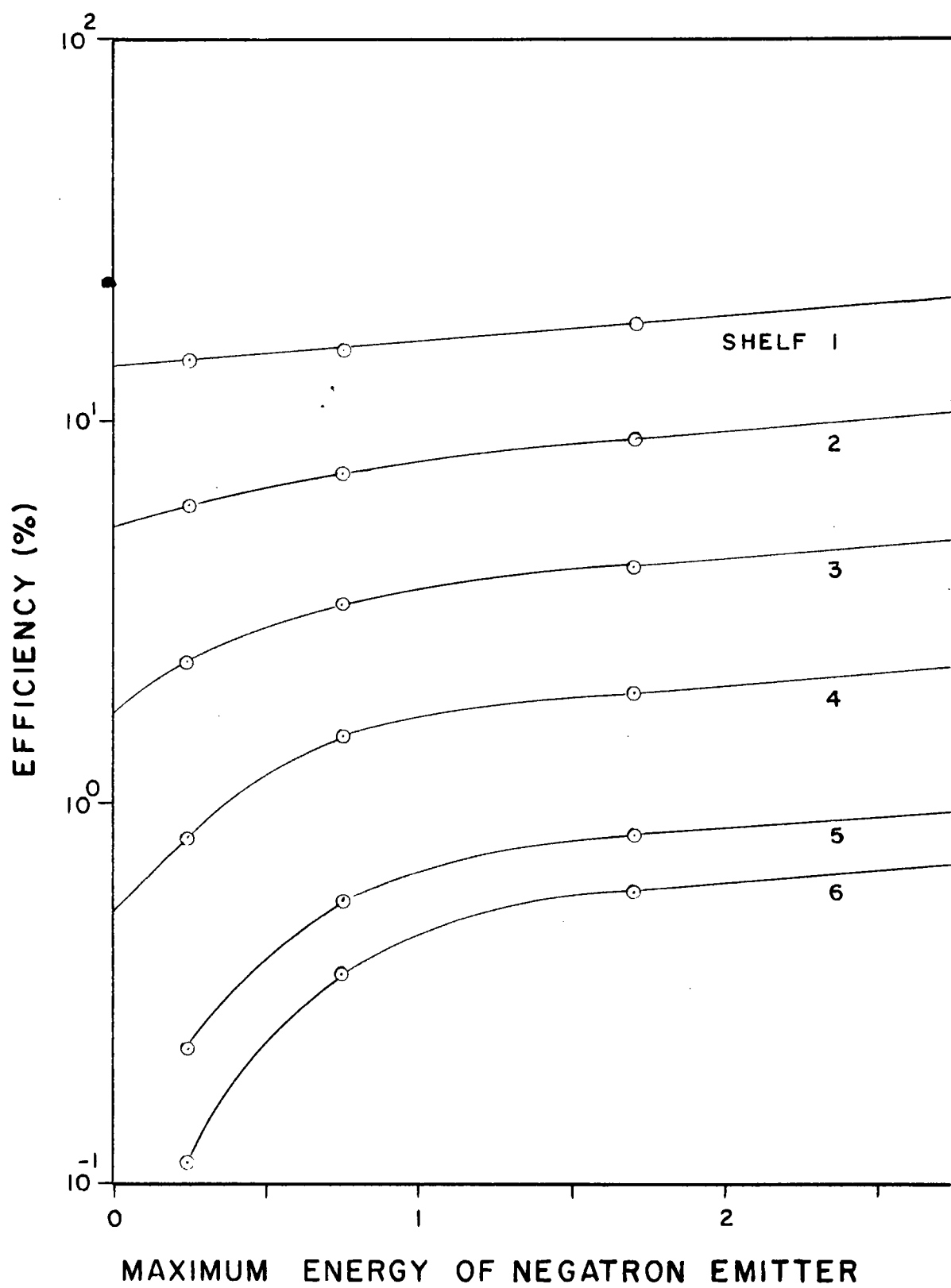Emitter for Each Shelf Position

FIG.14

2.   The Scintillation Spectrometer

After chemical separation, the decay of the gamma
activity of the separated fractions was followed on a single
channel pulse analyser using a NaI crystal (thallium act-
ivated).   The energy carried by the gamma rays caused dis-
turbance in the crystal lattice, the atoms of which emit
flashes of light when they return to their original energy
levels.   NaI is transparent to its own fluorescence, and
the light flashes or scintillations were received by the
photomultiplier tube (Dumont 6292) on which the crystal stood.
The crystal was a right cylinder, 1 1/2" in diameter and 1"
tall.   It stood on a photomultiplier tube, and Dow-Corning
Silicone Oil DC-200 was used to make an optical seal between
the crystal and photomultiplier.   The other surfaces of the
crystal were roughened.   Crystal and photomultiplier were
then sealed in a thin aluminum can, the inside of which
had been coated with MgO in water glass to make the surface
optically reflecting.   The canning was done in a gloved box
in a dry atmosphere because NaI is extremely hygroscopic.

The light pulses from the NaI crystal were detected
by the Dumont photomultiplier, the impressed voltage being
obtained from a Nichols AEP1007B High Voltage Set delivering
3,000 volts.   The pulses then passed from a pre-amplifier
into a single channel pulse analyser[*] where they were amplified

* The single channel pulse analyser was designed by Dr. R.E. Bell
 of the Radiation Laboratory at McGill University.

and sorted. A block diagram of the scintillation spectrometer is shown in Figure 15. The regulated power supply for the pre-amplifier was Model 28 and the regulated power supply for the pulse analyser was Model 32, both manufactured by the Lambda Electronics Corporation. The pulses were fed through a Marconi Scaler, AEP-908, and an N.R.C. Counting Rate Meter, AEP-1902-A. The counting rate was recorded by an Esterline-Angus Graphic Ammeter, Model AW.

The counting rate at which coincidence corrections were no longer negligible was determined by following the decay of the annihilation radiation of a high-activity source of 20.5 min. C^{11}. It was found that using a scanning speed of 1 scan/min., the instrument saturated at counting rates higher than 6×10^4 c/m for a 2% channel, i.e. a total counting rate of 3×10^6 c/m. In all bombardments, sample were placed on a shelf sufficiently far from the crystal so that coincidence losses were negligible.

Drifts in sensitivity of the scintillation spectrometer were checked every few hours by scanning a long-lived standard and normalizing the peak-heights of spallation products to a constant peak height of the standard. Decay curves were then plotted and extrapolated to time of separation or to end of bombardment. To convert the counting rate at zero time to the disintegration rate at zero time the following corrections were applied:

Figure 15

Block Diagram of Scintillation Spectrometer

FIG.15
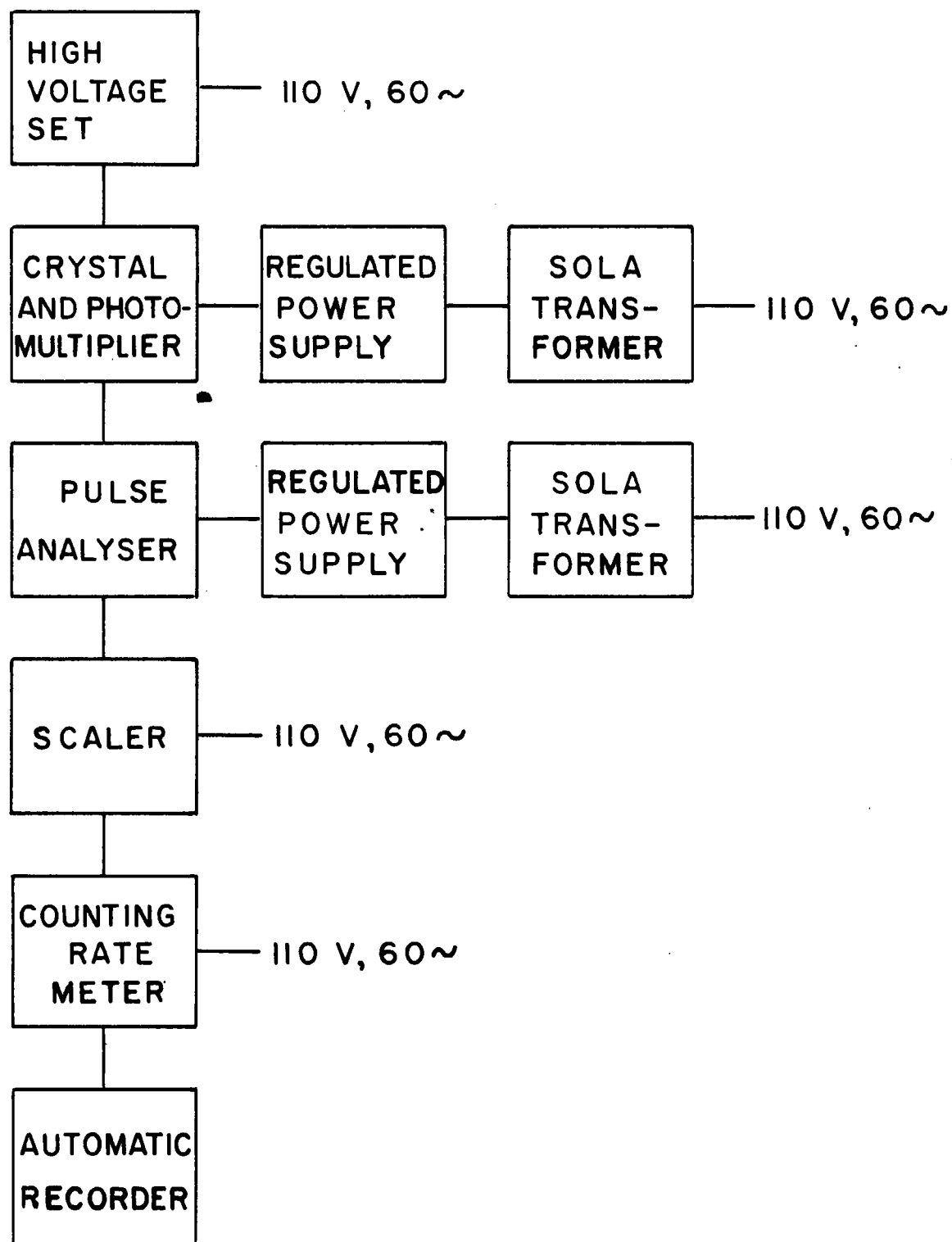
(1) Dilution factor

(2) Chemical yield factor for separations other than ion-exchange (e.g. dimethylglyoxime precipitations of nickel from calcium).

(3) Short-lived activities were counted using a scanning speed of 1 scan/min. Longer lived activities were scanned using 1 scan/30 min. in order to get improved resolution of the peaks in the gamma-ray spectrum. Peak heights in the slower scan were higher, and the experimentally determined ratio was 1.76.

(4) A factor of 2 was applied to the annihilation radiation peak at 0.511 Mev., because 2 quanta are emitted for each event.

(5) The contribution of the Compton peak to the peak of the characteristic gamma-ray was determined at several points on the decay curve. Counting rates were multiplied by the factor

$$\left(\frac{\text{peak height due to characteristic gamma}}{\text{peak height due to Compton plus characteristic gamma}} \right)$$

(6) Peak heights were multiplied by the factor

$$\left(\frac{\text{total area under the peak}}{\text{area inside a 2\% channel}} \right).$$

Consider a 0.51 Mev. peak in a scan of total energy range 3 Mev. Then the 0.51 Mev. peak occurs at $\frac{0.51}{3} \times 100 =$ 17% of full scale. If the % resolution at that date for 0.51 Mev. is 10%, then the half width (i.e. full width at

half height) is 17% x 10% = 2% of full scale. The equation
for the standard Gaussian* is

$$\phi(t) = \frac{1}{\sqrt{2\pi}} \ e^{-t^2/2}$$

Figure 16 is a graph of $\phi(t)$ versus t. Given a Gaussian
of any scale of drawing, mark in the half width of 1.7%.
The channel width of the pulse analyser was set at all
times at 2% of full scale. On the Gaussian, mark off an
area corresponding to 2%. From the graph, calculate the
ratio $\left(\dfrac{\text{total area under the peak}}{\text{area inside a 2\% channel}}\right)$.

(7) Pulse areas were divided by the overall efficiency
for producing a full energy pulse in the crystal = (a) x (b) x
(c)

where   (a) is the experimentally determined shelf factor.
The shelf factors were determined experimentally
by measuring the relative peak heights of a
Na^{22} standard source placed on the different
shelves.

           (b) is the total intrinsic efficiency, excluding
geometry. Values for the total intrinsic
efficiency were taken from Figure 19 in
Chapter V of Siegbahn "Beta - and Gamma-Ray
Spectroscopy". The efficiency values as

*   see, for example, Richardson C.H., "An Introduction to
Statistical Analysis" Harcourt Brace and Co., N.Y.(1944).

<u>Figure 16</u>

Illustration of Method of Calculating
Correction (6)

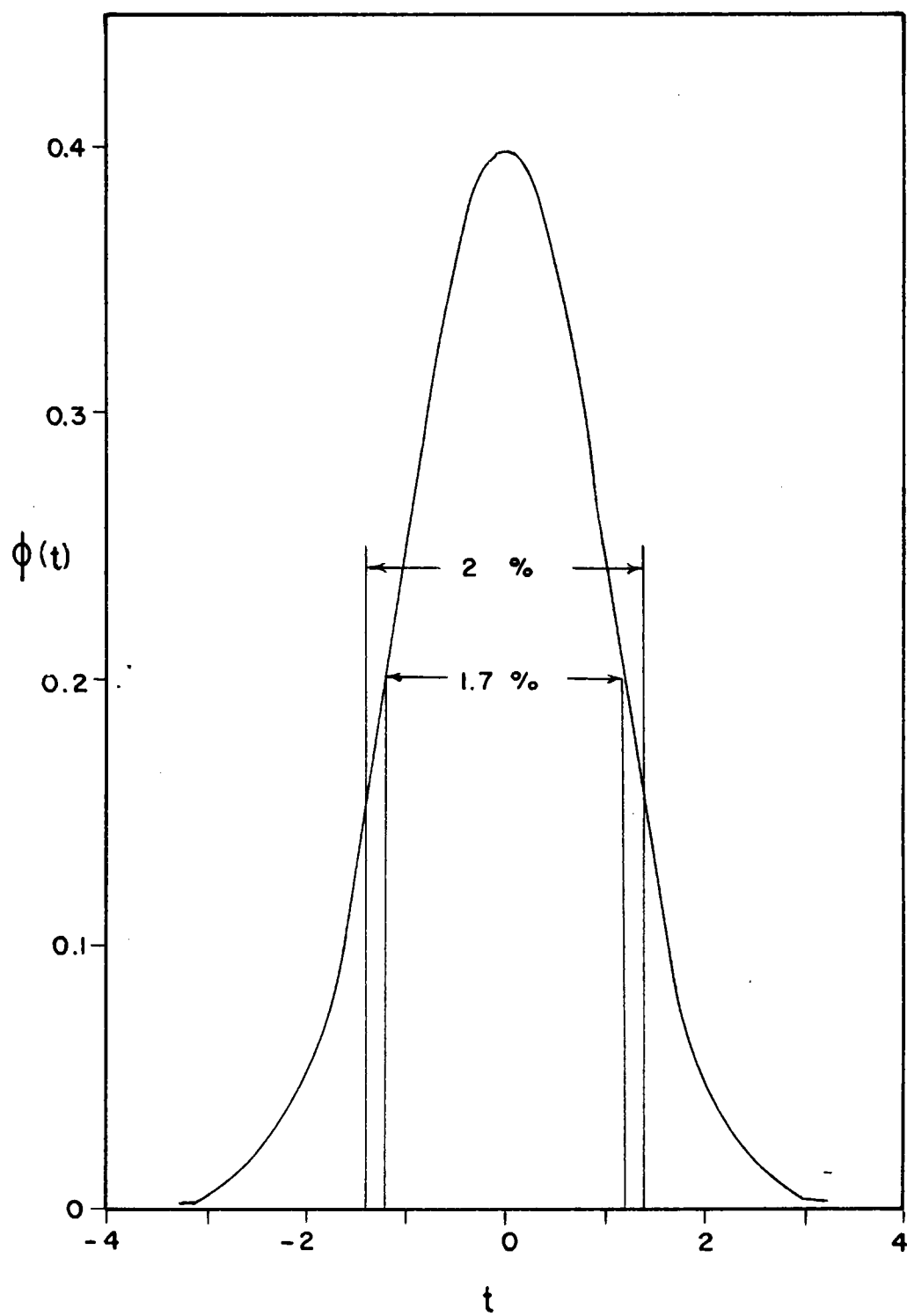Total Area Under the Peak $\div$ Area Inside a 2% Channel

FIG.16

published in Siegbahn were calculated from
the efficiency for Compton, photo-electric
and pair-production processes for a NaI(Tl)
crystal in the shape of a right cylinder
1 1/2" in diameter by 1" high. These values
do not take account of the variation of
efficiency with gamma energy.

(c)   is the ratio of pulses of maximum size (peak)
to all pulses produced for a 1 1/2" diameter, 1"
high crystal. The values used for this correction
factor were taken from Figure 6 in Chapter V of
Siegbahn "Beta - and Gamma-Ray Spectroscopy"(214).

III   RESULTS

Each radioactive nuclide measured was identified by chemical isolation, by half-life exhibited in beta or gamma counters or in both, and by gamma energies and gamma abundances.

Figures 17 to 19 are sample decay curves of the monitors.   Figure 17, the decay of the boron monitor irradiated at 42 Mev., shows the decay of the 0.51 Mev. annihilation gamma of the total sample before chemical separation.   Subtraction of the background activity of 36 hour Ni^{57} gives a 20.5 minute line used to calculate the yield of C^{11} in the $B^{11}(p,n)C^{11}$ monitoring reaction.

Figure 18 is the decay curve of the boron monitor irradiated with 55 Mev. protons.   The decay curve shown is that of the 0.51 Mev. annihilation gamma of the total sample before chemical separation.   Subtraction of 2.6 hour Mn^{56} leaves a composite curve (indicated by the triangles in Figure 18).   This curve was resolved into 20.5 min. C^{11} and 8.9 min. Fe^{53} by a combined graphical and analytical method used by several authors, e.g. Biller (62) and Kofstad (55).   The total observed activity of the sample may be written

$$\sum A = C_1 A_1^{\,0} e^{-\lambda_1 t} + C_2 A_2^{\,0} e^{-\lambda_2 t} \qquad \ldots (12)$$

where $A_1^{\,0}$ and $A_2^{\,0}$ are the disintegration rates at zero time, λ_1 and λ_2 are the decay constants, and C_1 and C_2 are the

Figure 17

Decay of Boron Monitor Irradiated at
42 Mev.

⊙	experimental points
—	36 hour Ni^{57}
---	20.5 minute C^{11}
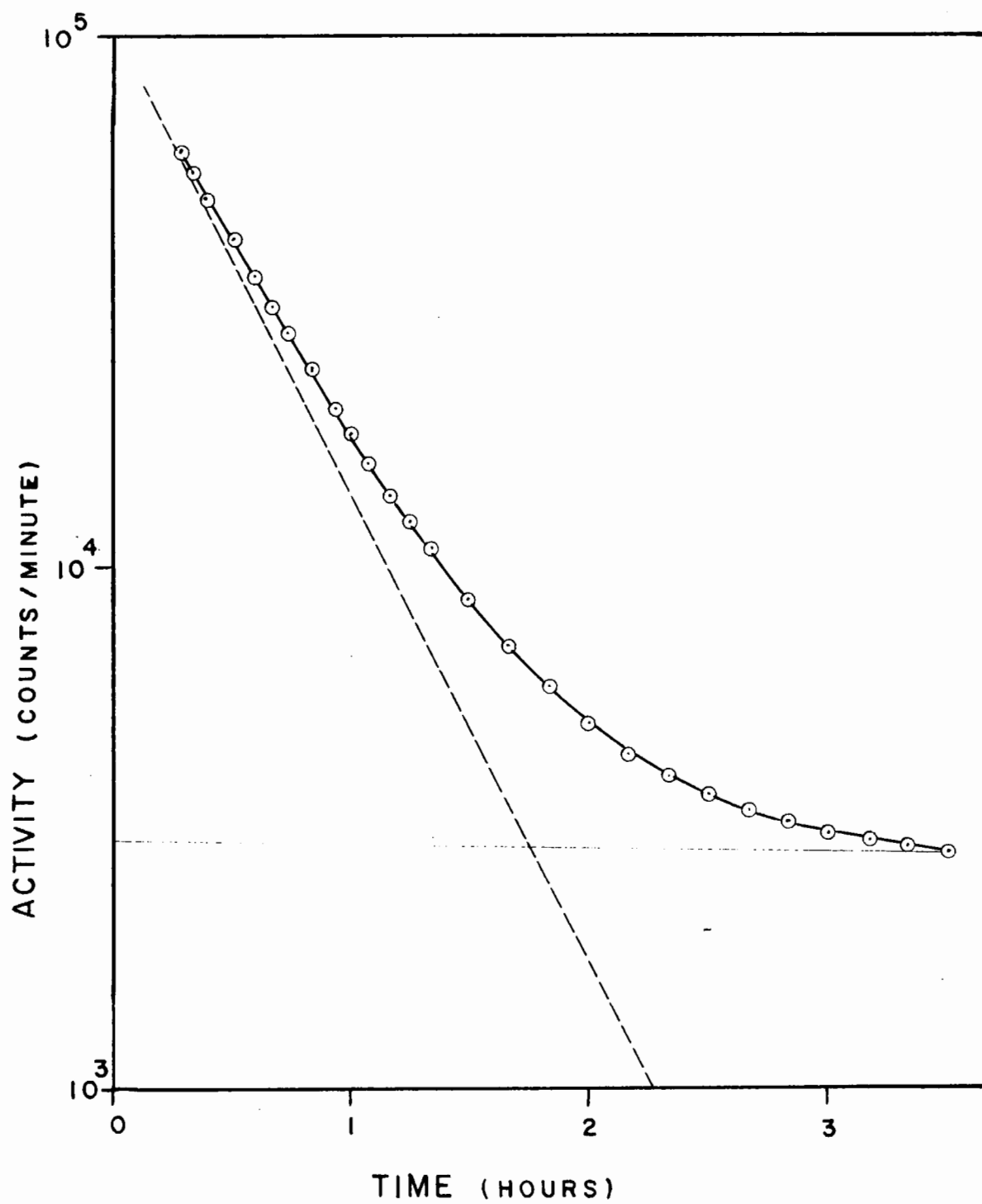
FIG.17

Figure 18

Decay of Boron Monitor Irradiated at
55 Mev.

⊙	Experimental Points
—	2.6 hour Mn^{56}
△	⊙ less 2.6 hour Mn^{56}
- - - -	20.5 minute C^{11}
— - — -	. 8.9 minute Fe^{53}
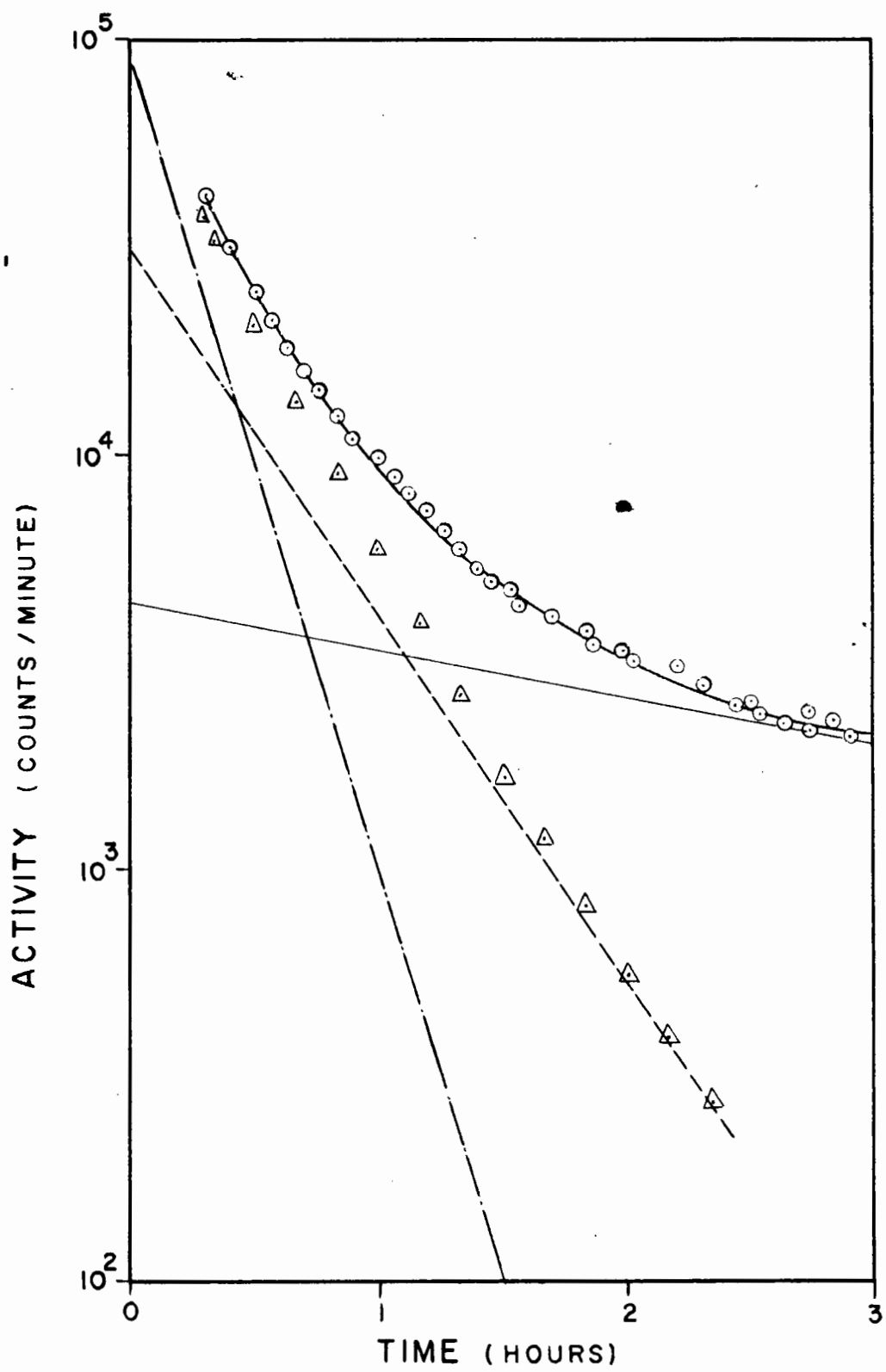
FIG.18

Figure 19

Decay of Aluminum Monitor Irradiated at
60 Mev.

⊙   Experimental decay curve of the

        magnetically separated alumina.

△   Experimental decay curve of the

        magnetically separted cobalt

        normalized to eventually coincide
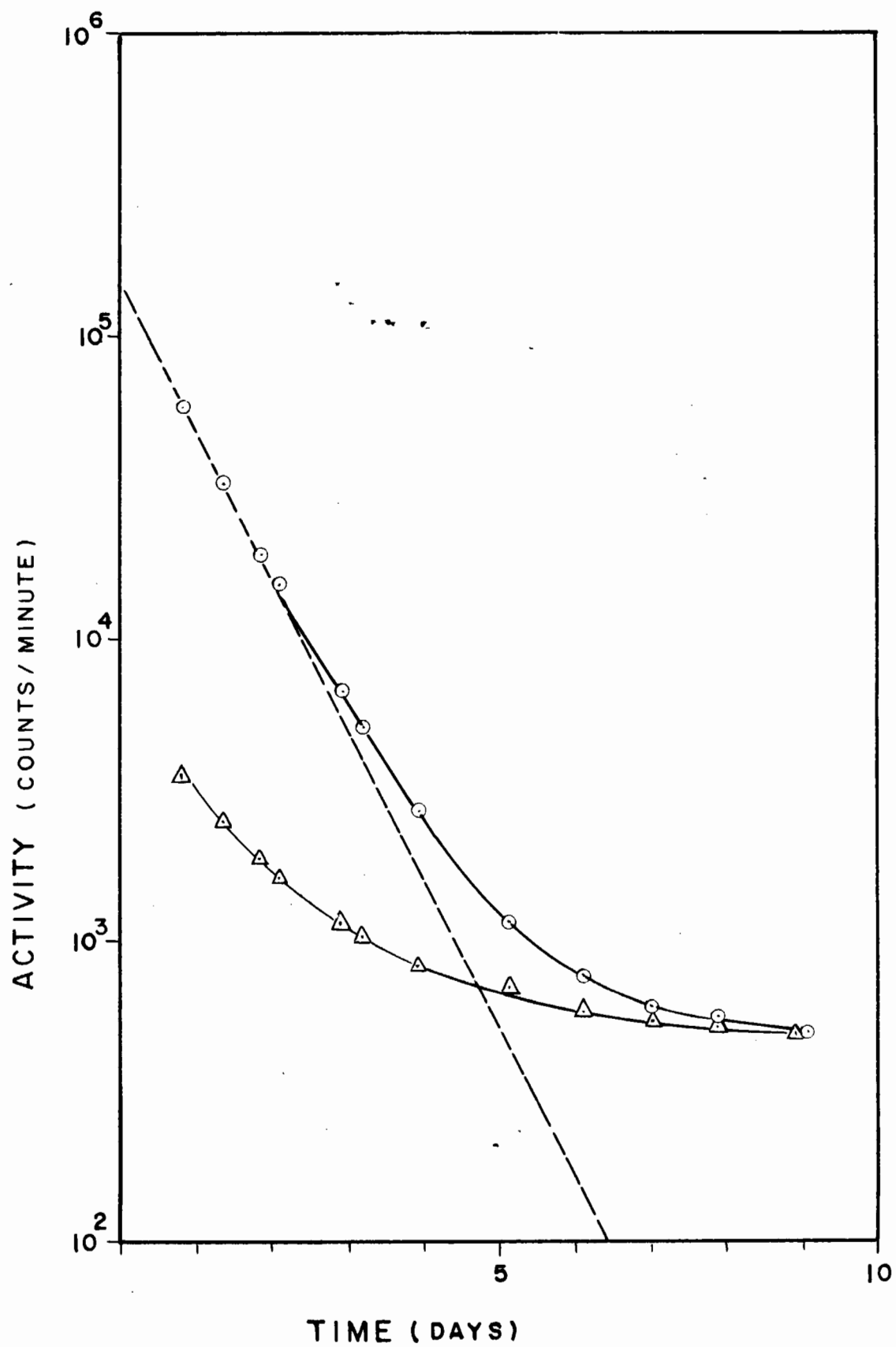
        with the cobalt curve.

----   15 hour Na^{24}.

FIG.19

decay constants, and C_1 and C_2 are the counting efficiencies. Multiplying by $e^{+\lambda_2 t}$ gives

$$e^{\lambda_2 t} \sum A = C_1 A_1^{\,o} e^{+(\lambda_2 - \lambda_1)t} + C_2 A_2^{\,o} \qquad \ldots (13)$$

The graph of $e^{\lambda_2 t}$ versus $e^{(\lambda_2 - \lambda_1)t}$ will be a straight line with intercept on the $e^{\lambda_2 t} \sum A$ axis of $C_2 A_2^{\,o}$ and slope $C_1 A_1^{\,o}$. The success of this method depends upon the accuracy of the values of the half-lives, which in the case of C^{11} and Fe^{53} are well established.

Figure 19 is the decay curve of the beta activity of the Na^{24} formed in the aluminum monitor by irradiation with 60 Mev. protons. A test irradiation to check the efficiency of the magnetic separation of cobalt from alumina showed that 0.1% of the alumina remained in the magnetic fraction, but that 7.2% of the irradiated cobalt remained in the non-magnetic fraction. Figure 19 shows how the separated magnetic fraction contains no 15 hour Na^{24}. The shortest half-life present is 36 hour Ni^{57}. In order to substract the decay curve of the magnetic fraction from the decay curve of the non-magnetic fraction it was necessary to dissolve the magnetic fraction in nitric acid, dilute to a known volume and reserve a small aliquot for counting together with the non-magnetic fraction (Na^{24} monitor). The decay curve of the magnetic fraction was normalized so as to coincide at infinite time with the decay curve of the non-magnetic fraction. The

counting rate of the magnetic fraction was not itself of interest at this point. Subtraction (see Figure 19) gave a 15 hour line which was used to calculate the yield of the Na^{24} monitor.

Figure 20 shows the decay of the 0.50 ± 0.02 Mev. γ in the nickel fraction. The decay curve is resolved into 6.4 day Ni^{56} (0.48 Mev. gamma) and 36 hour Ni^{57} (0.51 Mev. annihilation radiation). Search for the unreported nuclides Ni^{55} and Ni^{54} corroborated the work of Fink (88) in that both nuclides must be short-lived. From (1) a comparison with other nickel isotopes (2) an estimate of the total decay energy available and (3) a consideration of shell structure, Fink estimated the half-lives of Ni^{55} and Ni^{54} as being of the order of minutes or less. Experimentally, Fink reported that the half-lives of the two unreported nuclides were shorter than 5 minutes. In the work reported in this thesis no new activity was observed in the nickel fraction at any time. Table XIV shows that a search for Ni^{54} should be most profitable at a proton energy of 78 Mev. The Table was constructed by assuming 52 Mev. - 39 Mev. = 13 Mev. increase in proton energy for each neutron emitted. In Irradiation 25 a cobalt target was bombarded for 15 minutes with 78 Mev. protons and a rapid separation carried our for nickel. Both the beta and gamma decay of the separated nickel were followed within one hour after the end of

Figure 20

Sample Decay Curve of the $0.50 \pm .02$ Mev. Gamma
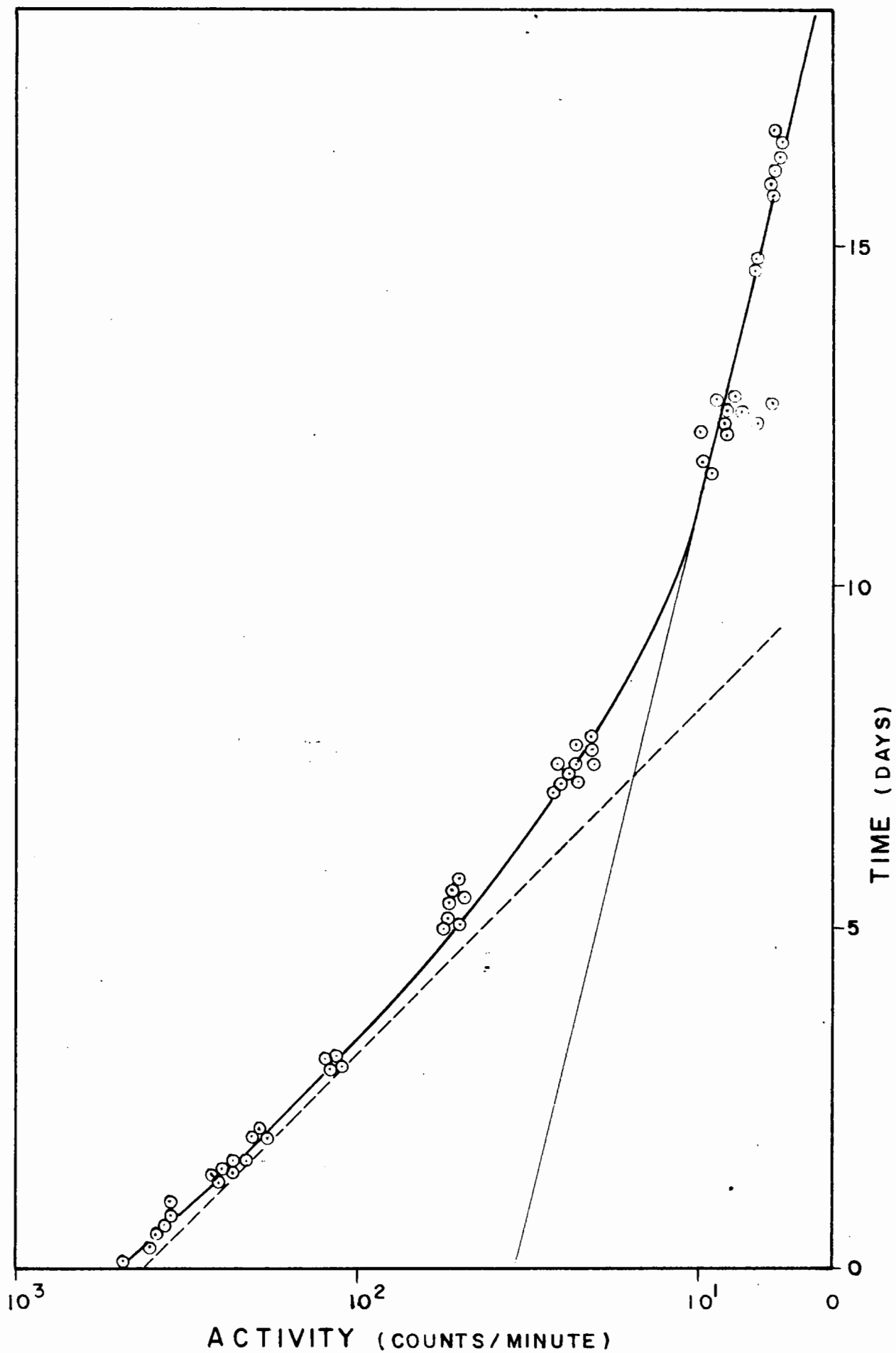in the Nickel Fraction

—— 6.4 day Ni^{56}

--- 36 hour Ni^{57}

ACTIVITY (COUNTS/MINUTE)

TIME (DAYS)

FIG.20

Table XIV

Proton Energy for Maximum Yield of
Nickel Isotopes

Reaction	Proton Energy (Mev.)
$Co^{59}(p,3n)Ni^{57}$	39 experimentally observed
$Co^{59}(p,4n)Ni^{56}$	52 experimentally observed
$Co^{59}(p,5n)Ni^{55}$	65?
$Co^{59}(p,6n)Ni^{54}$	78?

bombardment. One hour after bombardment the counting rate
of 36 hour Ni^{57} was 15,000 counts per minute. No shorter
activity was observed. We conclude that the half-lives of
Ni^{55} and Ni^{54} are both shorter than about 5 minutes.

Figure 21 shows a typical decay curve of the
0.81 Mev. gamma in the cobalt fraction bombarded at energies
in the 30 Mev. range. The circles indicate the scatter of
the experimental points. The shape of the curve is caused
by the growth of a long-lived daughter from the decay of a
9 hour parent which is itself not counted by the instrument.
9 hour Co^{58m} decays by isomeric transition to 72 day Co^{58}
which decays by position emission followed by a 0.805 Mev.
gamma ray. Extrapolation of curve A to end of bombardment
enables us to draw B where B = Co^{58} formed by direct yield

<u>Figure 21</u>

Sample Decay Curve of the 0.81 Mev. Gamma
<u>in the Cobalt Fraction</u>

A = experimental points = Co^{58} direct yield

plus Co^{58} formed by decay of Co^{58m}.

B = Co^{58} direct yield

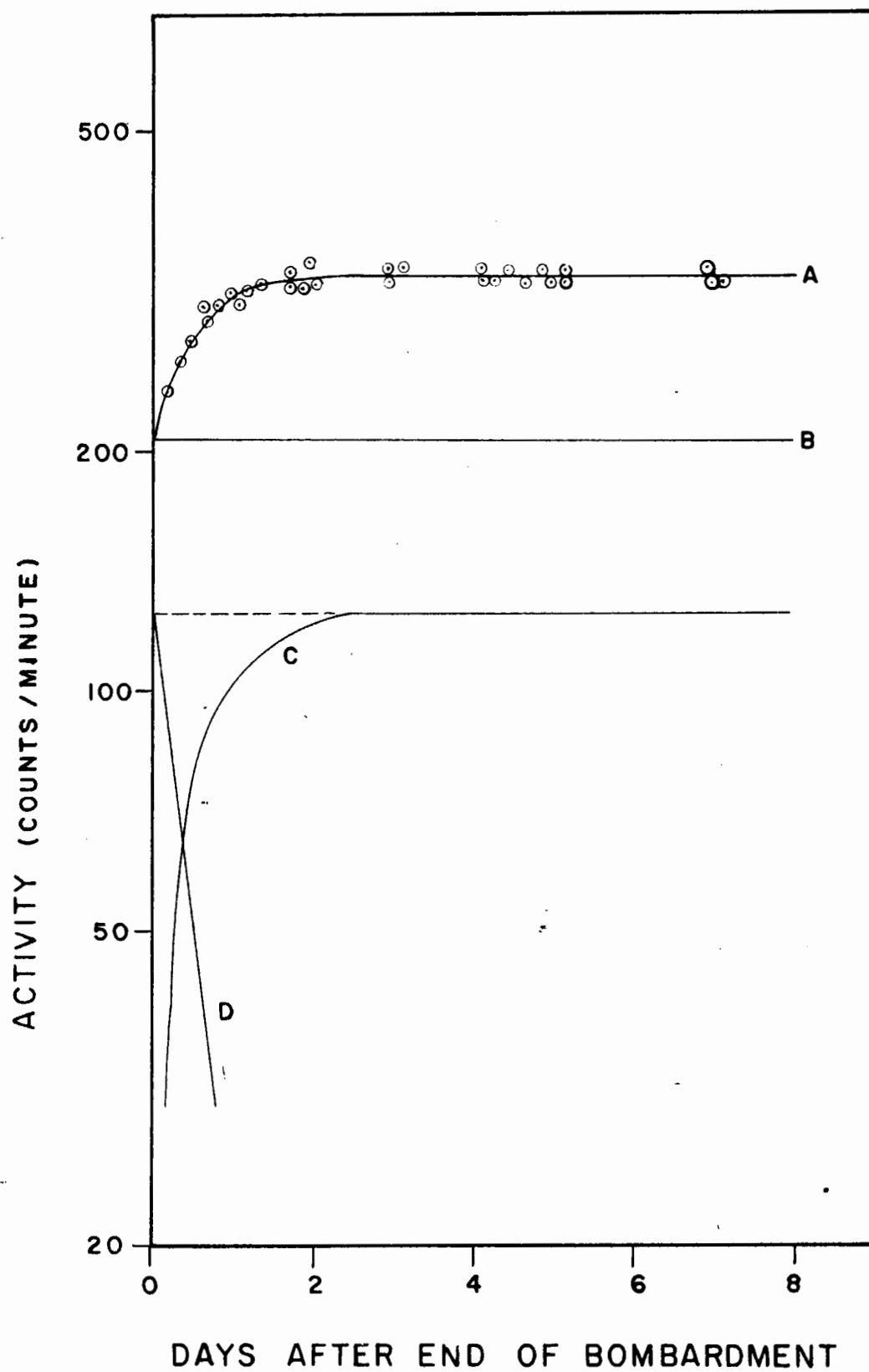C = growth of Co^{58} formed by decay of

Co^{58m} = A − B

D = decay of Co^{58m}

FIG.21

(see Figure 21). Curve C is obtained by the subtraction
of B from A. Curve D, the decay of Co^{58m} is obtained by
subtracting values on the curve C from the maximum value of
C. The fact that D emerges as a straight line with a 9
hour half-life is a check on the accuracy of placement of
curves A,B and C.

Figures 22 and 23 are sample decay curves used to
calculate the yields of Co^{56} and Co^{55} respectively. The
large scatter in Figure 23 is due to the low counting rate
obtained for long-lived Co^{56}.

Figures 24 to 28 are self-explanatory. Figures
29 and 30 show the decay of the scandium activity. Figure
30 shows the first 10 hours of Figure 29 in greater detail.

Figure 31 is the decay curve of the calcium fraction.
The uncertainties are very large because of the low counting
rate. An 8 day line has been drawn through the points follow-
ing Belmont (193) who showed that a composite decay of Ca^{47}
in equilibrium with its daughter Sc^{47} exhibits an 8 day live.

In three irradiations, numbers 29, 30 and 31, pot-
assium was separated from the target. In each case the
potassium decay curve (e.g. Figure 32) showed the presence
of an activity with a half-life of approximately 16 days.
The experimental results are summarized in Table XV.

Figure 22

Sample Decay Curve of the 1.24 Mev.
Gamma in the Cobalt Fraction Used to
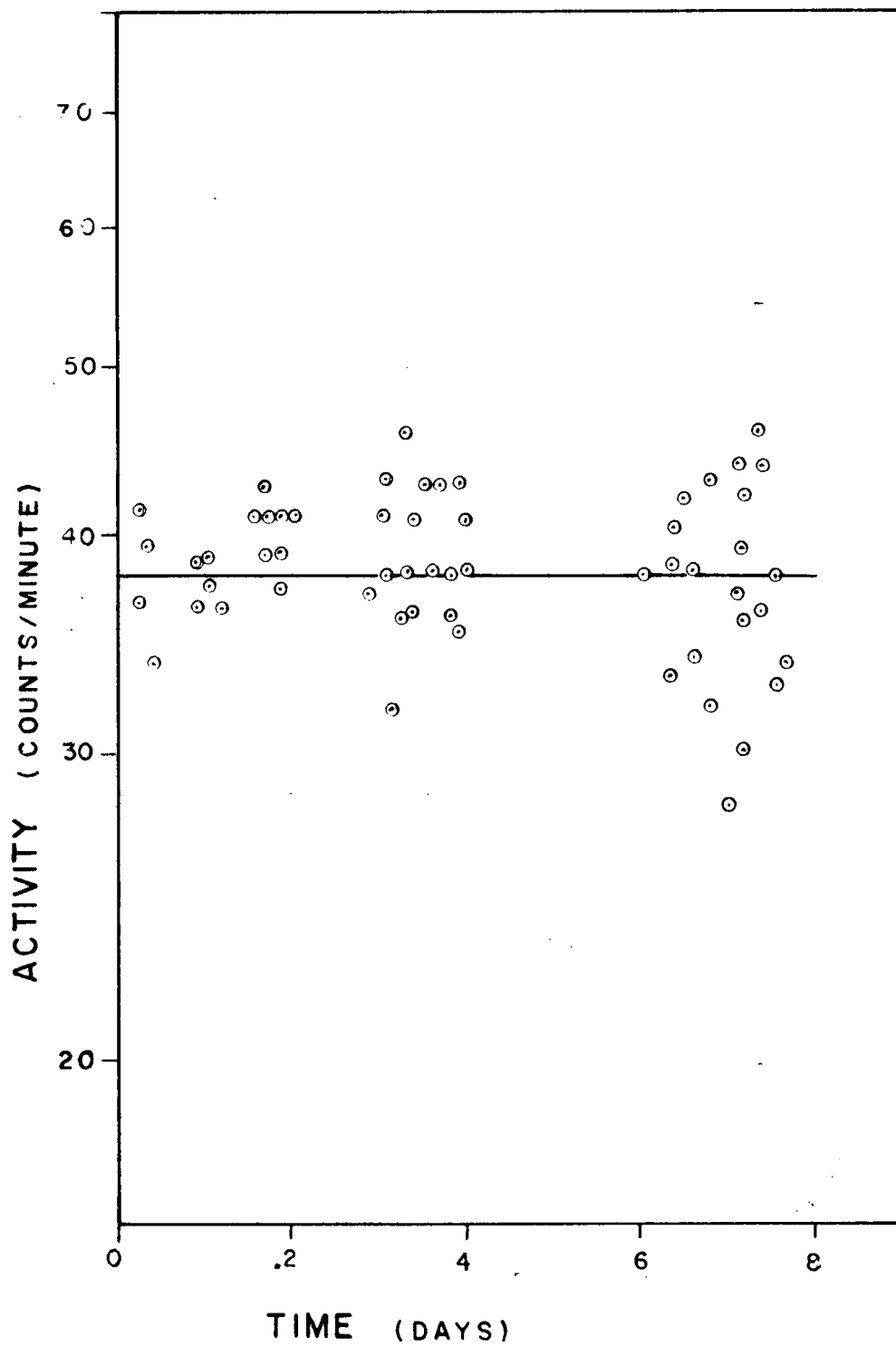Calculate the Yield of Co^{56}.

FIG. 22

Figure 23

Sample Decay Curve of the 0.51 Mev. Annihilation Radiation of the Cobalt Fraction Used to Calculate the Yield of Co^{55}.

——— long-lived $Co^{58,56}$

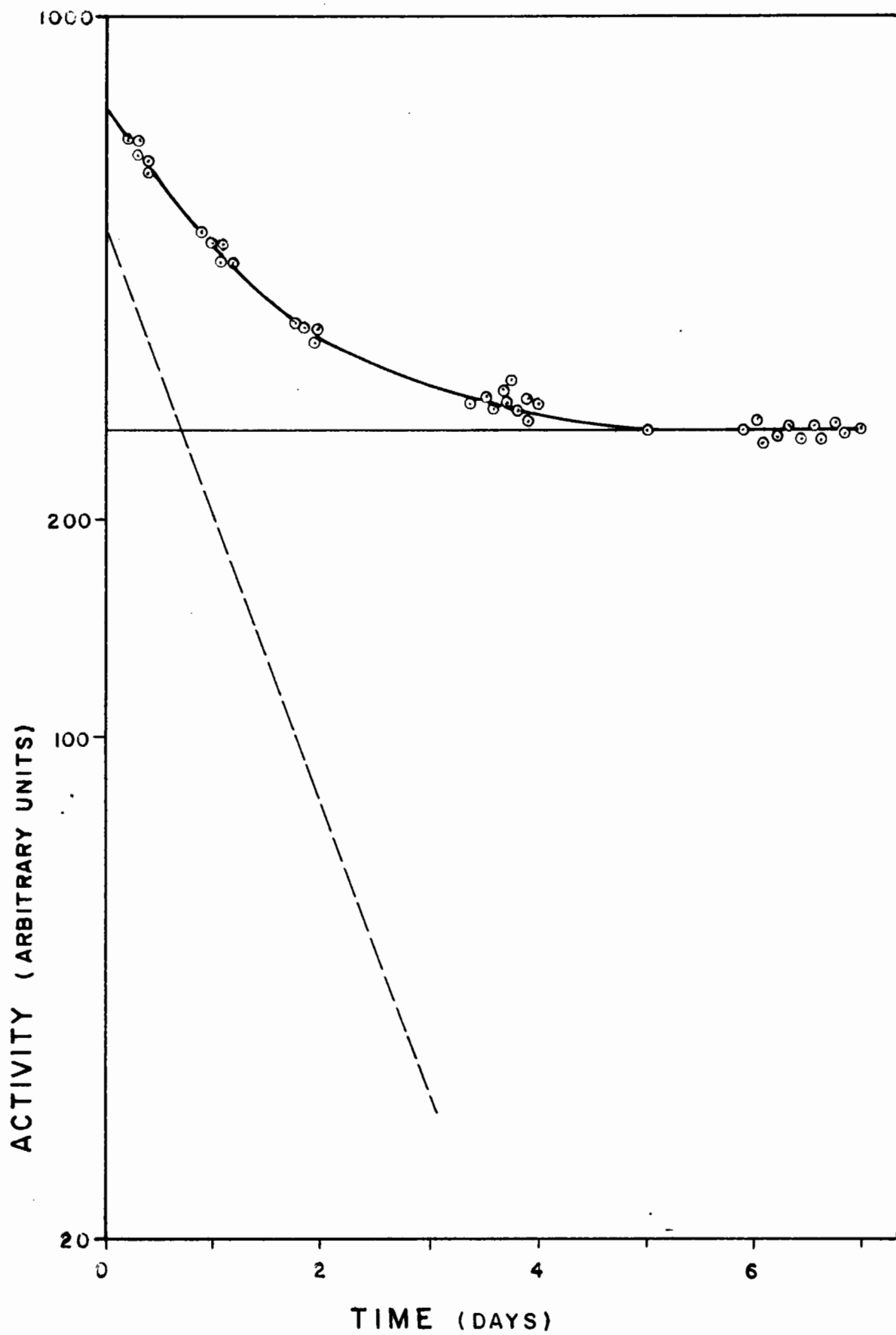- - - 18 hour Co^{55}

FIG.23

Figure 24

Sample Decay Curve of the Beta Activity
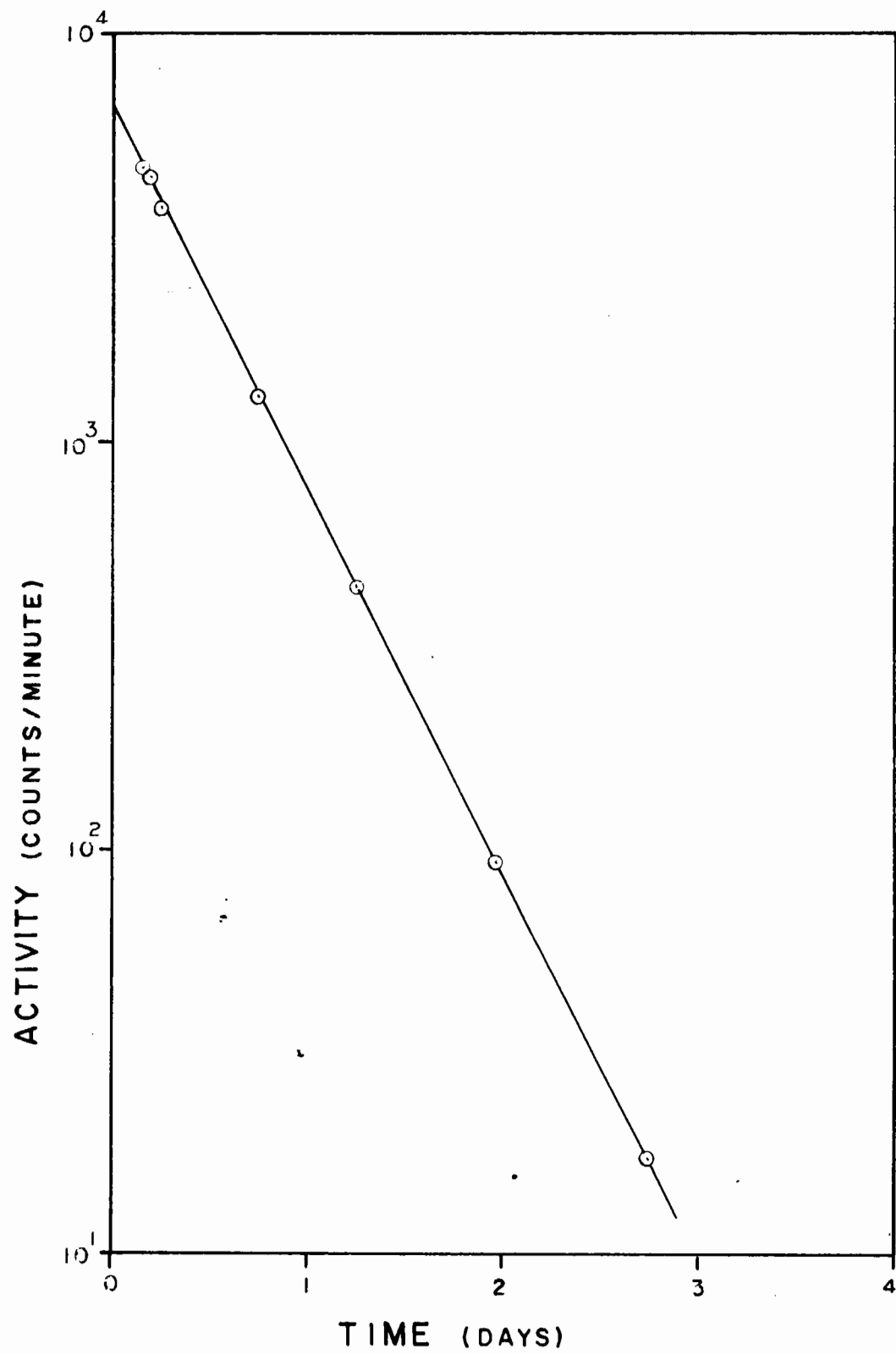in the Iron Fraction used to Calculate
the Yield of 7.8 hour Fe^{52}.

FIG.24

Figure 25

Sample Decay Curve of the 0.84 Mev. Gamma
in the Manganese Fraction Used to Calculate
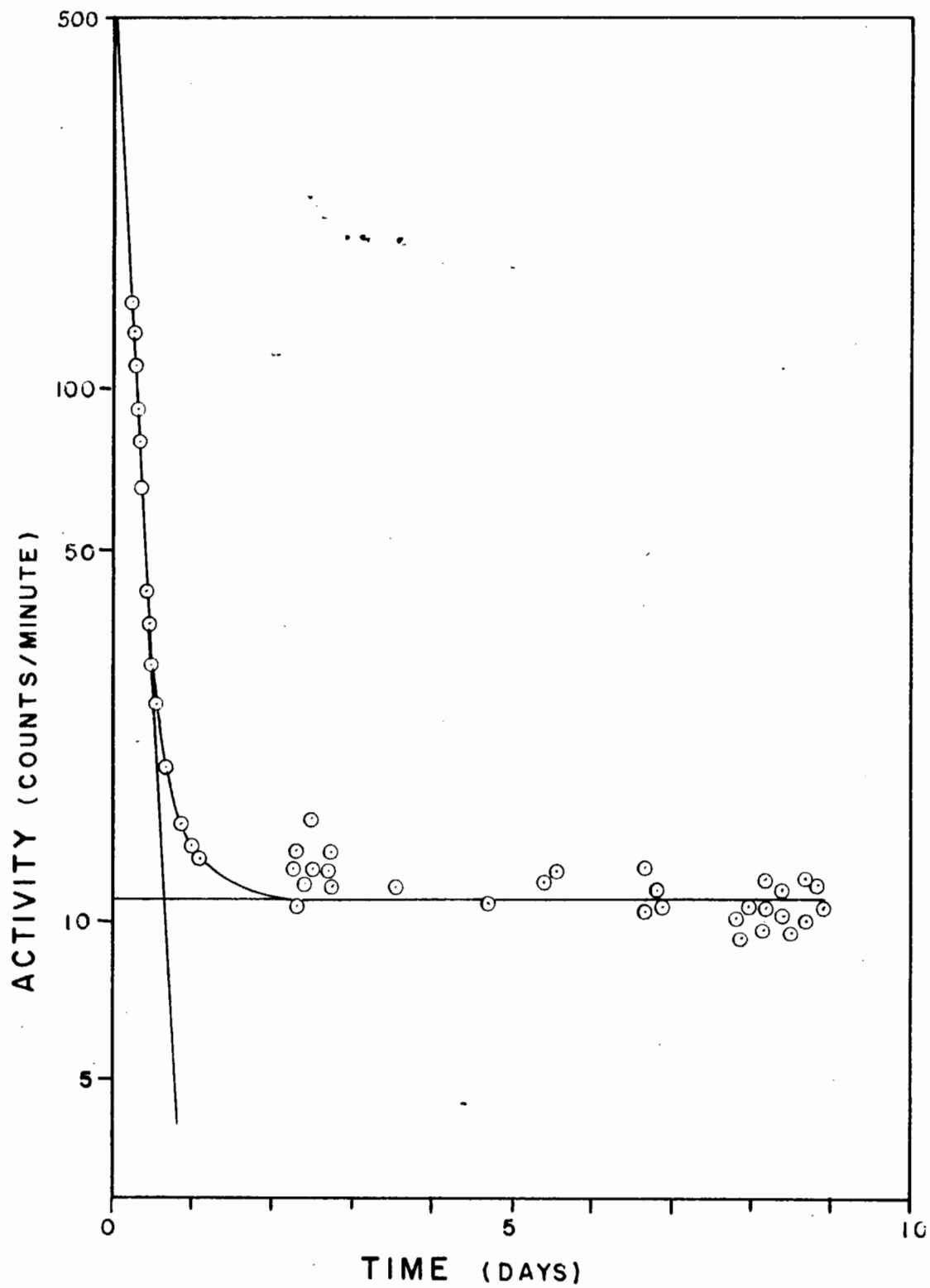the Yield of 291 day Mn^{54}. The Short-Lived
Activity is 2.58 hour Mn^{56}.

FIG.25

Figure 26

Sample Decay Curve of the 0.51 Mev. Annihil-
ation Radiation of the Manganese Fraction
Used to Calculate the Yield of Mn^{52}.   The
Decay Curve is Resolved into 5.7 day Mn^{52}
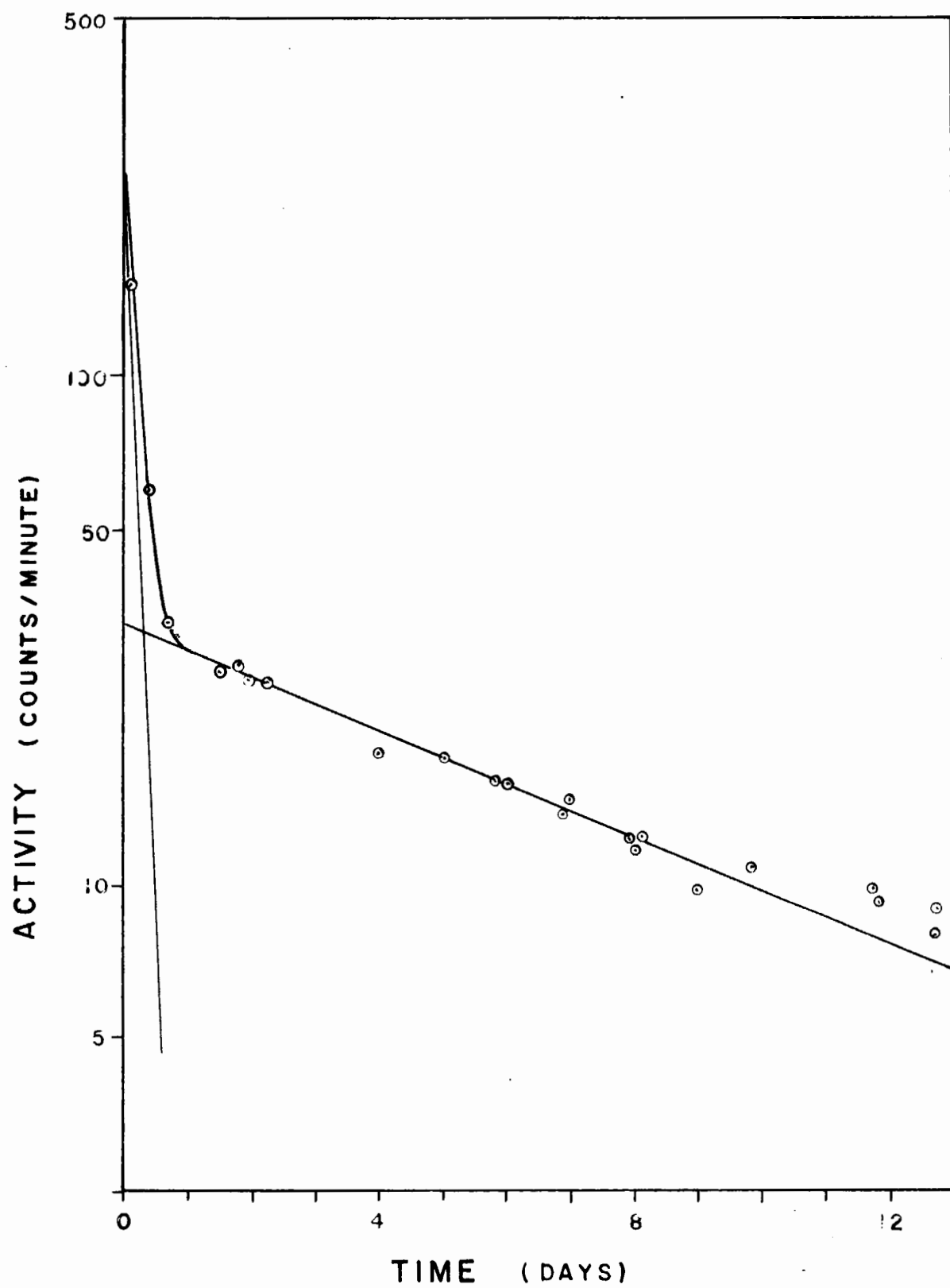and 2.58 hour Mn^{56}.

FIG.26

Figure 27

Sample Decay Curve of the Beta Radiation in
the Manganese Fraction after the Substraction
of 5.7 day Mn^{52}. The Curve is Resolved into
2.58 hour Mn^{56} and 21 minute Mn^{52m}.
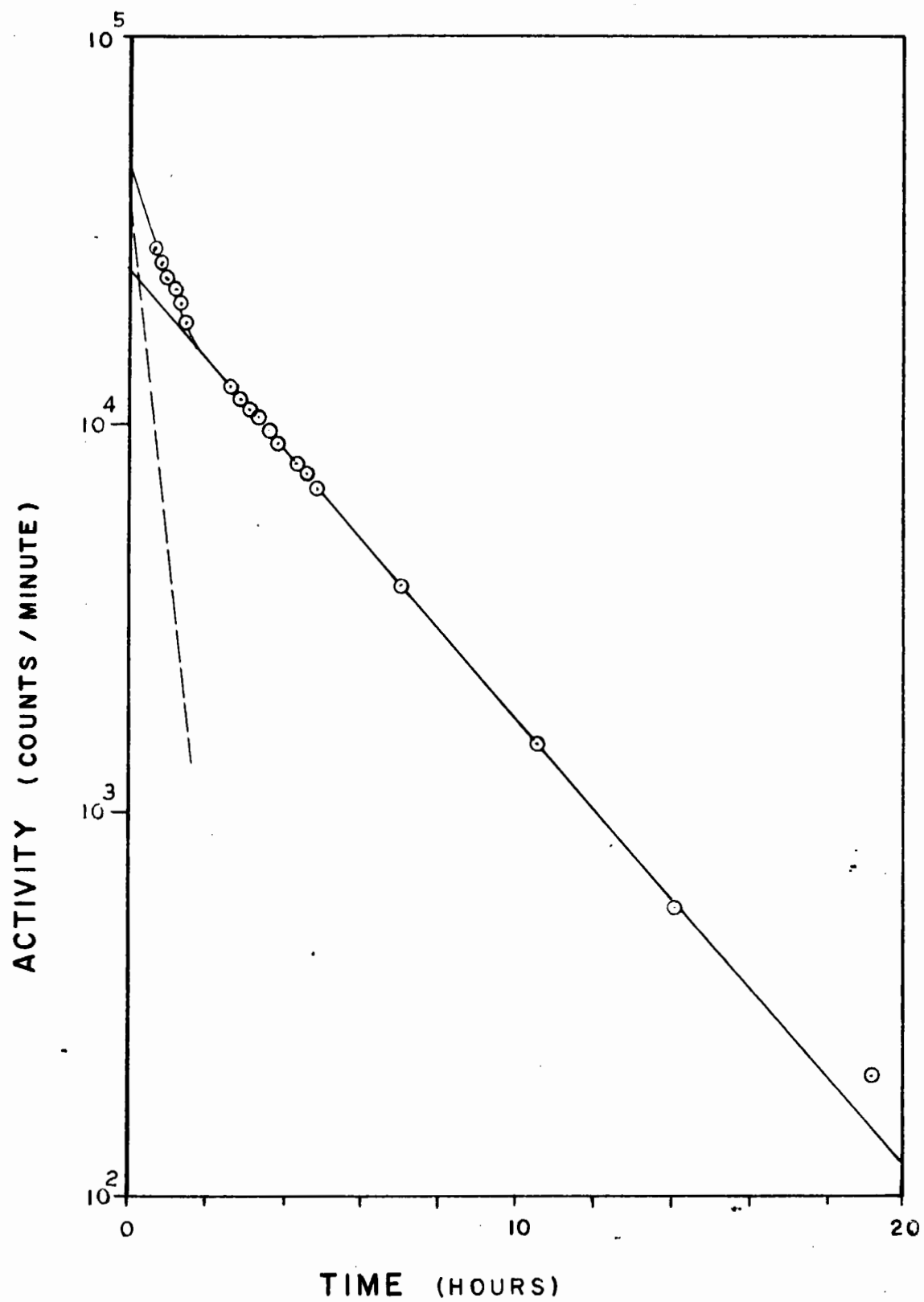
FIG.27

Figure 28

Sample Decay Curve of the Beta Activity
of the Chromium Fraction Showing 42
Minute Cr^{49} and 27 day Cr^{51}.
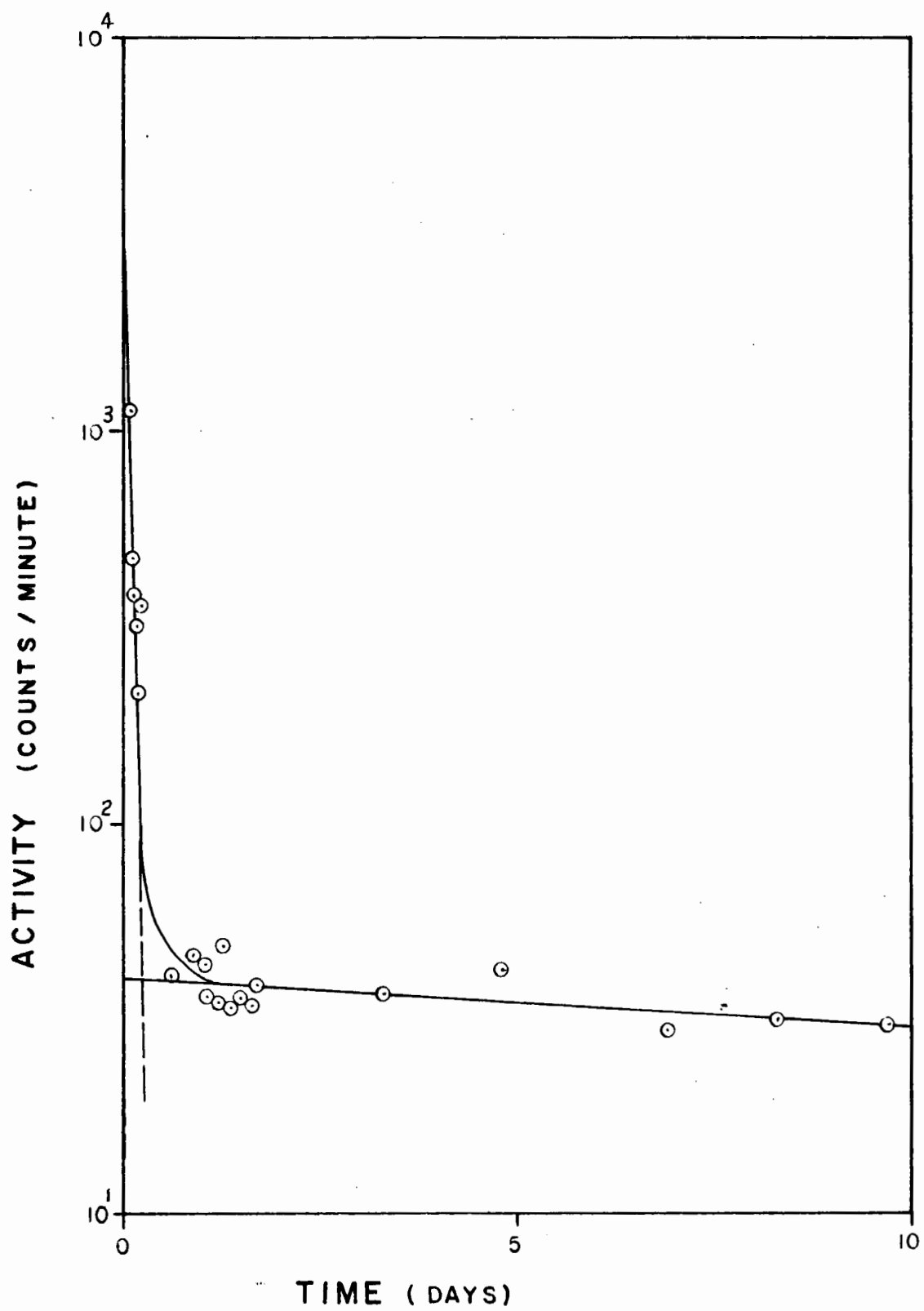
FIG.28

Figure 29

Sample Decay Curve of the Beta Activity
of the Scandium Fraction Used to Calculate
the Yield of 85 day Sc^{46}. Substraction of
Sc^{46} gives a 44 hour line used to calculate
the yield of Sc^{48}. The short-lived act-
ivities are Sc^{43}, Sc^{44} and Sc^{49}.
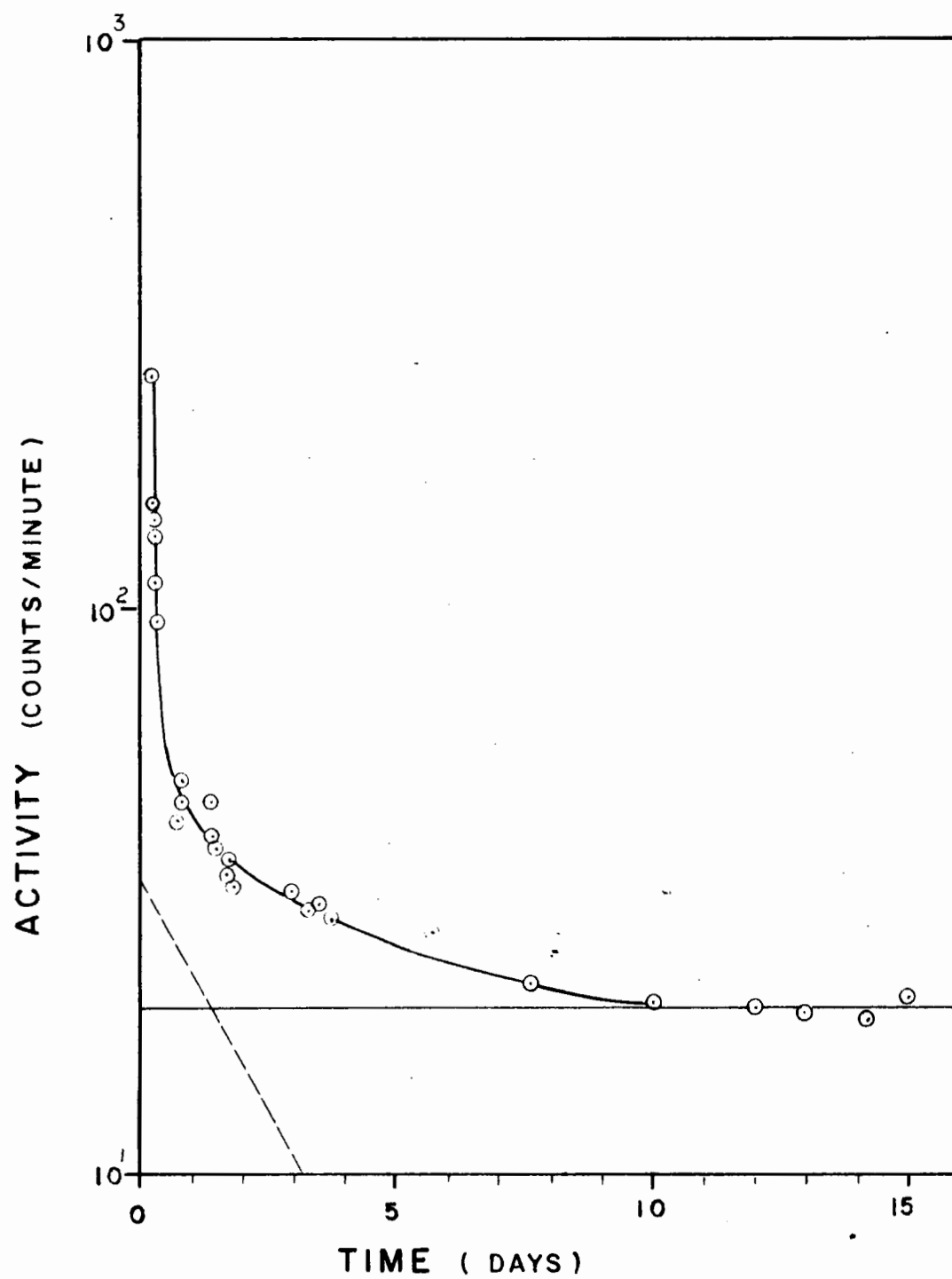
FIG.29

<u>Figure 30</u>

Sample Decay Curve of the Beta Decay of the
Scandium Fraction after Subtraction of the 85
day Sc^{46} and 44 hour Sc^{48}

    ⊙   Experimental Points

    —   4 hour $Sc^{43,44}$

    △   Experimental points less 4 hour
                      $Sc^{43,44}$

    - - - -   57 minute Sc^{49}
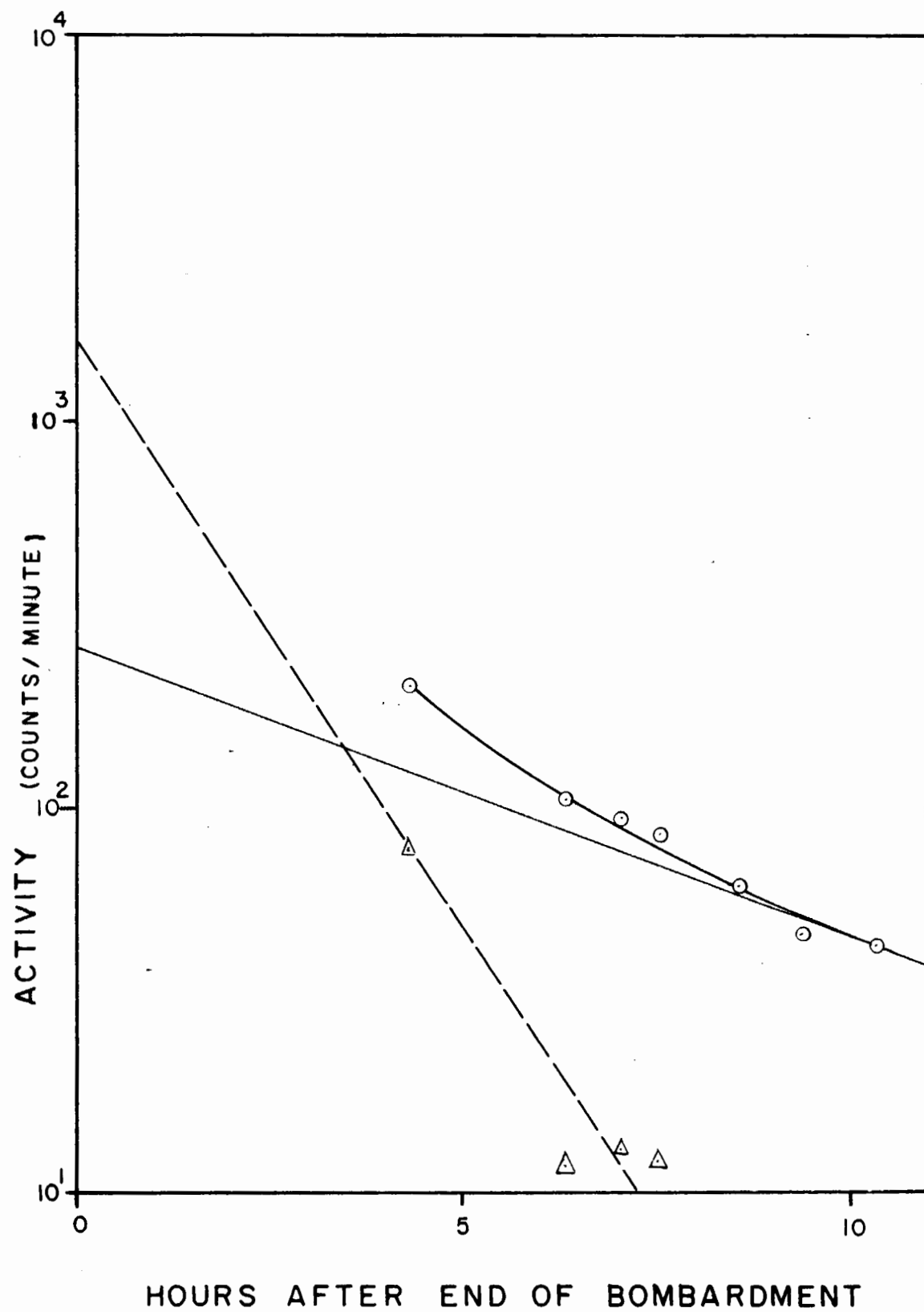
FIG. 30

Figure 31

Sample Decay Curve of the Beta Activity of
the Calcium Fraction Used to Calculate the
Yield of 4.8 day $Ca^{47} \rightarrow$ 3.43 day Sc^{47}.

FIG. 31

<u>Figure 32</u>

Sample Decay Curve of the Beta Activity of
the Potassium Fraction in Irradiation 30
Showing the Presence of a 19 ± 5 day Activity
as Well as 22 Hour K^{43}.
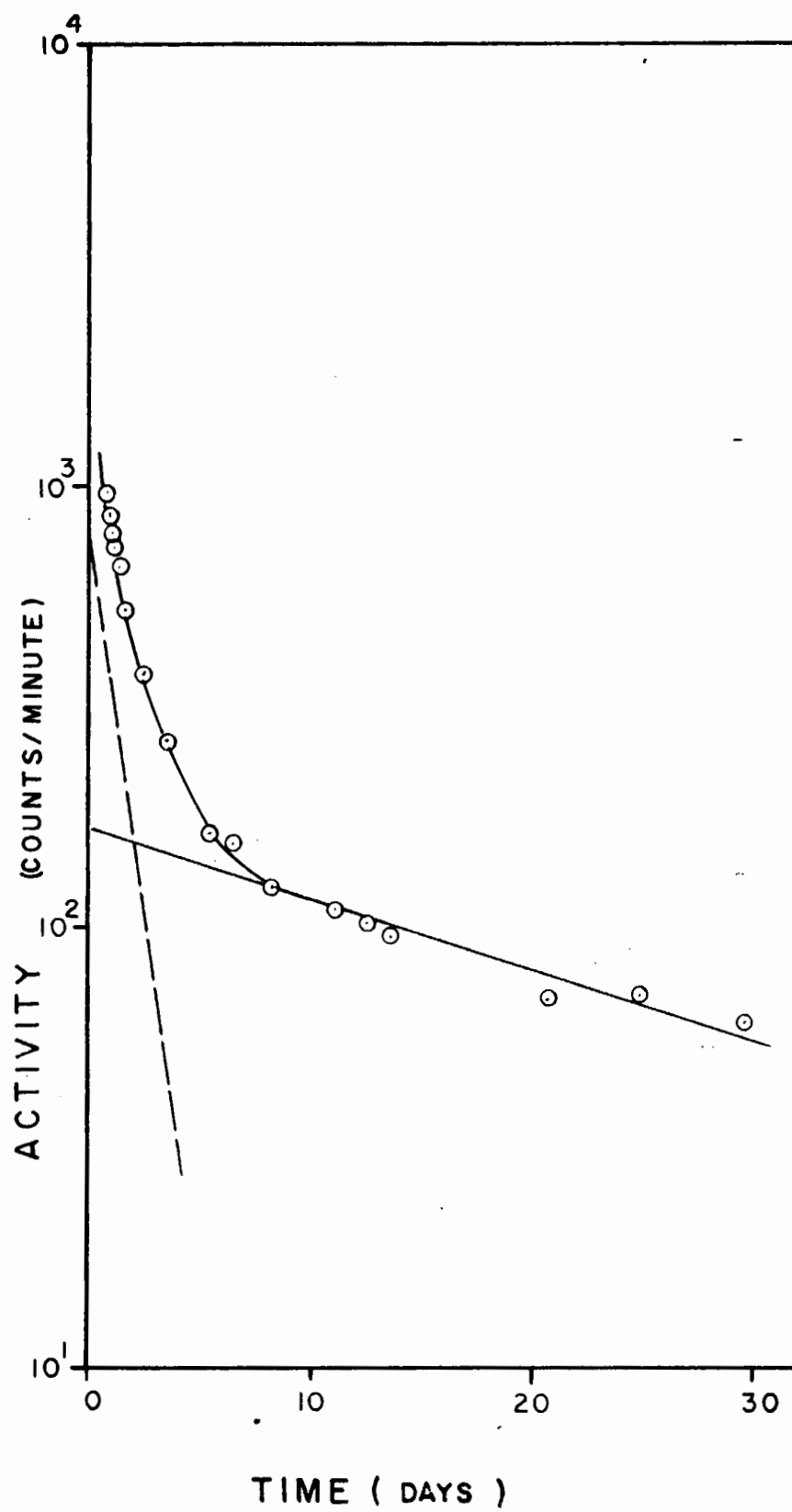
FIG. 32

Table XV

Sixteen Day Activity in the Potassium Fraction

Irrad. Number	Proton Energy (Mev.)	Activity (c/m)	Half-life (days)
30	88.1	160	19 ± 5
29	81.7	200	12 ± 5
31	67.4	7	30 ± 20

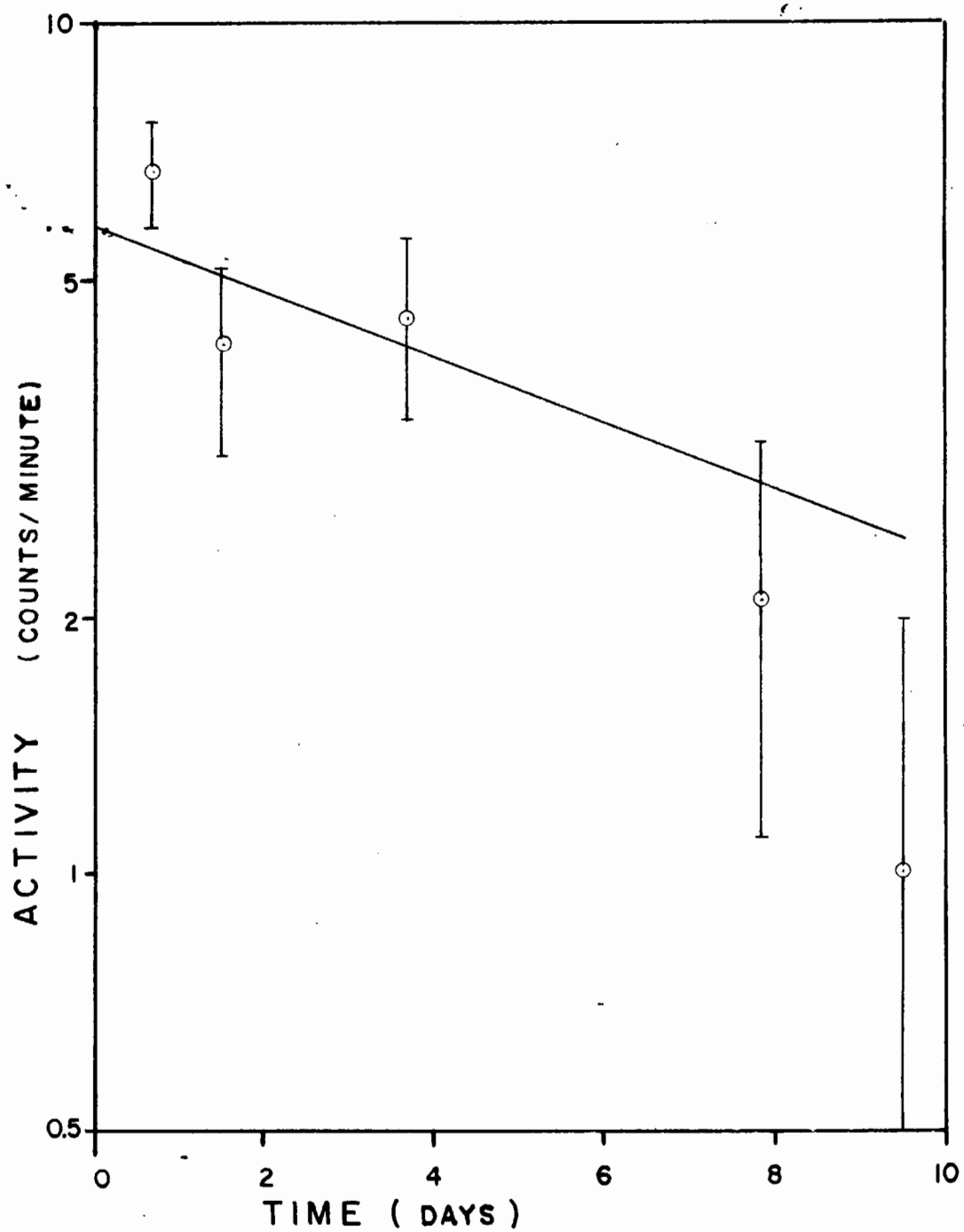The nuclides expected in the potassium fraction are

$$22 \text{ min.} \quad K^{44} \rightarrow Ca^{44}(\text{stable})$$
$$22 \text{ hr.} \quad K^{43} \rightarrow Ca^{43}(\text{stable})$$
$$12.4 \text{ hr.} \quad K^{42} \rightarrow Ca^{42}(\text{stable})$$
$$7.6 \text{ min. or } 0.9 \text{ sec. } K^{38} \rightarrow A^{38} (\text{stable})$$

All the daughter nuclides are stable, so that the 16 day activity cannot be a daughter growing in. Gamma-ray analysis of the potassium fraction after the short-lived activities had decayed away gave the spectrum shown in Figure 33. A spectrum of the background activity is included for purposes of comparison. From Figure 33 the gamma-ray energies are

X-ray peak	0.11 ± 0.01 Mev.
annihilation radiation	0.51 ± 0.01 Mev.
γ_1	0.96 ± 0.03 Mev.
γ_2	1.30 ± 0.02 Mev.

Figure 33

Gamma-ray Analysis of the Sixteen Day
Activity in the Potassium Fraction

      (a)   Sixteen Day Activity

      (b)   Background

RELATIVE PEAK HEIGHT

GAMMA ENERGY (Mev.)
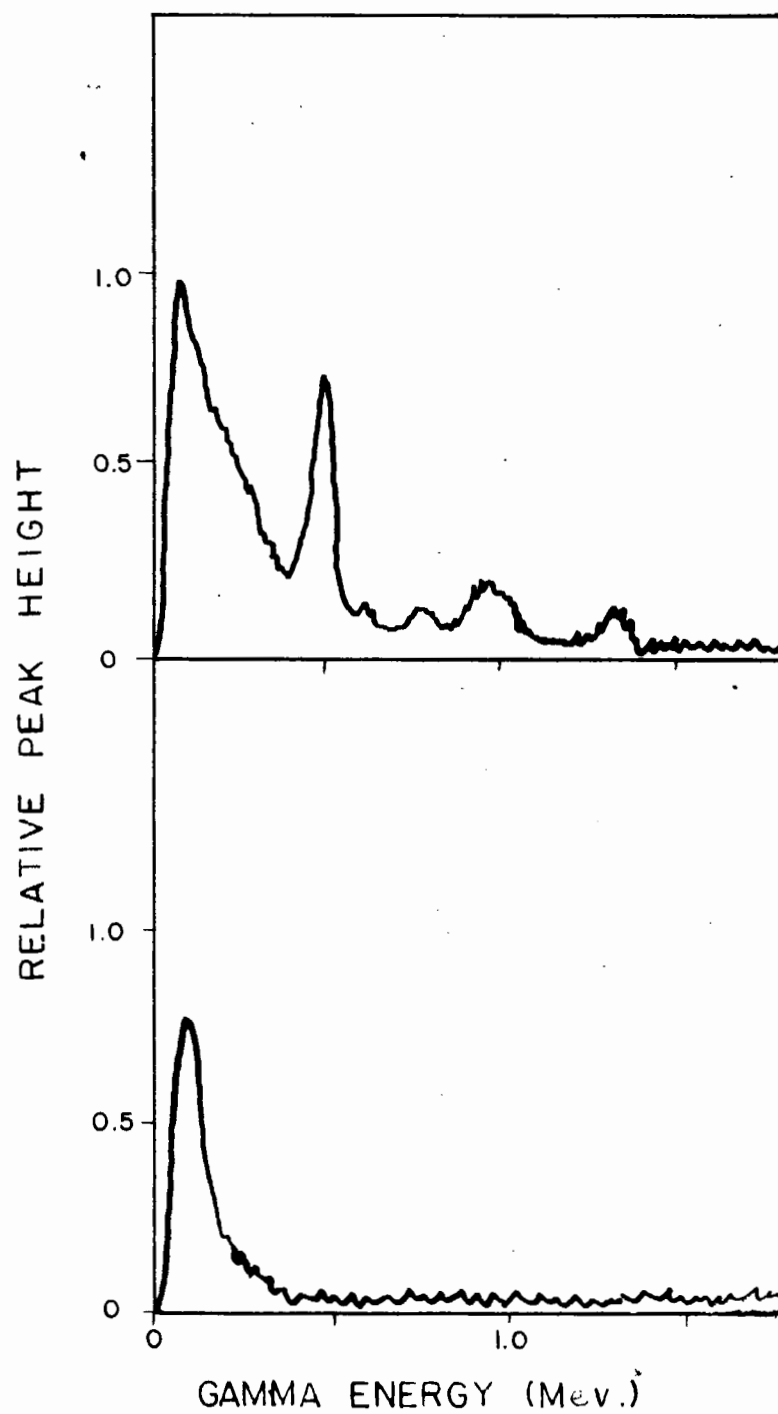
FIG. 33

The sharp peak at 0.51 Mev. indicates that the 16 ± 5 day
activity is a positron emitter. Comparison with the decay
characteristics of possible spallation products suggest
that the activity is due to contamination of V^{48} -
half-life 16 days, positron emission 58%, gamma-rays of
0.99, 1.32 and 2.23 Mev. The 2.23 Mev. gamma-ray would not
have been seen because the voltage and gain settings on the
scintillation spectrometer were such that gamma-rays more
energetic than 1.8 Mev. would not have been recorded.

Figure 34

Sample Decay Curve of the Beta Activity of the
Potassium Fraction in Irradiation 30 After the
Subtraction of 19 ± 5 day Activity.

The 22 hour line drawn through the points was
used to calculate the yield of 22 hr. K^{43}.
Subtraction of the 22 hour line gives 27 Min.
K^{44}.
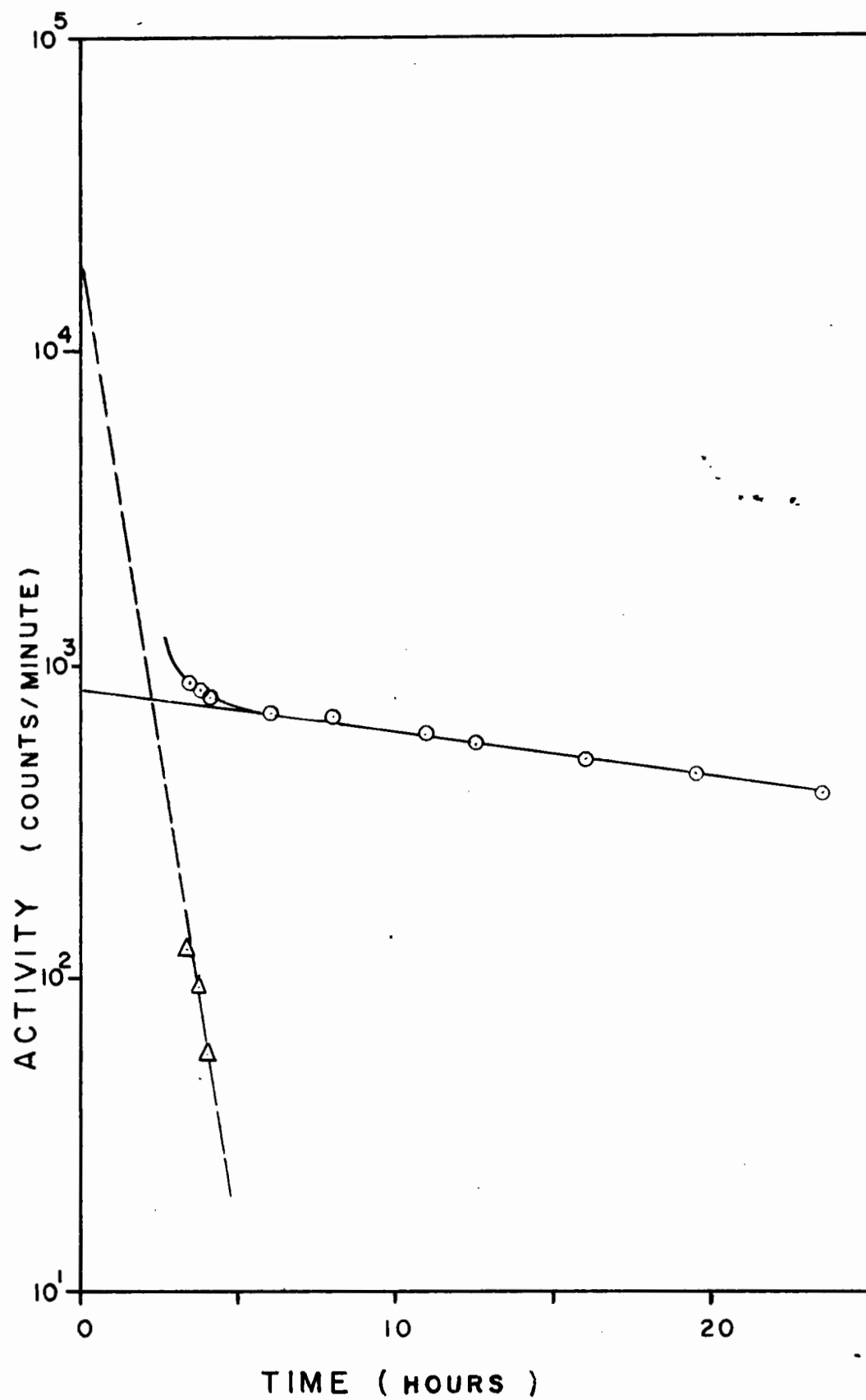
FIG. 34

Table XVI

Branching Ratios Used in the Calculation of Cross-Sections

Nuclide	Radiation Used in Calculations	Abundance %	Reference
Ni^{57}	β^+	50 ± 25	(85)
Ni^{56}	0.48 Mev. γ	unknown	
Co^{58m}	0.81 Mev. γ of Co^{58}	100 ± 2	(100)(92)(96)(95)
Co^{58}	0.81 Mev. γ	100 ± 2	(100)(92)(96)(95)
Co^{56}	β^+ 0.85 Mev. 1.24 Mev.	25 ± 20 100 ± 2 55 ± 2	(103)(104) (105) (105)
Co^{55}	β^+	60 ± 25	(107)
Fe^{53}	β^+	100 ± 20	(45)
Fe^{52}	β^+	38 ± 8	(116)
Mn^{56}	β^-	100 ± 1	(45)
Mn^{54}	0.84 Mev. γ	100 ± 1	(45)
Mn^{52m}	β^+	99.95 ± 0.05	(123)
Mn^{52}	β^+	35 ± 2	(93)
Mn^{51}	β^+	100 ± 20	(45)
Cr^{51}	E.C.	100 ± 1	(132)
Cr^{49}	β^+	88.5 ± 1.0	(134)
Sc^{49}	β^-	100 ± 10	(149)
Sc^{48}	β^-	100 ± 10	(141)
Sc^{47}	β^-	100 ± 10	(151)

Table XVI (Contd.)

Nuclide	Radiation Used in Calculations	Abundance %	Reference
Sc^{46}	β^-	100 ± 1	(153)
Sc^{44}	β^+, E.C.	93.2 ± 1.5	(158)
Sc^{43}	β^+, E.C.	80 ± 15	(156)
Ca^{47}	β^-	100 ± 10	(161)
Ca^{45}	β^-	100 ± 2	(164)
K^{44}	β^-	100 ± 10	(166)
K^{43}	β^-	100 ± 10	(7)
K^{42}	β^-	100 ± 10	(168)

<u>Sample Calculation of the Cross-Section</u>

Example: Formation of Ni^{57} in Irradiation 30, bombarded at
88.1 Mev. for 55 minutes.

total disintegrations/minute of Ni^{57} in target =
3.3×10^3 c/m(on shelf 1 of Geiger)

   $\times \dfrac{100}{15.8}$ (Geiger efficiency shelf 1 for 0.835 Mev.)

   $\times \dfrac{1}{0.92}$ $\left(\dfrac{\text{negatron back-scattering factor}}{\text{positron} \quad \text{''} \quad \text{''} \quad \text{''}}\right)$

   $\times \dfrac{100}{1.6}$ (dilution)

   $\times \dfrac{100}{50.1}$ (chemical yield)

   $= 2.81 \times 10^6$ disintegrations/minute.

total disintegrations/minute of Na^{24} monitor

   $= 2.86 \times 10^5$ c/m(on shelf 6 Geiger)

   $\times \dfrac{100}{0.519}$ (Geiger efficiency shelf 6 for 1.39 Mev. Beta)

   $\times \dfrac{1}{1}$ $\left(\dfrac{\text{negatron back-scattering}}{\text{negatron} \quad \text{''} \quad \text{''}}\right)$

   $= 5.50 \times 10^7$ disintegrations/minute.

Let Ni^{57} be represented by x, Na^{24} by y.
Then from equation (11) in Section I

$$\sigma_x = \sigma_y \times \left\{\dfrac{\text{abundance of y radiation counted}}{\text{abundance of x radiation counted}}\right\} \times \left\{\dfrac{\text{dis./min. } x}{\text{dis./min. } y}\right\} \times \left\{\dfrac{n_{Al}}{n_{Co}}\right\}$$

$$\times \quad \dfrac{1 - e^{-\lambda_y t}}{1 - e^{-\lambda_x t}}$$

where $\left\{\dfrac{n_{Al}}{n_{Co}}\right\}$ is the ratio of the number of atoms of Al:Co in
the target.

Substituting in the above equation,

$$\sigma_x = \sigma_y \times \frac{\text{abundance of y radiation counted}}{\text{abundance of x radiation counted}} \times \frac{2.81 \times 10^6}{5.50 \times 10^7} \times \frac{1}{7.707}$$

$$\times \frac{4.151 \times 10^{-2}}{1.749 \times 10^{-2}}$$

$$= \sigma_y \times \frac{\text{abundance of y radiation counted}}{\text{abundance of x radiation counted}} \times 0.0157$$

where 0.0157 is the "saturation activity of the nuclide $\div$ saturation activity of the monitor" tabulated in Table XVII.

Therefore, $\sigma_x = 10.69$ mb. $\times \dfrac{100\% \quad \beta^-}{50\% \quad \beta^+} \times 0.0157$

$$= 0.336 \text{ mb.}$$

The cross-sections are tabulated in Table XVII. Following Rudstam (207) the nuclides investigated can be divided into

(1) shielded nuclides;

(2) nuclides for which the cross-section of the parent nuclide is unknown;

(3) nuclides for which the cross-section of the parent nuclide is known.

All nickel isotopes belong in the first group, as well as other nuclides shielded by stable isobars or by isobars long-lived relative to the 1-2 hours between bombardment and separation. The measured cross-sections for nuclides in this group can be regarded as independent. Nuclides in group (1)

are: Ni^{57}, Ni^{56}, Co^{58m}, Co^{58} (see discussion in pages following) Co^{56}, Mn^{54}, Mn^{52}, Sc^{48}, Sc^{47}, Sc^{46}, Sc^{44} and K^{42}.

Nuclides falling into the second category are Co^{55}, Fe^{53}, Fe^{52}, Mn^{56}, Mn^{51}, Cr^{49}, Sc^{49}, Sc^{43}, Ca^{47}, Ca^{45}, K^{44} and K^{43}. The nuclides in this group all have short lived parents, so that the cross-sections reported in this thesis are the cumulative cross-sections.

Only two nuclides fall into the third group - Mn^{52m} and Cr^{51}. The following is an example of the method used to calculate the independent cross-section. Mn^{52m} was chosen for detailed discussion, but the argument may be applied similarly to calculation of the independent yield of Cr^{51}.
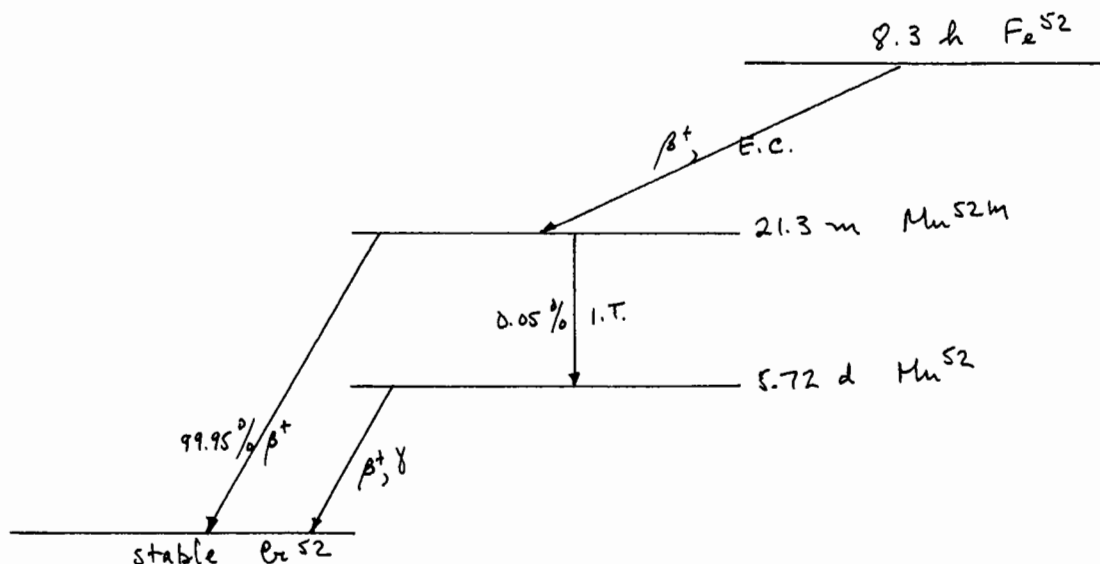
Table XVII

Values of the Cross-Section of Spallation Products

Nuclide	Irrad. No.	Proton Energy (Mev.)	Cross-Section Used for Monitor (mb.)	Sat. Act. Nuclide Sat. Act. Monitor	Nuclide Cross-Section (mb.)
Ni57	16	24.2	36.2 C^{11}	0	< 1
	15	29.7	29.2 C^{11}	0.0883	5.16
	17	35.2	24.2 C^{11}	0.648	31.4
	34	40.5	21.0 C^{11}	1.39	59
	21	42.4	19.9 C^{11}	1.06	42.4
	26	46.6	17.5 C^{11}	0.696	24.4
	22	52.5	14.8 C^{11}	0.474	14.0
	20	55.3	13.65 C^{11}	0.357	9.7
	13	60.3	12.40 C^{11}	0.0295	0.73
	31	67.4	7.50 Na^{24}	0.0452	0.68
	30	88.1	10.69 Na^{24}	0.0157	0.336
Ni56	18	40.5	21.0 C^{11}	0	< 0.12
	21	42.4	19.9 C^{11}	0	< 0.38
	26	46.6	17.5 C^{11}	0.0396	0.7
	8	50.3	15.65 C^{11}	0.0693	1.08
	22	52.5	14.8 C^{11}	0.0739	1.1
	20	55.3	13.65 C^{11}	0.0860	1.18
	13	60.3	12.40 C^{11}	0.104	1.3
	31	67.4	7.50 Na^{24}	0.00710	0.053
	30	88.1	10.69 Na^{24}	0.000905	0.010

Table XVII (Contd.)

Nuclide	Irrad. No.	Proton Energy (Mev.)	Cross-Section Used for Monitor (mb.)	Sat. Act. Nuclide Sat. Act. Monitor	Nuclide Cross-Section (mb.)
Co^{58m}	16	24.2	36.2 C^{11}	3.51	876
	15	29.7	29.2 C^{11}	3.16	636
	17	35.2	24.2 C^{11}	2.15	360
	21	42.4	19.9 C^{11}	2.65	364
	26	46.6	17.5 C^{11}	1.39	168
	22	52.5	14.8 C^{11}	1.53	156
	20	55.3	13.65 C^{11}	0.342	32
Co^{58}	16	24.2	36.2 C^{11}	1.94	484
	15	29.7	29.2 C^{11}	1.76	354
	17	35.2	24.2 C^{11}	1.34	224
	21	42.4	19.9 C^{11}	2.42	332
	26	46.6	17.5 C^{11}	2.30	278
	22	52.5	14.8 C^{11}	2.10	214
	20	55.3	13.65 C^{11}	1.93	182
Co^{56}	26	46.6	17.5 C^{11}	0	< 13
	22	52.5	14.8 C^{11}	2.35	140
	20	55.3	13.65 C^{11}	3.08	167
	29	81.7	10.42 Na^{24}	0.190	7.9
	30	88.1	10.69 Na^{24}	0.130	5.6
	28	94.9	10.70 Na^{24}	0.538	< 24

Table XVII (Contd.)

Nuclide	Irrad. No.	Proton Energy (Mev.)	Cross-Section Used for Monitor (mb.)	Sat. Act. Nuclide Sat. Act. Monitor	Nuclide Cross-Section (mb.)
Co^{55}	26	44.6	17.5 C^{11}	0	< 0.5
	22	52.5	14.8 C^{11}	0.0831	2.1
	20	55.3	13.65 C^{11}	0.188	4.28
	29	81.7	10.42 Na^{24}	0.0897	1.54
	30	88.1	10.69 Na^{24}	0.0399	0.71
	28	94.9	10.70 Na^{24}	0.107	1.9
Fe^{53}	18	40.5	21.0 C^{11}	0	< 0.3
	21	42.4	19.9 C^{11}	0	< 0.3
	26	44.6	17.5 C^{11}	0.271	4.7
	22	52.5	14.8 C^{11}	0.598	8.9
	20	55.3	13.65 C^{11}	0.863	11.7
Fe^{52}	18	40.5	21.0 C^{11}	0	< 0.015
	21	42.4	19.9 C^{11}	0.000629	0.033
	20	55.3	13.65 C^{11}	0.000608	0.022
	33	83.7	10.57 Na^{24}	0.00670	0.185
	32	92.5	10.70 Na^{24}	0.00580	0.164

Table XVII (Contd.)

Nuclide	Irrad. No.	Proton Energy (Mev.)	Cross-Section Used for Monitor (mb.)	Sat. Act. Nuclide Sat. Act. Monitor	Nuclide Cross-Section (mb.)
Mn^{56}	34	40.5	21.0 C^{11}	0.0186	0.39
	21	42.4	19.9 C^{11}	0.0229	0.46
	26	46.6	17.5 C^{11}	0.129	2.26
	22	52.5	14.8 C^{11}	0.506	7.5
	20	55.3	13.65 C^{11}	0.989	13.5
	13	60.3	12.4 C^{11}	0.536	6.65
	33	83.7	10.57 Na^{24}	0.0888	0.939
	32	92.5	10.70 Na^{24}	0.0712	0.762
Mn^{54}	17	35.2	24.2 C^{11}	5.61	136
	18	40.5	21.2 C^{11}	11.4	242
	21	42.4	19.9 C^{11}	10.5	210
	26	46.6	17.5 C^{11}	7.53	132
	22	52.5	14.8 C^{11}	6.56	97
	20	55.3	13.65 C^{11}	10.75	147
	13	60.3	12.4 C^{11}	5.84	73
Mn^{52m}	20	55.3	13.65 C^{11}	0	< 0.3
	13	60.3	12.4 C^{11}	0	< 0.3
	33	83.7	10.57 Na^{24}	0.478	5.0
	32	92.5	10.70 Na^{24}	0.403	4.8

Table XVII (Contd.)

| Nuclide	Irrad. No.	Proton Energy (Mev.)	Cross-Section Used for Monitor (mb.)	Sat. Act. Nuclide Sat. Act. Monitor	Nuclide Cross-Section (mb.)
Mn^{52}	17	35.2	$24.2\ C^{11}$	0	<0.20
	34	40.5	$21.0\ C^{11}$	0.0213	1.28
	21	42.4	$19.9\ C^{11}$	0.0257	1.46
	26	46.6	$17.5\ C^{11}$	0.0684	3.42
	22	52.5	$14.8\ C^{11}$	0.0316	1.34
	20	55.3	$13.65\ C^{11}$	0.106	4.14
	13	60.3	$12.4\ C^{11}$	0.176	6.2
	33	83.7	$10.57\ Na^{24}$	0.155	4.66
	32	92.5	$10.70\ Na^{24}$	0.0872	2.66
Mn^{51}	13	60.3	$12.4\ C^{11}$	<0.011	<0.14
	33	83.7	$10.57\ Na^{24}$	<0.029	<0.30
	32	92.5	$10.70\ Na^{24}$	<0.040	<0.43
Cr^{51}	31	67.4	$7.50\ Na^{24}$	0.0586	0.44
	29	81.7	$10.42\ Na^{24}$	0.0751	0.78
	30	88.1	$10.69\ Na^{24}$	0.219	2.34
Cr^{49}	31	67.4	$7.50\ Na^{24}$	0.00106	0.0090
	29	81.7	$10.42\ Na^{24}$	0.00119	0.014
	30	88.1	$10.69\ Na^{24}$	0.00618	0.075
Sc^{49}	33	83.7	$10.57\ Na^{24}$	0.000331	0.0035
	32	92.5	$10.70\ Na^{24}$	0.000215	0.0023

Table XVII (Contd.)

Nuclide	Irrad. No.	Proton Energy (Mev.)	Cross-Section Used for Monitor (mb.)	Sat. Act. Nuclide Sat. Act. Monitor	Nuclide Cross-Section (mb.)
Sc^{48}	31	67.4	7.50 Na^{24}	0.000911	0.0068
	33	83.7	10.57 Na^{24}	0.000393	0.0041
	32	92.5	10.70 Na^{24}	<0.00043	<0.0047
Sc^{47}	31	67.4	7.50 Na^{24}	<0.00039	<0.0029
	33	83.7	10.57 Na^{24}	<0.00020	<0.0021
	32	92.5	10.70 Na^{24}	<0.00066	<0.0071
Sc^{46}	31	67.4	7.50 Na^{24}	0.0263	0.197
	29	81.7	10.42 Na^{24}	0.0156	0.163
	33	83.7	10.57 Na^{24}	0.0111	0.117
	32	92.5	10.70 Na^{24}	0.0074	0.079
$Sc^{43,44}$	33	83.7	10.57 Na^{24}	0.000200	0.00243
	32	92.5	10.70 Na^{24}	0.000240	0.00295
Ca^{47}	31	67.4	7.50 Na^{24}	0.00193	0.014
	30	88.1	10.69 Na^{24}	<0.0004	<0.004
Ca^{45}	31	67.4	7.50 Na^{24}	<0.013	<0.10
	30	88.1	10.69 Na^{24}	0.0319	0.34
K^{44}	29	81.7	10.42 Na^{24}	0.00280	0.029
	30	88.1	10.69 Na^{24}	0.0216	0.23

Table XVII (Contd.)

Nuclide	Irrad. No.	Proton Energy (Mev.)	Cross-Section Used for Monitor (mb.)	Sat. Act. Nuclide Sat. Act. Monitor	Nuclide Cross-Section (mb.)
K^{43}	29	81.7	10.42 Na^{24}	0.000702	0.0073
	30	88.1	10.69 Na^{24}	0.00296	0.0316
K^{42}	29	81.7	10.42 Na^{24}	0.000182	0.00190
	30	88.1	10.69 Na^{24}	< 0.000503	< 0.0054

Ignoring the 0.05% decay of Mn^{52m} to Mn^{52}, the decay chain may be written

$$Fe^{52} \quad \underset{\beta^+}{\underline{7.8h}} \quad Mn^{52m} \quad \underset{\beta^+}{\underline{21.3m}} \quad Cr^{52} \text{ (stable)}$$
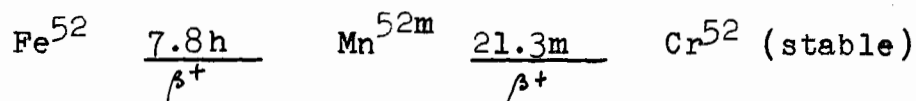
Since no data are available on the parent of Fe^{52}, we shall consider Fe^{52} as a primary product, i.e. all the Fe^{52} atoms are formed directly in the spallation process. The Mn^{52m} atoms are, however, formed in two ways: as direct reaction products, and by the decay of Fe^{52}, so that at any given time the total number of atoms of Mn^{52m} (1) number of atoms of Mn^{52m} formed directly PLUS (2) number of atoms of Mn^{52m} formed by decay of Fe^{52} MINUS (3) number of atoms of Mn^{52m} which have decayed in the interval between end of bombardment and the given time. We wish to calculate (1) in order to quote the independent yield of formation of Mn^{52m}. Extrapolation of the Mn^{52} decay curve to the time of end of bombardment gives (1) PLUS (2), and from the cross-section of Fe^{52} it is possible to calculate (2).

Knowing (2) as well as (1) PLUS (2), subtraction gives (1), the independent yield of Mn^{52m}.

Example: Suppose the independent cross-section at bombardment time of Fe^{52} is 1 mb., and suppose the cumulative cross-section at bombardment time of Mn^{52m} is 1 mb. Suppose 2 hours elapse between end of bombardment and time of separation. During these 2 hours, 15.5% of the 8.3 hour Fe^{52} decayed to Mn^{52m}. It follows that, during these 2 hours, the amount of Fe^{52} that

decayed to Mn^{52m} was 15.5%. That is, of the measured cross-section for the formation of Mn^{52m} 15.5%, i.e. 0.155 mb., is due to the decay of Fe^{52} to Mn^{52m}. What will be the amount of Mn^{52m} formed from the decay of Fe^{52}? From equation (11) in Section I of this thesis

$$\frac{N_A}{N_B} = \frac{\sigma_A}{\sigma_B} \frac{(1-e^{-\lambda_A t})}{(1-e^{-\lambda_B t})}$$

where A refers to Fe^{52}, and B refers to Mn^{52m}. σ_B is the cross-section of Mn^{52m} formed from the decay of Fe^{52}. For every atom of Fe^{52} which decays, one atom of Mn^{52} is formed. Therefore $N_A = N_B$.

$$\sigma_B = \sigma_A \times \frac{(1-e^{-A^t})}{(1-e^{-B^t})}$$

$$= 0.155 \frac{(1-e^{-1.395 \times 10^{-3} \times 120})}{(1-e^{-3.25 \times 10^{-2} \times 120})} \text{ mb.}$$

$$= 0.155 \left(\frac{1-0.846}{1-0.021}\right) \text{ mb.} = 0.022 \text{ mb.}$$

But we had postulated that the cumulative cross-section at bombardment time of Mn^{52m} was 1 mb. Therefore the independent yield of Mn^{52m} is 1 mb. MINUS **0.022** mb. = 0.98 mb.

Figure 35

Absolute Excitation Function for Co^{59} $(p,3n)Ni^{57}$.

The dashed line represents the results of Sharp, Diamond and Wilkinson.

FIG. 35

Figure 36

Absolute Excitation Function for Co^{59} $(p,4n)Ni^{56}$.

The dashed line represents the results of Sharp, Diamond and Wilkinson.

FIG. 36

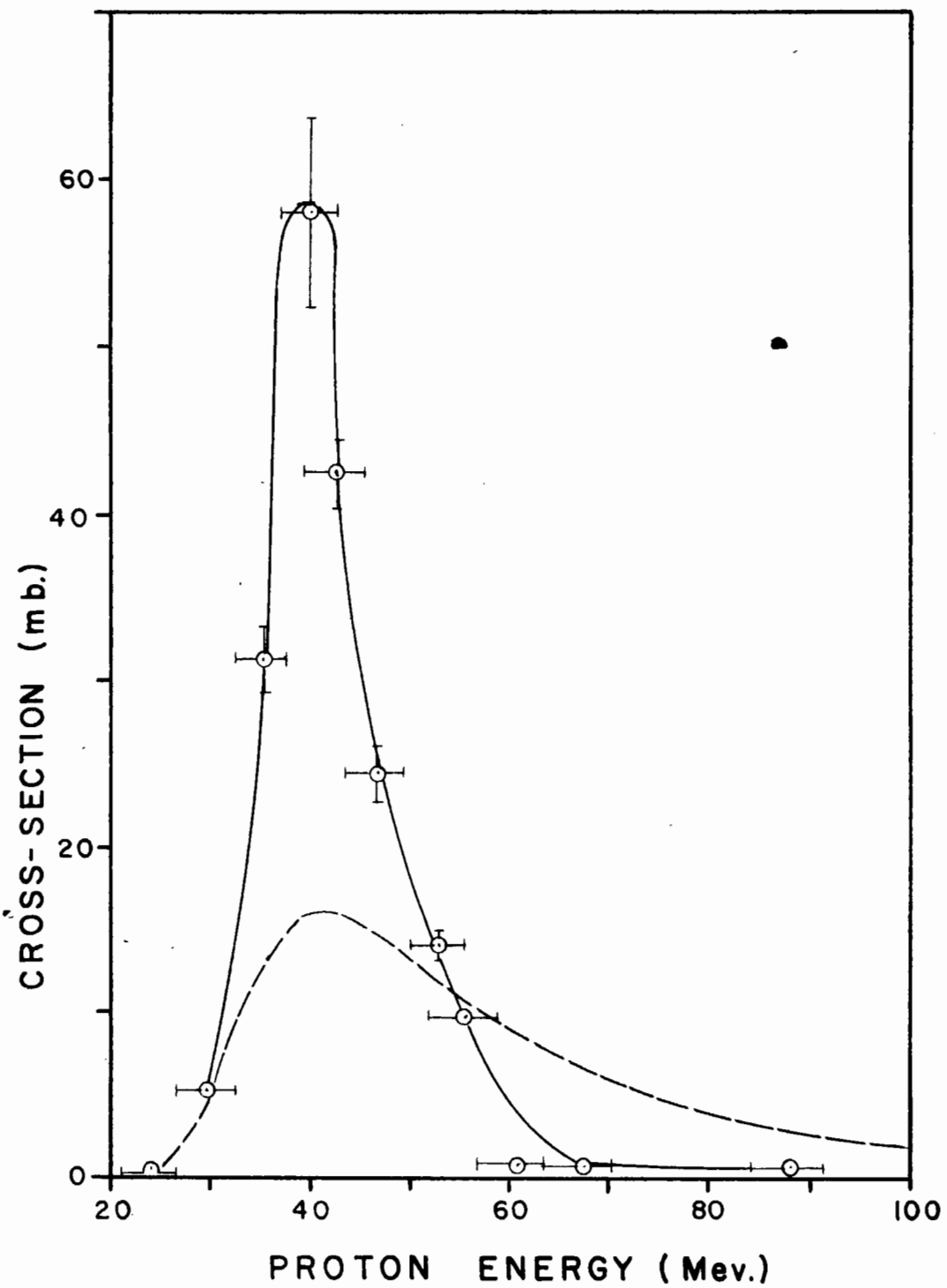## Figure 37
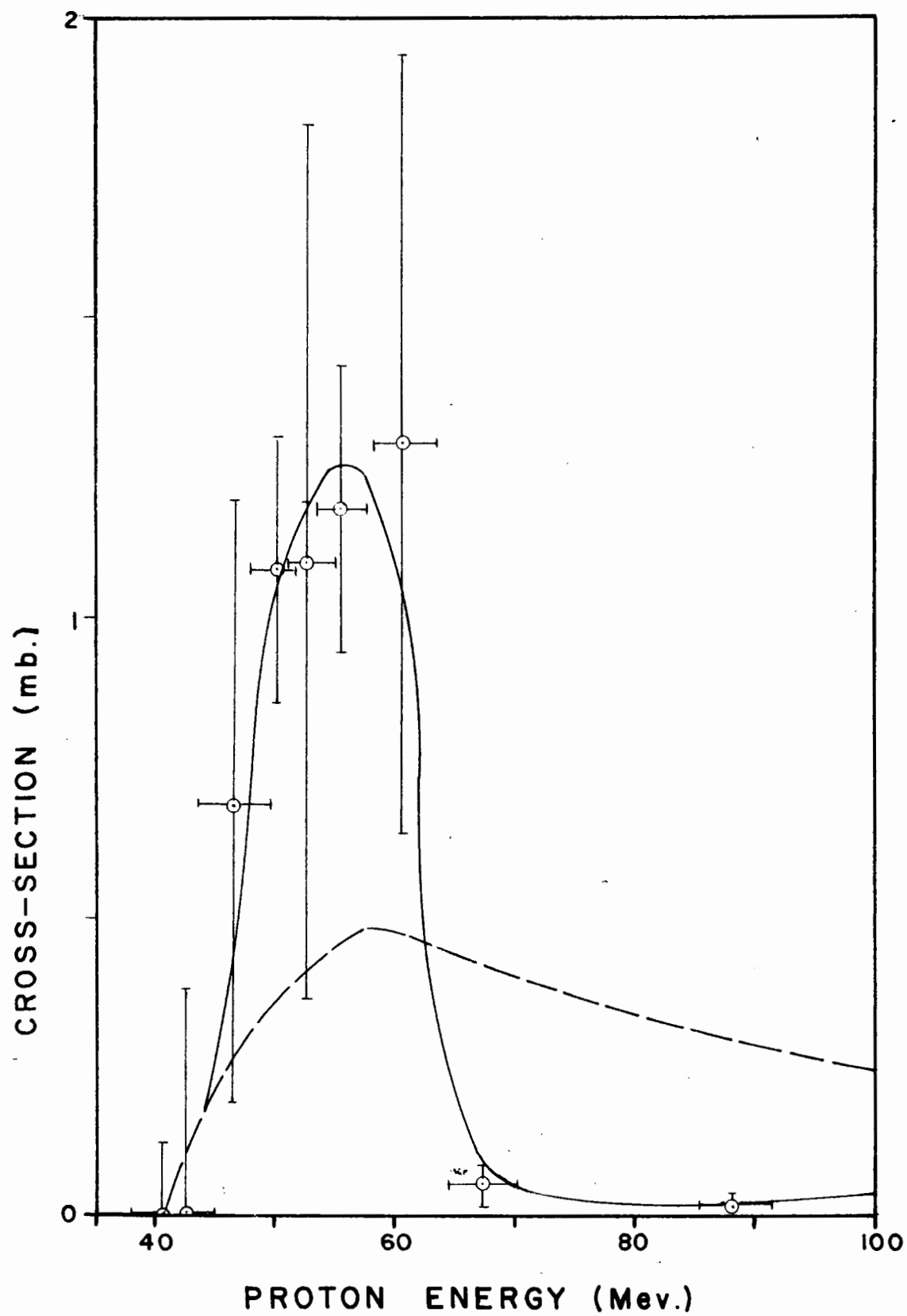
Absolute Excitation Function for Co^{59}
$(p,pn)Co^{58m}$.

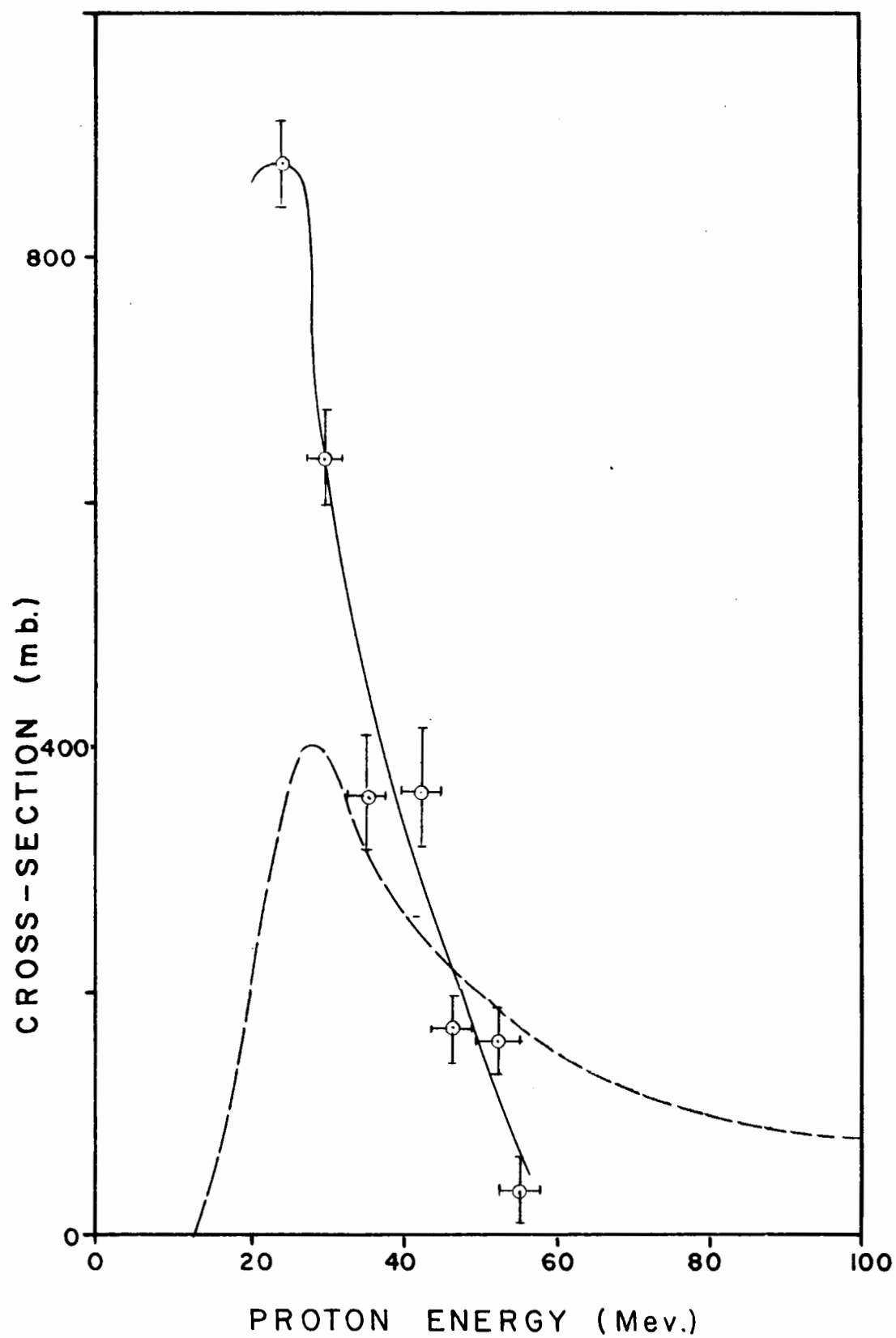The dashed line represents the results of
Sharp, Diamond and Wilkinson.

FIG. 37

Figure 38

Absolute Excitation Function for $Co^{59}(p,pn)Co^{58}$

- - - -   Sharp, Diamond and Wilkinson

— . — . Wagnes and Wiig

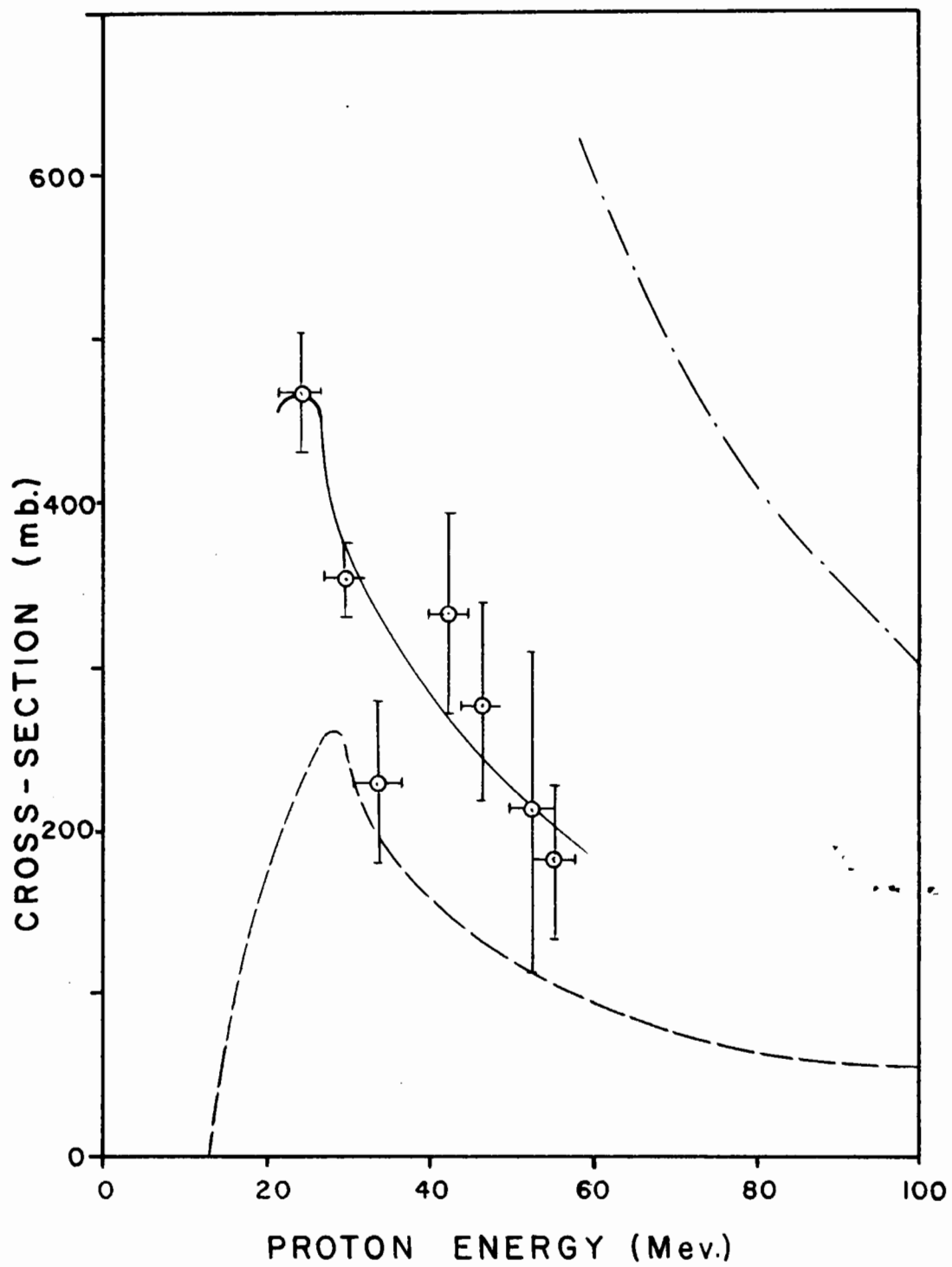FIG. 38

Figure 39

Absolute Excitation Function for Co^{59} (p,p3n)Co^{56}

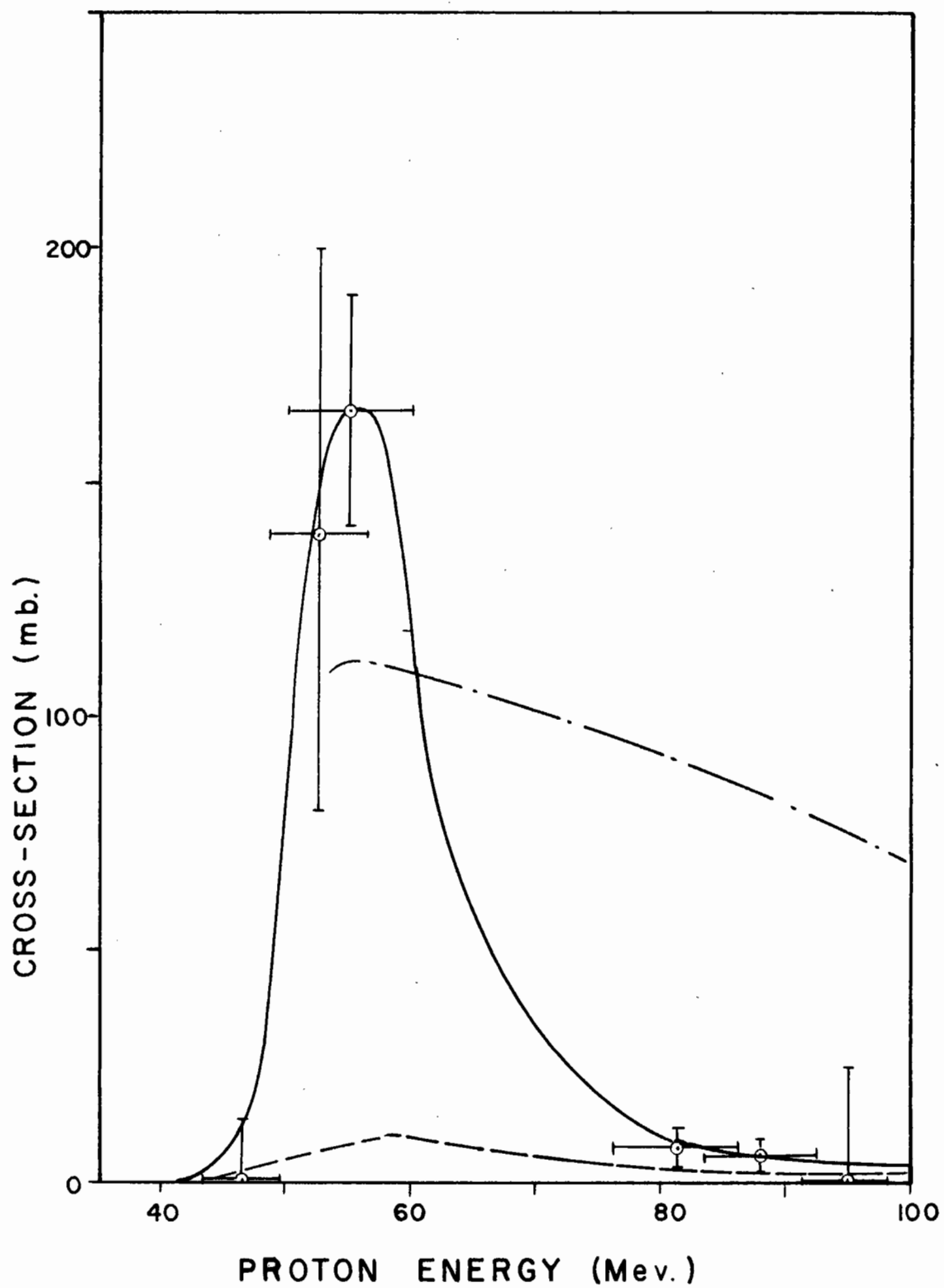----   Sharp, Diamond and Wilkinson

—.—.   Wagner and Wiig

FIG. 39

Figure 40

Absolute Excitation Function for Co^{59} $(p,p4n)Co^{55}$.

----   Sharp, Diamond and Wilkinson

— . — . Wagner and Wiig

FIG.40

Figure 41

Absolute Excitation Function for Co^{59} $(p,2p5n)Fe^{53}$.

The dashed line represents the results of Sharp, Diamond and Wilkinson.

FIG.41

Figure 42

Absolute Excitation Function for Co^{59}
$(p,2p6nFe^{52})$.

The dashed line represents the results of
Sharp, Diamond and Wilkinson.

FIG.42

Figure 43

Absolute Excitation Function for Co^{59} $(p,3pn)Mn^{56}$.

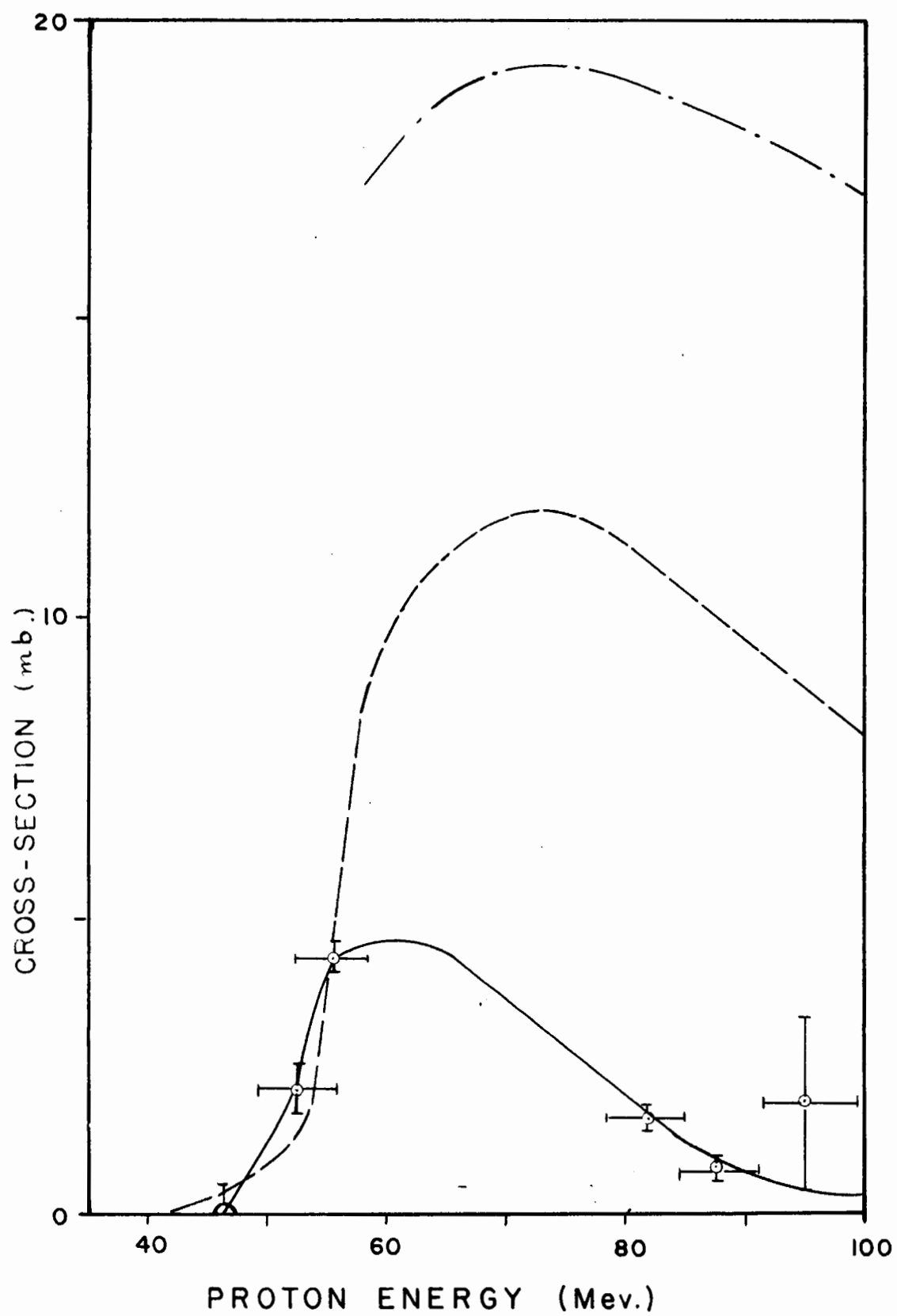   ----   Sharp, Diamond and Wilkinson

    — . — .   Wagner and Wiig
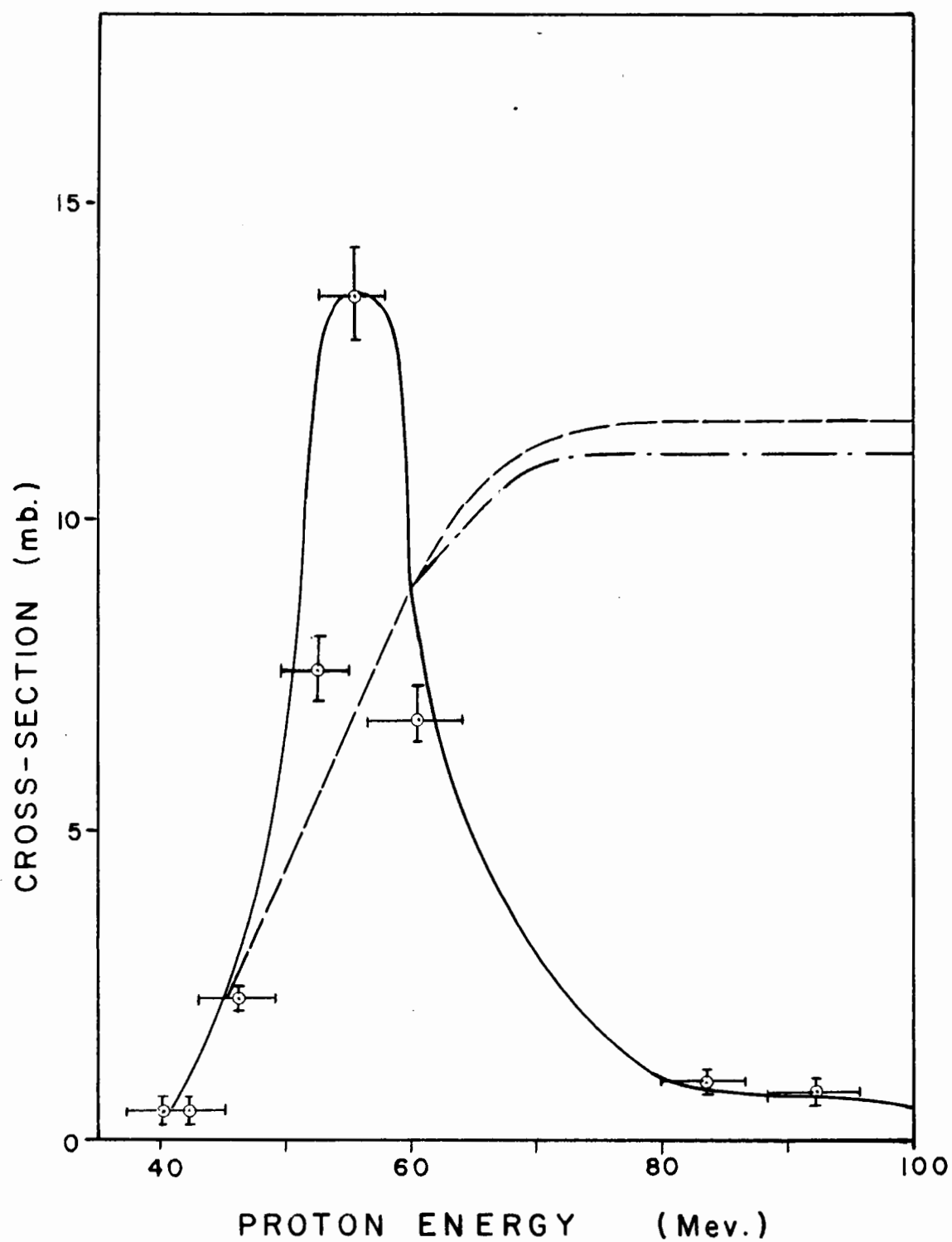
FIG.43

Figure 44

Absolute Excitation Function for Co^{59} $(p,3p3n)Mn^{54}$.

The dashed line represents the results of Sharp, Diamond and Wilkinson.
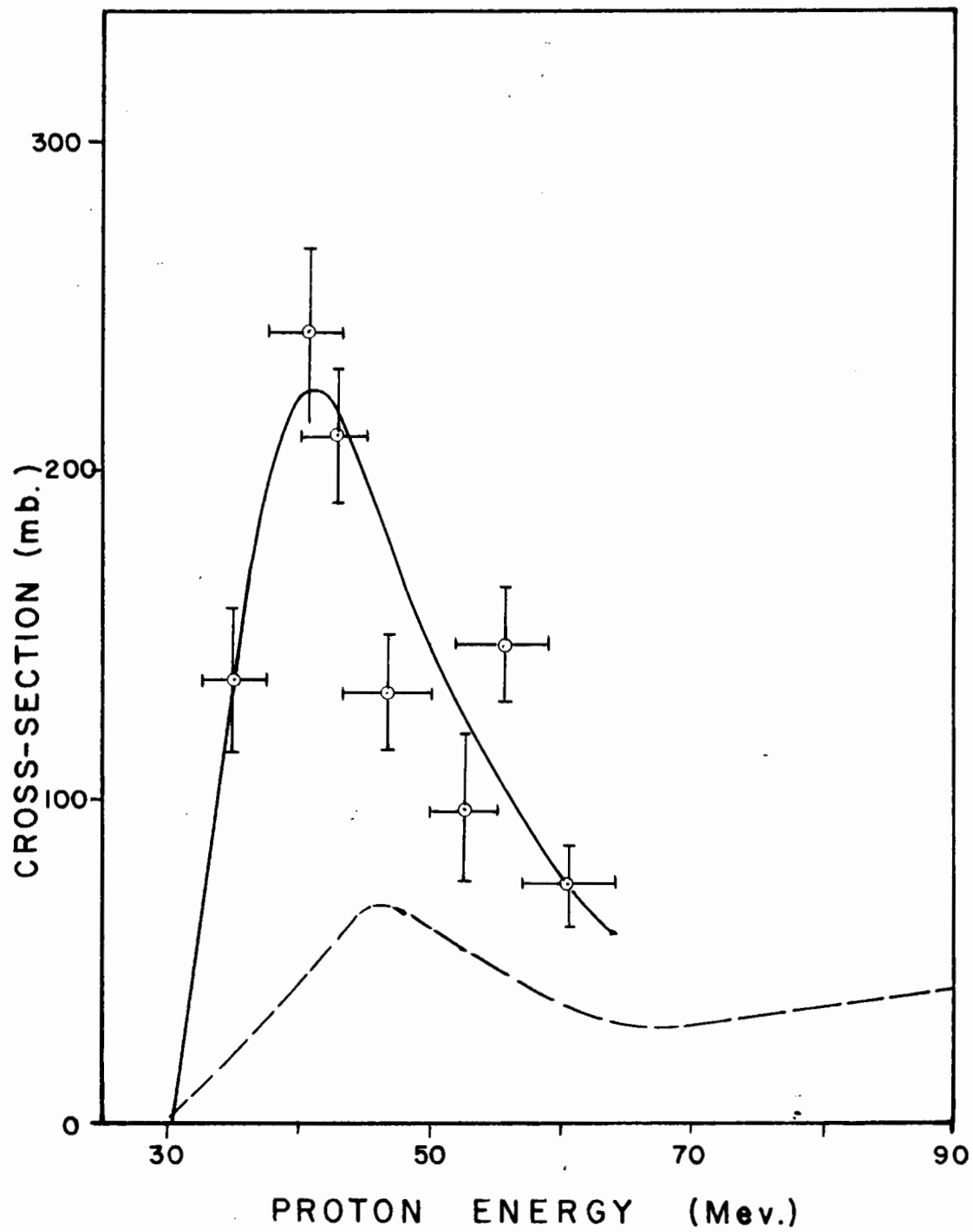
FIG. 44

Figure 45

Absolute Excitation Function for Co^{59} $(p,3p5n)Mn^{52m}$.

The dashed line represents the results of Sharp, Diamond and Wilkinson.
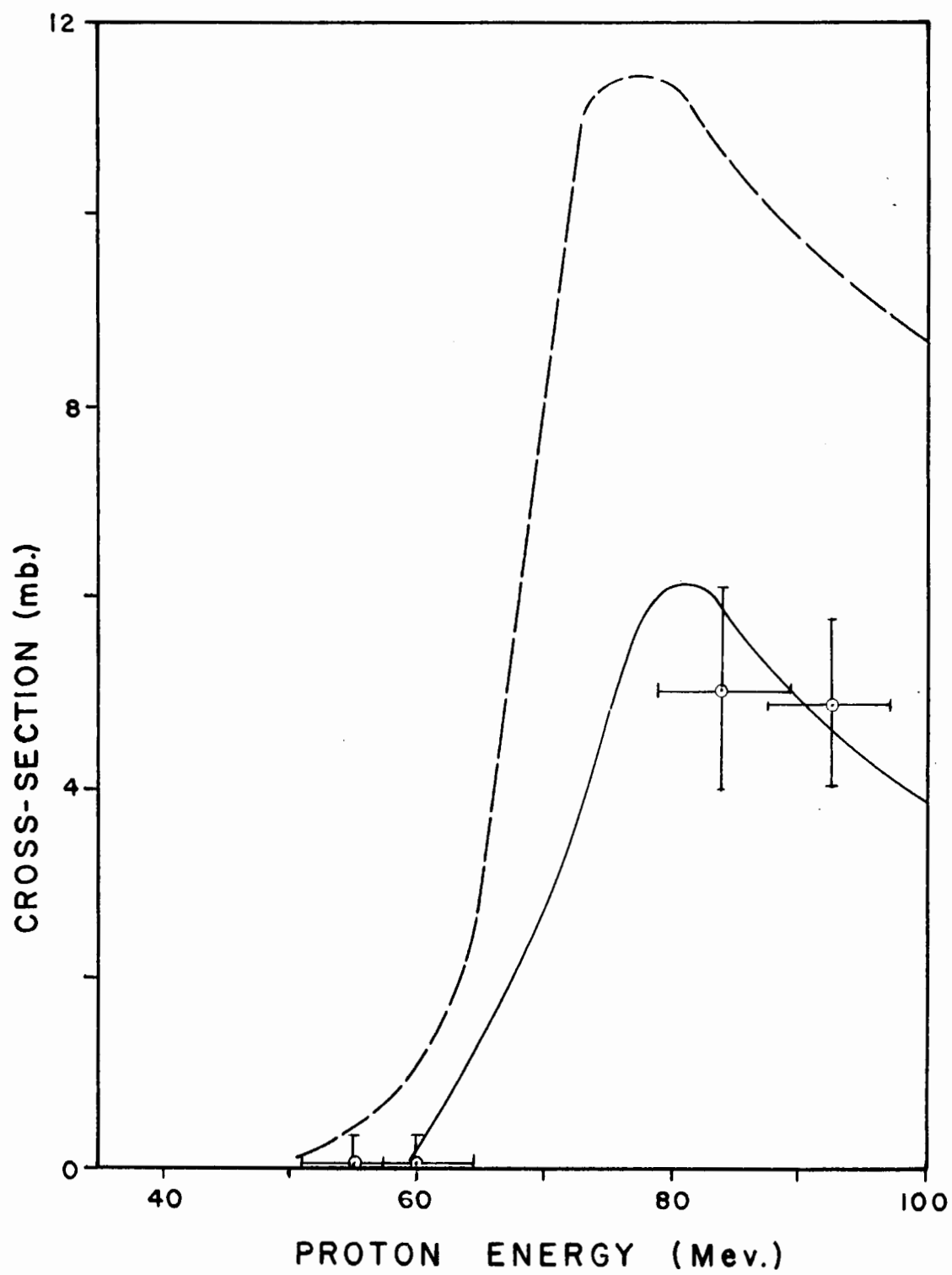
FIG. 45

Figure 46

Absolute Excitation Function for Co^{59} $(p,3p5n)Mn^{52}$.

The dashed line represents the results of Sharp, Diamond and Wilkinson.
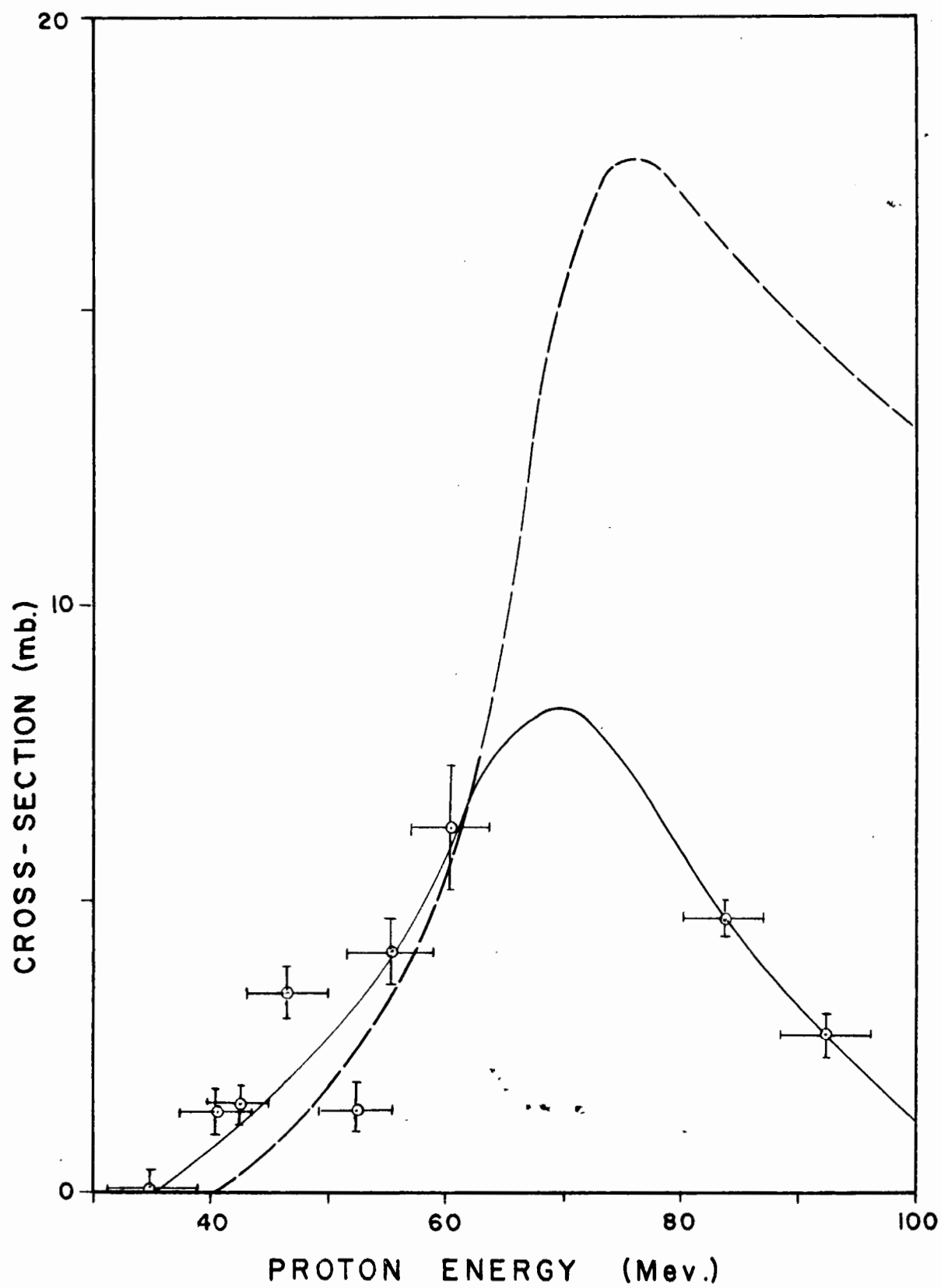
FIG. 46

Figure 47
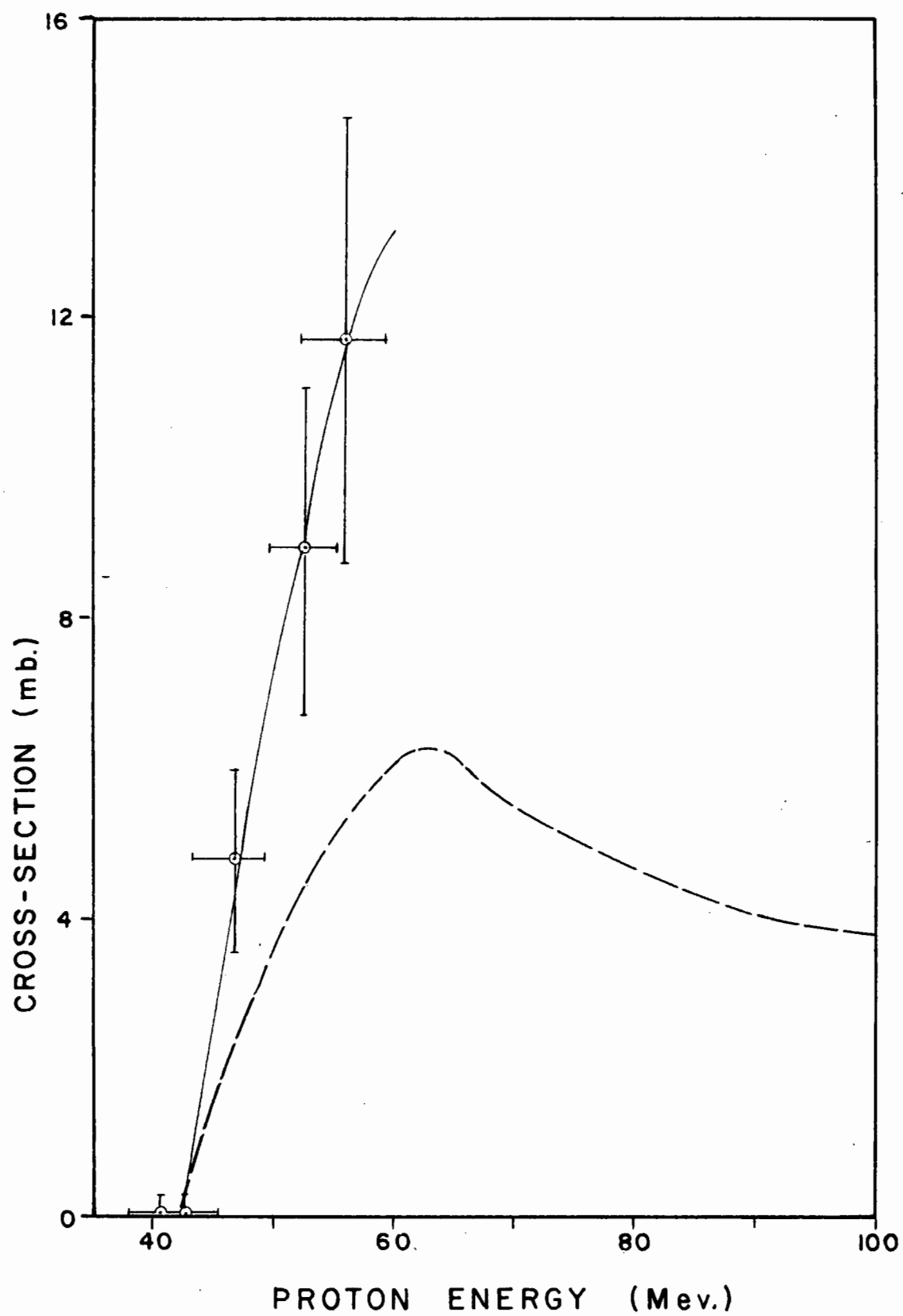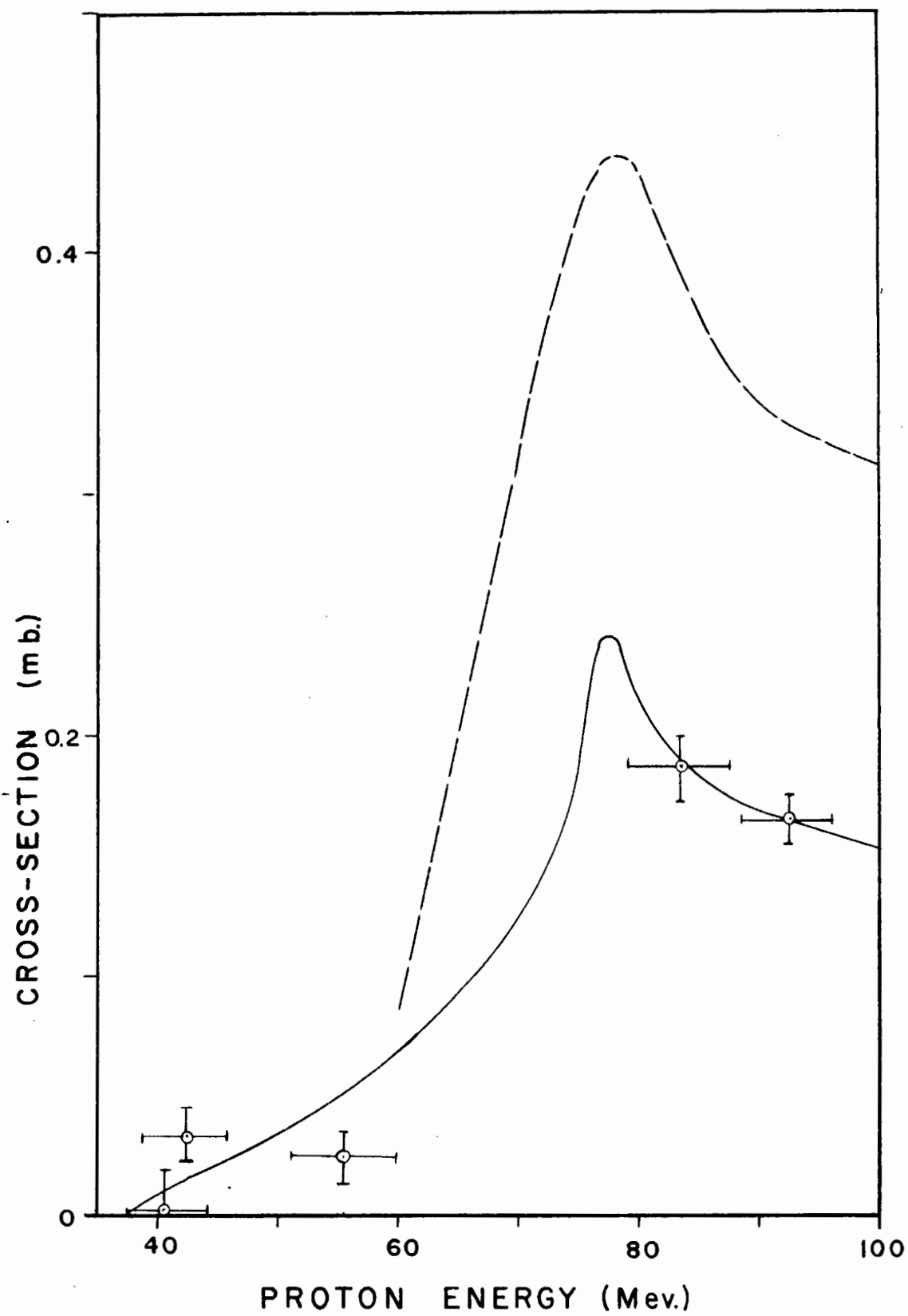
Absolute Excitation Function for Co^{59} $(p,4p5n)Cr^{51}$.

The dashed line represents the data of Sharp, Diamond and Wilkinson $\pm$ 10.
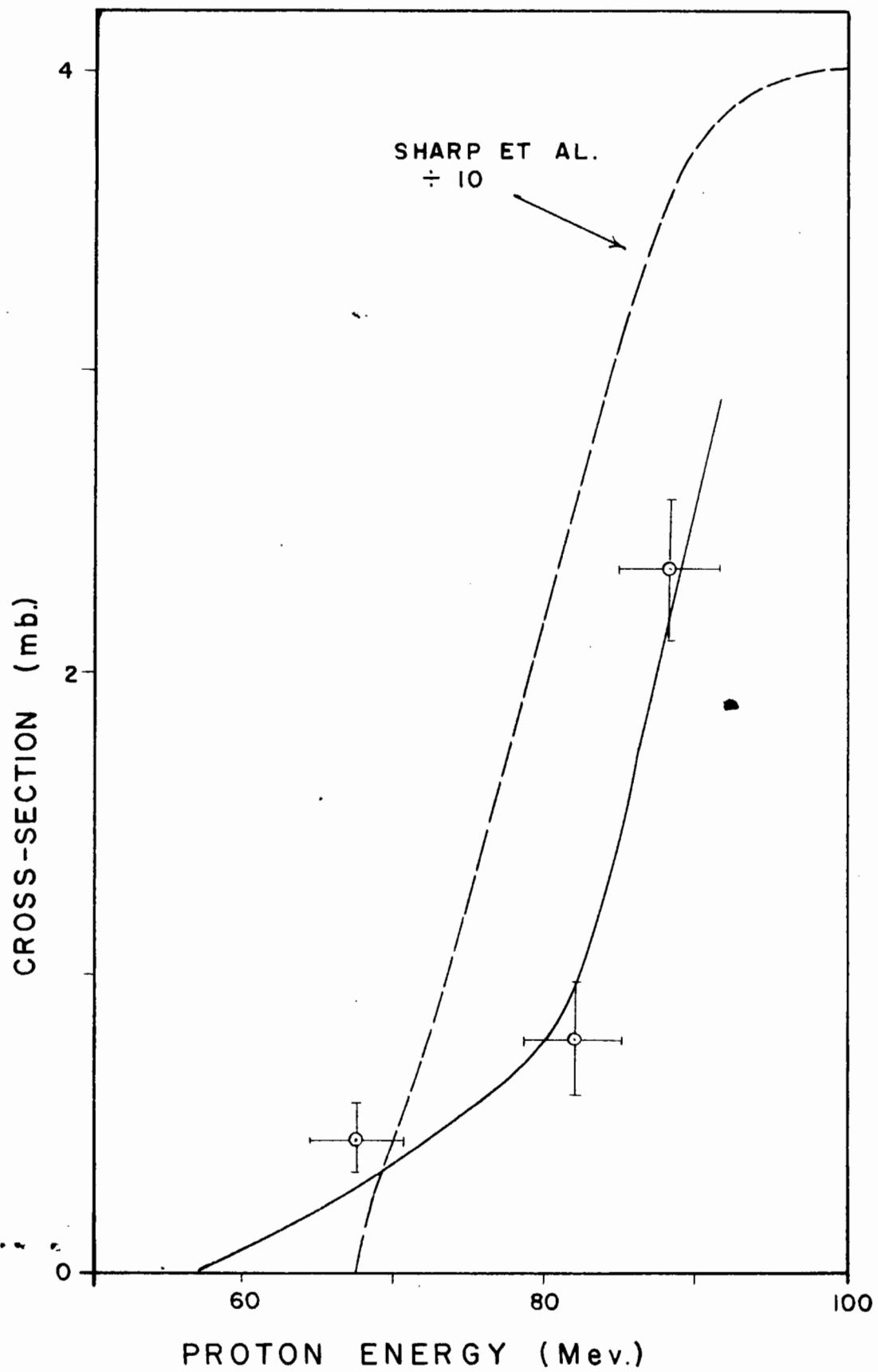
FIG.47

Figure 48

Absolute Excitation Function for $Co^{59}(p,4p7n)Cr^{49}$
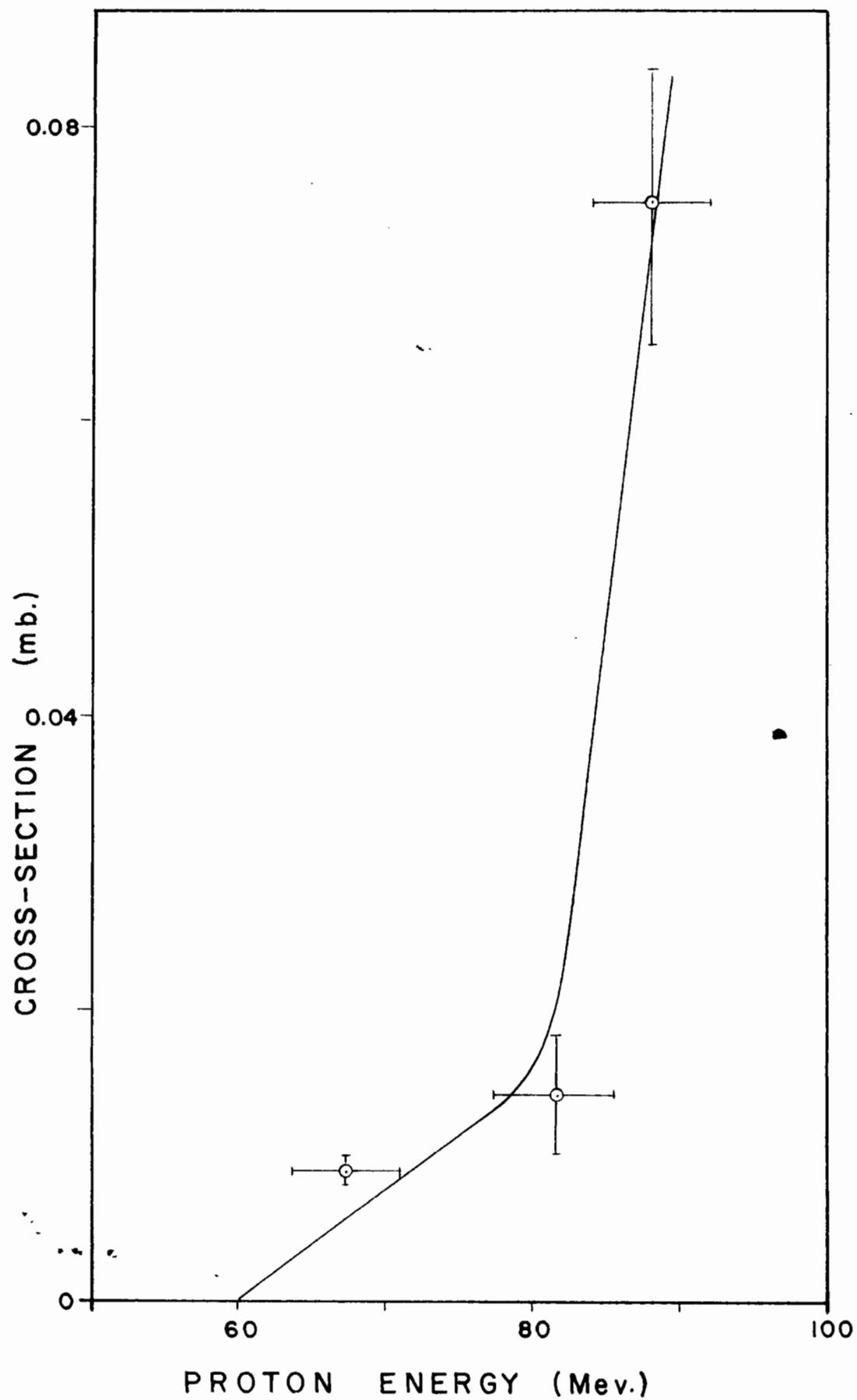
FIG.48

Figure 49

Absolute Excitation Functions for the Formation of Sc^{49} and Sc^{48}.

$\square$ $Co^{59}(p, 7p4n)Sc^{49}$

$\odot$ $Co^{59}(p, 7p5n)Sc^{48}$
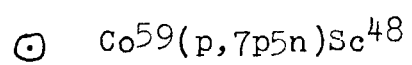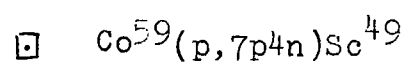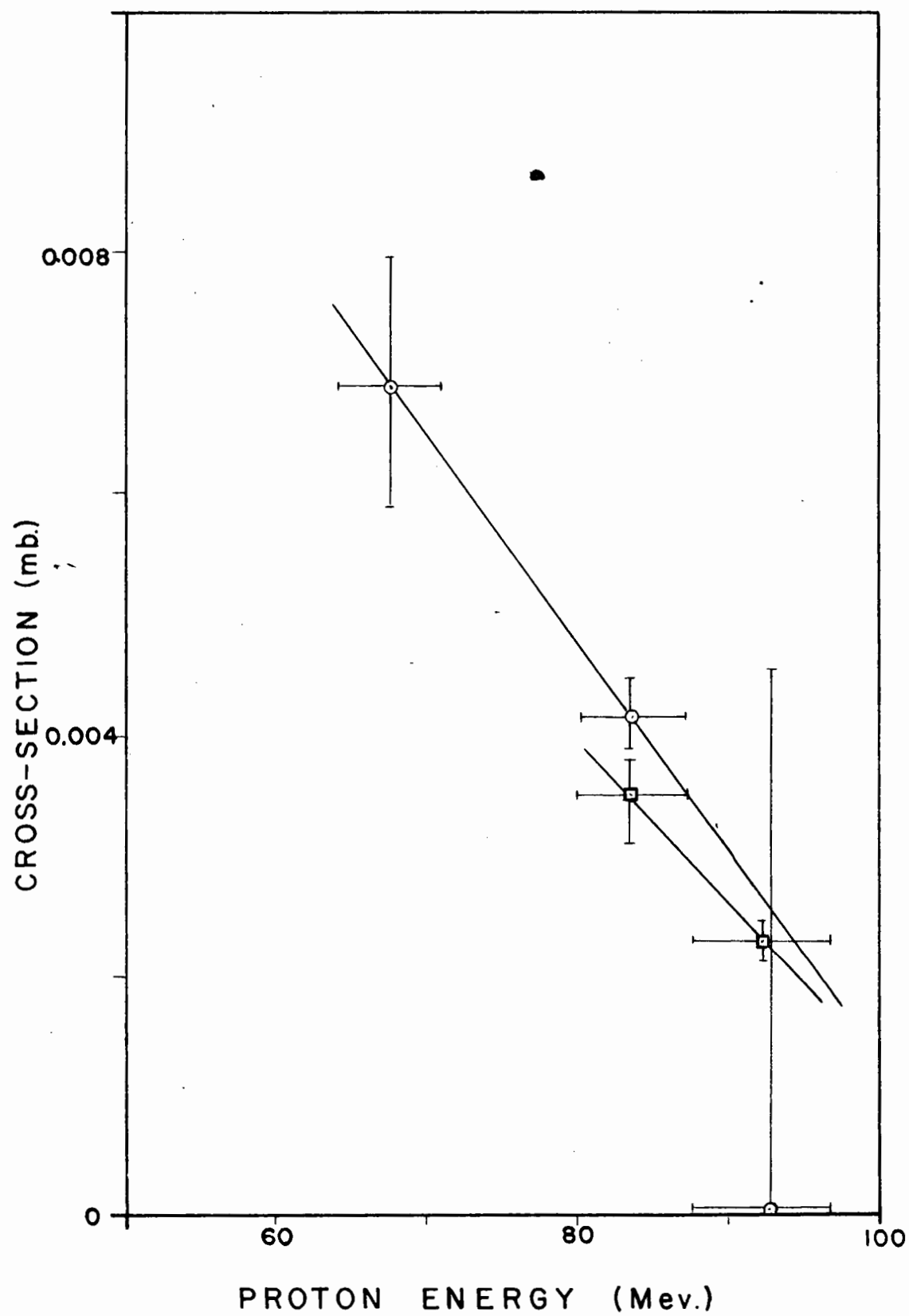
FIG.49

Figure 50

Absolute Excitation Functions for the Formation of Sc^{46} and of $Sc^{43,44}$.

- ⊙ $Co^{59}(p,7p7n)Sc^{46}$

- ⊡ $Co^{59}(p,7p9n)Sc^{44}$ PLUS $Co^{59}(p,7p10n)Sc^{43}$
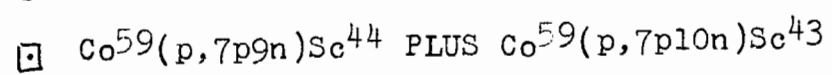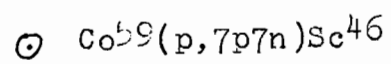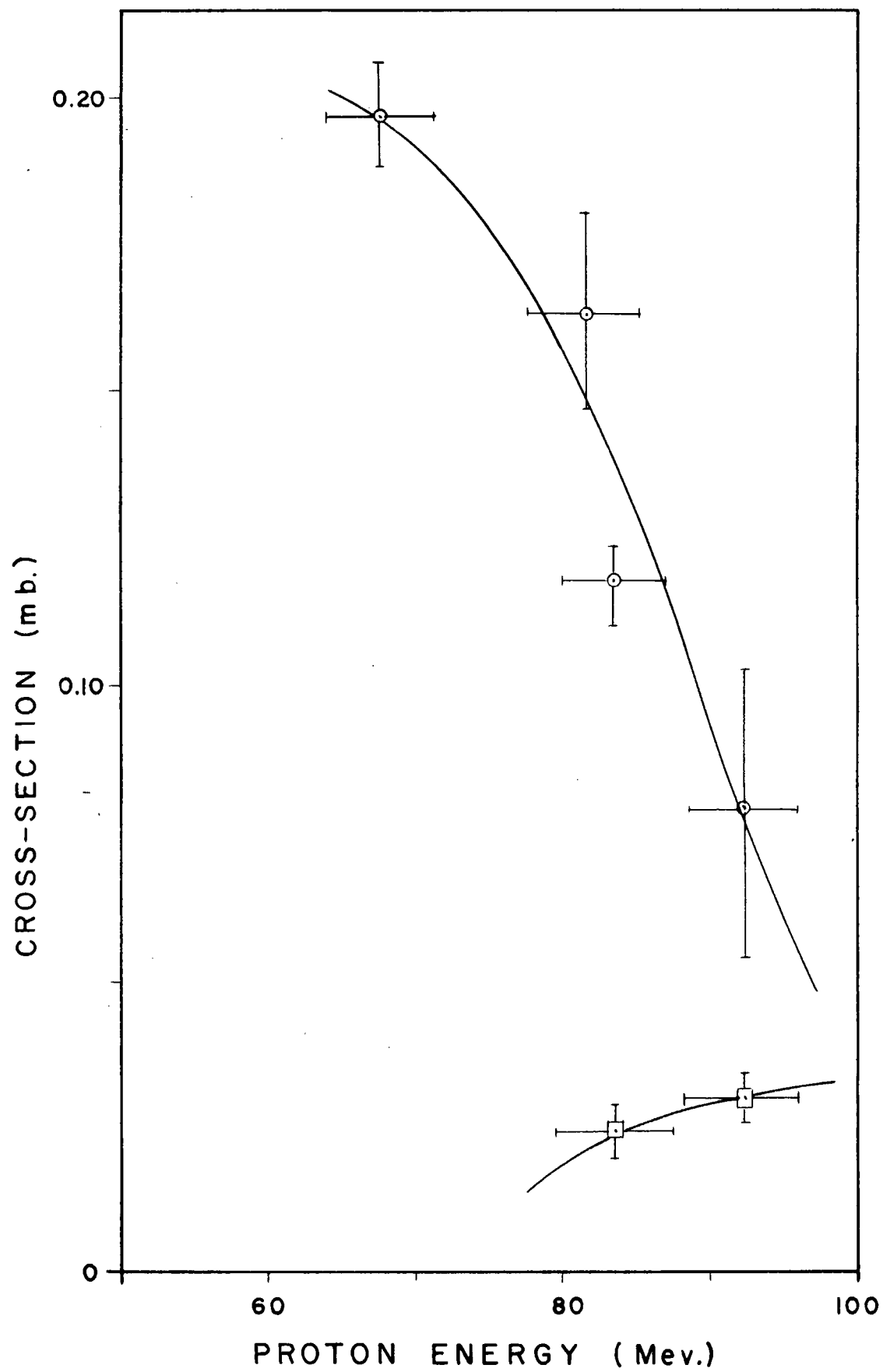
FIG. 50

Figure 51

Absolute Excitation Function for the Formation of
Ca^{47} and Ca^{45}.

Note the separate ordinates.

⊙ $Co^{59}(p,8p5n)Ca^{47}$

⊡ $Co^{59}(p,8p7n)Ca^{45}$
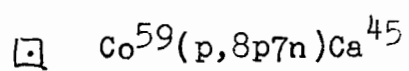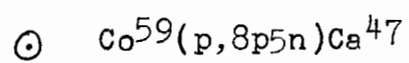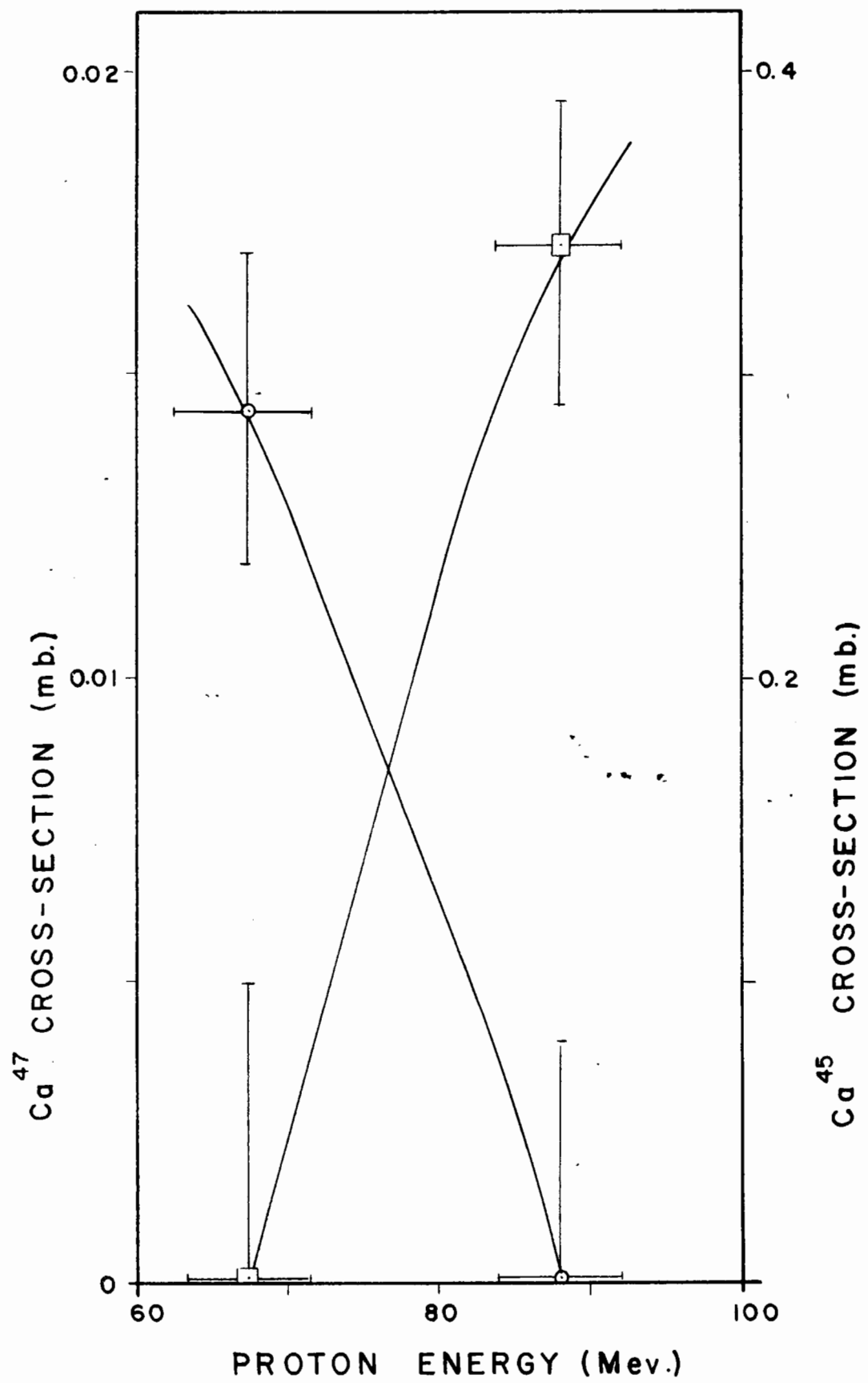
FIG.51

Figure 52

Absolute Excitation Function for Co^{59} $(p,9p7n)K^{44}$.
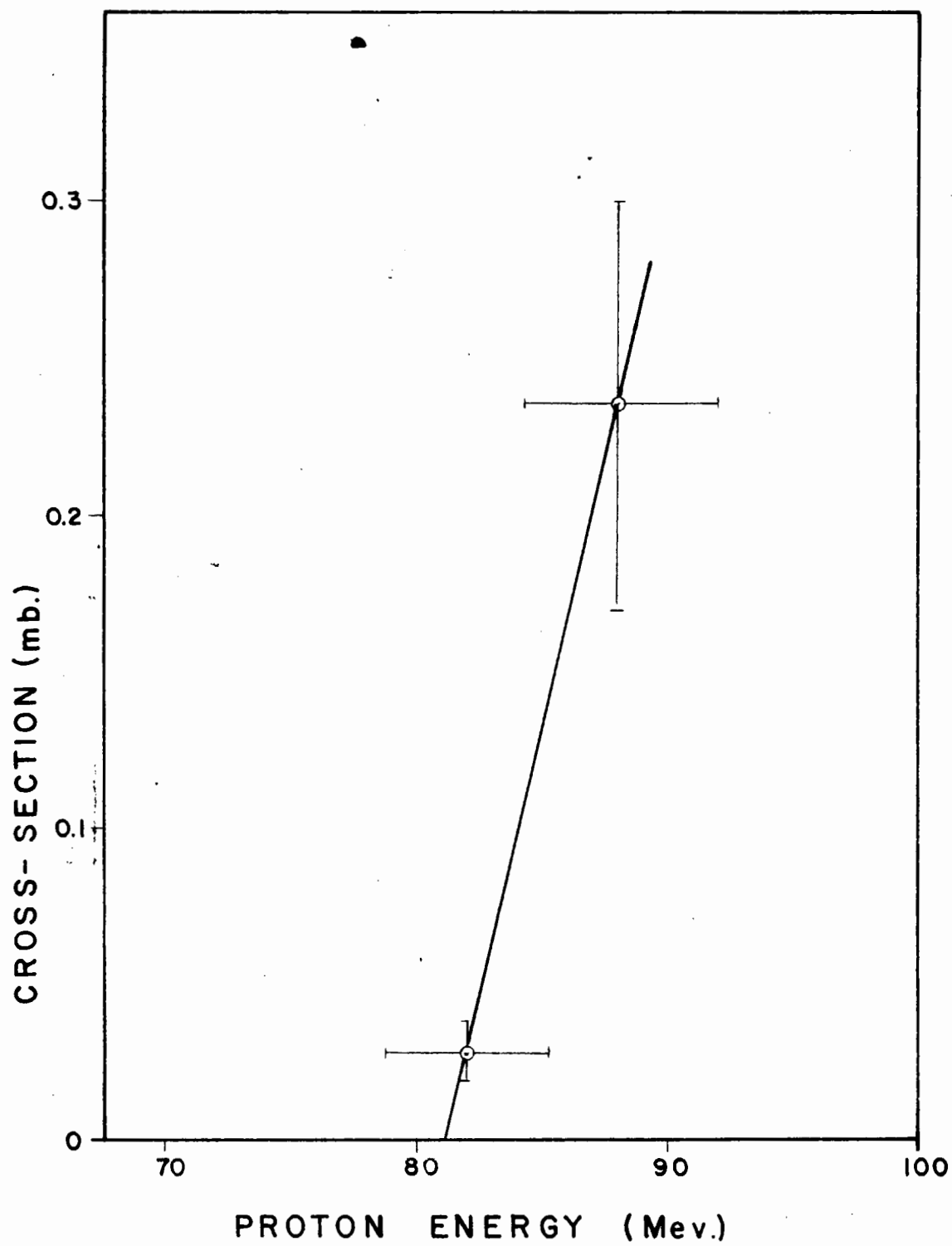
FIG.52

Figure 53

Absolute Excitation Functions for the Formation of K^{43} and K^{42}.

⊙ $Co^{59}(p,9p8n)K^{43}$

⊡ $Co^{59}(p,9p9n)K^{42}$
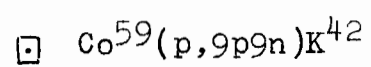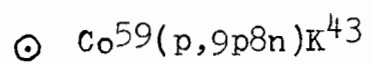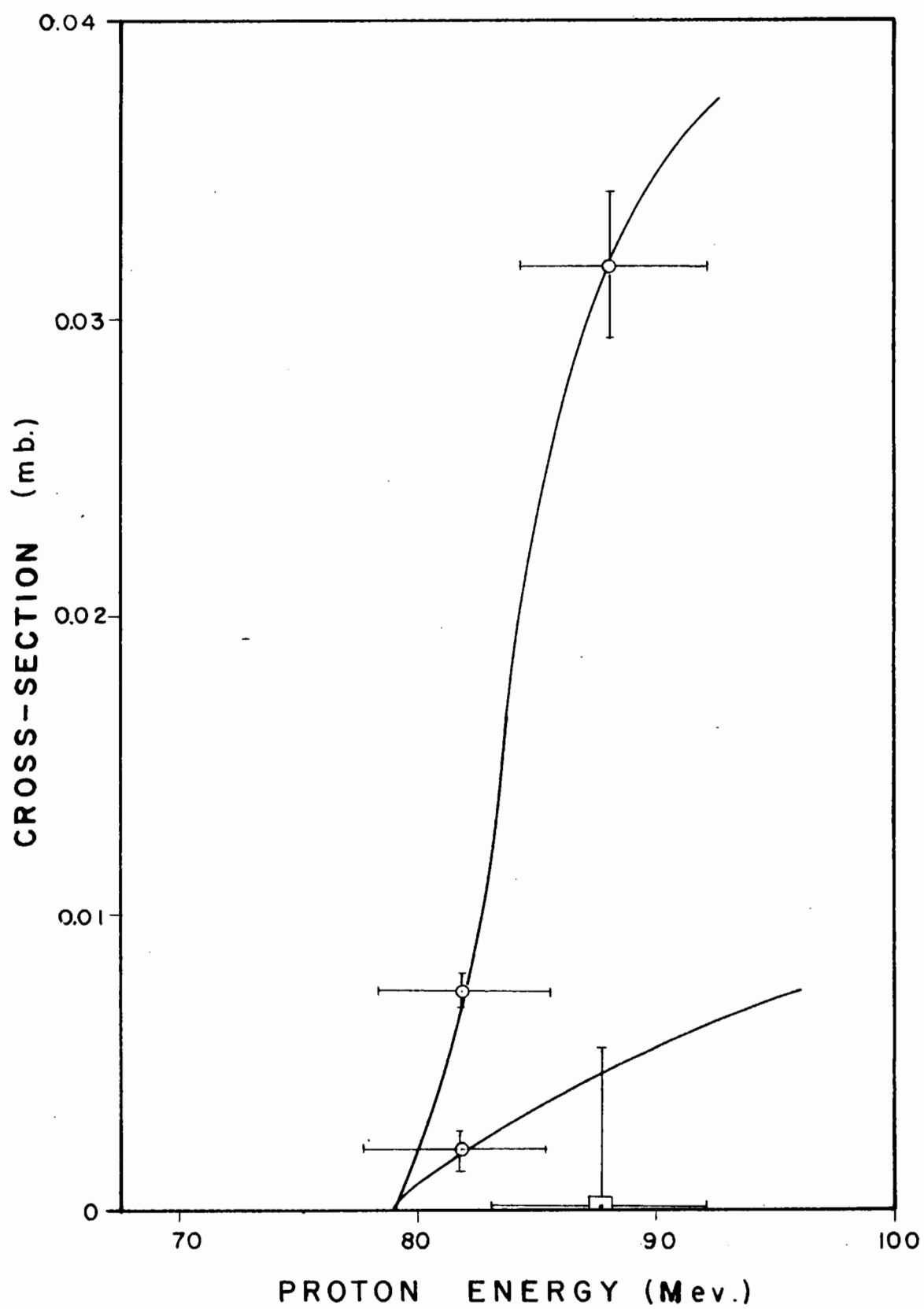
FIG. 53

The two main sources of error in the determination of the cross-sections are:

(1) Uncertainty in the published value of the cross-section of the monitoring reaction. Hintz and Ramsey (190) quote an error in the boron reaction of $\pm 15\%$, and attribute the uncertainty to absorption and scattering in beta counting. Hicks, Stevenson and Nervik (69) do not place any limit of error on their determination of the $Al^{27}(p,3pn)Na^{24}$ cross-sections. The precision of their work is of the order of 3 or 4%. Including an error of about 6% in the determination of the carbon monitor (189) used by Hicks, Stevenson and Nervik, the total error in their values for the aluminum reaction is of the order of 7%.

(2) The second large source of error, the uncertainty in the published branching ratios, is compiled in Table XVII. A reference is quoted for each branching ratio.
Oter sources of error include:

(3) The duration of bombardment was generally known to about 15 seconds. An error of 15 seconds in timing a 15 minute bombardment causes an error in the exponential of the C^{11} monitor of 1.2%. An error of 15 seconds in timing a 30 minute bombardment causes an error of 0.5%.

(4) The estimated error involved in reading the graph of activity versus time for each nuclide ranged from 1% to 40%, depending on the yield, decay scheme and half-life of the nuclide.

(5) Sensitivity Drift of Scintillation Spectrometer   1.3%

(6) Geometry Calibration of Scintillation Spectrometer   3%

(7) Calibration of Geiger-Muller Counter   3%

(8) Reading the Graph of the Monitor   0.5%

(9) In the separation of calcium from nickel by successive dimethylglyoxime precipitations, duplicate chemical yield determinations were made and the uncertainty in chemical yield is an added cause of error in such irradiations.

Table XVIII

Chemical Yield Determination

Irradiation No.	Element	Chemical Yield, %
30	Ni	50.7 ± 2.0
30	Ca	13.9 ± 2.0
31	Ni	42.4 ± 2.0
31	Ca	16 ± 6

(10) Dilution - negligible

(11) Reproducibility of counting grometry - negligible

(12) Ratio of Co:B or Co:Al_2O_3 of the targets - negligible

(13) Recoils of reaction products out of the target will be an additional source of error. Sugarman, Campos, and Wielgoz (215) found that for bismuth targets of thickness

32 mg/cm^2 bombarded with 450 Mev. protons less than 0.08% of the total activity recoiled out of the target. Since (a) proton energies in this work were less than 100 Mev. and (b) the targets used were about 4 times as thick as those used by Sugarman et al., the fraction of the total activity recoiling out of the target will be very much less than 0.08%, i.e. negligible.

The errors shown in Figures 35 to 53 do not include errors (1) and (2) above, because these errors are not un-certainties in the experimental work described in this thesis. The square root of the sum of the squares of the remaining errors as calculated in Table XIX is the vertical uncertainty shown in the excitation functions.

The limit of error shown horizontally on Figure 35 to 53 is the error in cyclotron energy, due to oscillations of the proton beam. This uncertainty causes an error ranging from 2.3 Mev. at 25 Mev. to 3.8 Mev. at 95 Mev.

Table XIX

Typical Calculation of Error in the Values of the Cross-Sections

Nuclide	Irrad. No.	% Error Due to					Root of Sum of Squares (%)
		Counter Calib.	Nuclide Graph	Monitor Graph	Timing	Chem. Yield	
Ni^{57}	21	4	0.71	0.64	0.8	–	4.2
	31	3	0.22	2.1	0.0	4.7	5.9
Ni^{56}	31	6	50	2.1	0.0	4.7	51
Co^{58m}	21	4	12.5	0.6	0.8	–	13
Co^{58}	21	4	17	0.6	0.8	–	18
Co^{56}	29	4	38	7.8	0.0	–	39
Co^{55}	29	3	3.2	7.8	0.0	–	9
Fe^{53}	26	4	25	4.9	1.2	–	26
Fe^{52}	21	4	36	0.6	0.8	–	36
Mn^{56}	26	4	1.2	4.9	1.2	–	7
Mn^{54}	21	4	10	0.6	0.8	–	10
Mn^{52m}	33	3	19	2.6	0.0	–	20
Mn^{52}	22	4	16	1.3	1.2	–	16
Cr^{51}	31	3	24	2.1	0.0	–	24
Cr^{49}	31	3	11	2.1	0.0	–	11
Sc^{49}	33	3	7	2.6	0.0	–	8
Sc^{48}	33	3	6	2.6	0.0	–	7
Sc^{46}	33	3	4	2.6	0.0	–	6
$Sc^{43,44}$	33	3	3	2.6	0.0	–	5
Ca^{47}	31	3	20	2.1	0.0	37	42

Table XIX (Contd.)

Nuclide	Irrad. No	% Error Due to				Chem. Yield	Root of Sum of Squares (%)
		Counter Calib.	Nuclide Graph	Monitor Graph	Timing		
Ca^{45}	30	3	1.4	7.8	0.0	14	16
K^{44}	30	3	24	7.8	0.0	-	25
K^{43}	30	3	0.6	7.8	0.0	-	8
K^{42}	29	3	5	7.8	0.0	-	10

IV. DISCUSSION AND CONCLUSIONS

The discrepancy between the excitation function for the formation of Ni^{57} reported in this thesis (see Figure 35) and that reported by Sharp, Diamond and Wilkinson (45) is fairly large. The thresholds and energies for maximum yield of the two curves agree closely. However, the shapes of the two curves differ greatly.

For proton energies above 60 Mev. the values obtained in the present work are considerably lower than those previously reported. The discrepancy cannot be due to use of monitoring reaction, since both Ni^{57} excitation functions are based on the same monitoring reaction--the formation of Na^{24} in aluminum. Identical values of the cross-section of the monitoring reaction (see Figure 4) were used in both cases.

For proton energies below 60 Mev. the excitation function reported in this thesis has higher values than the curve published by Sharp, Diamond and Wilkinson, rising to a value 3.6 times larger than the maximum yield published by them. Sharp, Diamond and Wilkinson used the $Al^{27}(p,3pn)Na^{24}$ reaction. For proton energies below 60 Mev., the present work is based on the monitoring reaction $B^{11}(p,pn)C^{11}(190)$ which has an associated error of about 15% (see discussion of errors in Section III). The discrepancy between our results

and those of Sharp, Diamond and Wilkinson may be due, at
least below 60 Mev., to error either in the boron or in the
aluminum monitoring reaction. The quoted error of 15% for
the boron excitation function will not, however, explain the
360% discrepancy observed.

The value shown in Figure 35 at 68 Mev. was obtained
using the Na^{24} monitor, whereas the value at 60 Mev. was obtain-
ed using C^{11} monitor. The continuity between these two values
is a check on the validity of the results reported here un-
less some unknown error is being systematically made. As a
further check, the value at 40 Mev. was obtained by counting
the beta radiation of Ni^{57} with a Geiger-Mueller tube, while
the values at 33 Mev. and 42 Mev. were obtained by counting the
annihilation radiation of Ni^{57} in a NaI(Tl) scintillation spect-
rometer. The values at 33, 40, and 42 Mev. lie on a smooth
curve. Sharp, Diamond and Wilkinson used a stacked foil tech-
nique. On the other hand, each of the points shown in Figure
35 is an independent determination. For these three reasons,
it is the author's opinion that the values reported in this
thesis may more closely represent the Ni^{57} excitation function
than the values reported by Sharp, Diamond and Wilkinson.

The very high yield of $Co^{58,58m}$ observed by previous
investigation (42) (45) has been confirmed in the present work.
This high yield may be explained by the so-called "pick-up"
process, in which the incoming proton interacts with a neutron
in the nucleus and departs as a deuteron.

The excitation functions for 4 particle emission are of special interest. The Ni^{56}, Co^{56} and Mn^{56} excitation functions observed here are quite different from those reported by Sharp, Diamond and Wilkinson (see Figures 36, 39 and 43). Figure 54 shows the excitation functions for 4 particle emission normalized to the same maximum yield. The striking similarity among the three curves is an argument for the accuracy of the work described in this thesis.

Yields for 9 particle emission, i.e. Cr^{51} and Mn^{51}, were smaller than the yields reported by Sharp, Diamond and Wilkinson by a factor of about ten.

It is of interest to intercompare the scandium results. The excitation functions of Sc^{49}, Sc^{48} and Sc^{46}, 11, 12 and 14 particle emission respectively, follow the same pattern, rising from a threshold at about 60 Mev. to a peak at about 67 Mev. and then falling off. This fall-off coincides with a rise in the yield of $Sc^{44,43}$ (16 and 17 particle emission).

Examination of the various yields as a function of Z shows that the bulk of the yield occurs in the elements with Z within 2 or 3 units of that of the target. Similar results have been obtained in previous spallation studies (see Section I). Such a yield pattern gives evidence for the fact that the incoming proton leaves only a small fraction of its energy in the nucleus.

Figure 54

Excitation Functions for Four Particle
Emission Normalized to Identical Maximum
Yield

— . — .	Ni^{56}
- - - - - - -	Co^{56}
——————	Mn^{56}
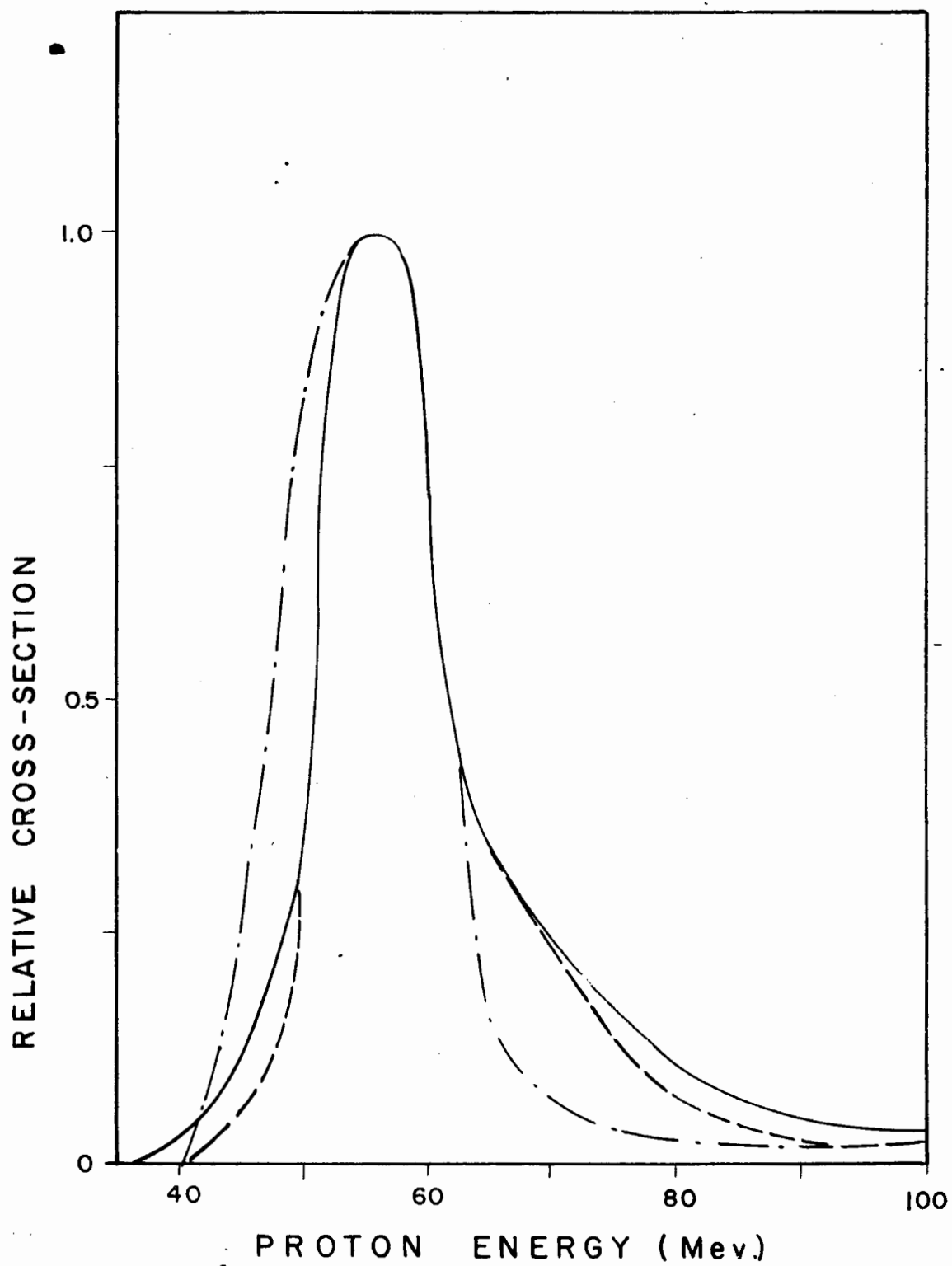
FIG. 54

Rudstam (38) (216) (207) has proposed an empirical formula which describes the cross-sections of the spallation products of medium weight elements. Rudstam has applied his formula to several spallation studies and has shown agreement between experimental and calculated cross-sections within a factor of about two on the average for most spallation groups. The formula is

$$\ln \sigma (A, Z) = PA - Q - R(Z - SA)^2 \qquad ...(14)$$

where $\sigma(A, Z)$ is the formation cross-section of the nuclide with the mass number A and the atomic number Z, and P,Q,R and S are constants.

The cross-section formula (14) for a given element bombarded with particles of a given kind and a given energy is determined from the experimentally determined cross-sections by choosing an arbitrary value for the parameter S, and then using the method of least squares to determine the best values of P,Q and R from the known data of $\ln \sigma(A, Z)$, A and $(Z - SA)^2$.

The experimental cross-sections for the determination of the parameters in equation (14) should be the independent cross-sections for primary spallation products. However, Rudstam points out that, since the independent cross-section of a nuclide is usually much lower than the independent cross-section of its daughter, the measured cross-sections can be used.

For comparison with the formula, the cross-section of a nuclide must be the sum of its isomers, e.g. Mn^{52m} plus Mn^{52}. Rudstam suggests that the calculations be limited to between 30 and 3 mass numbers below the lowest mass number of the target isotopes, in this case, limited to between $A = 56$ and $A = 29$.

Cross-sections were calculated for comparison with the experimental data obtained at 90 Mev. and at 60 Mev. A sample calculation for the data at 90 Mev. follows.

Applying the general method of least squares (217) to the case of k unknowns $(k = 3)$ determined by 14 sets of experimental results

$$z = u_1 x_1 + u_2 x_2 + u_3 x_3 \qquad \ldots (15)$$

where z, u_1, u_2, and u_3 are quantities that can be observed. Let n $(n = 14)$ sets of observations be made giving

$$_1z = {_1u_1}x_1 + {_1u_2}x_2 + {_1u_3}x_3$$

$$_2z = {_2u_1}x_1 + {_2u_2}x_2 + {_2u_3}x_3$$

$$_3z = {_3u_1}x_1 + {_3u_2}x_2 + {_3u_3}x_3 \qquad \ldots (16)$$

Since $n > k$, the problem is to assign values to x_1, x_2, and x_3 which minimize inconsistencies. Then by the method of least squares, one obtains 3 equations giving the 3 unknowns x_1, x_2, and x_3.

$$x_1 \sum (u_1)^2 + x_2 \sum (u_1 u_2) + x_3 \sum (u_1 u_3) = \sum (u_1 z)$$

$$x_1 \sum (u_1 u_2) + x_2 \sum (u_2)^2 + x_3 \sum (u_2 u_3) = \sum (u_2 z)$$

$$x_1 \sum (u_1 u_3) + x_2 \sum (u_2 u_3) + x_3 \sum (u_3)^2 = \sum (u_3 z)$$
$$\ldots (17)$$

Changing symbols to agree with the form of Rudstam's equation

$$z = u_1 x_1 + u_2 x_2 + u_3 x_3 \qquad \ldots (15)$$

becomes

$$\ln \sigma (A,Z) = AP - Q - (Z - SA)^2 R \qquad \ldots (14)$$

where $x_1 = P$ $\qquad u_1 = A$

$\qquad x_2 = Q$ $\qquad u_2 = -1$

$\qquad x_3 = R$ $\qquad u_3 = -(Z - SA)^2$

$\qquad z = \ln \sigma (A,Z)$

Tabulation of $u_1 u_2$ etc. gave $\sum u_1 u_2$, $\sum u_2 u_3$ etc. For example, assuming $S = 0.4680$, for the experimental data at 90 Mev., the 3 equations defining x_1, x_2, and x_3 are

$$34,965 \ x_1 - 696.5 \ x_2 - 957.4 \ x_3 = -1136.9$$

$$-696.5 \ x_1 + 14.00 \ x_2 + 19.00 \ x_3 = 23.90$$

$$-957.4 \ x_1 + 19.00 \ x_2 + 38.61 \ x_3 = 46.12 \qquad \ldots (18)$$

Solution of the equation (18) may be carried out by several methods. The method chosen was the Doolittle method (218)

for solving a system of symmetric simultaneous equations[*].
Application of the method gave

$$x_1 = P = 0.2151$$
$$x_2 = Q = 10.687$$
$$x_3 = R = 1.269 \qquad \qquad \dots(19)$$

The logarithms of the calculated cross-sections were then
found from equation (14).

The difference between the calculated and observed
logarithms of the cross-sections, y, was tabulated for the 14
nuclides. The root mean square error, E, of the logarithm of
the cross-sections was then calculated from

$$E = \sqrt{\frac{\sum_{i=1}^{14} y_i}{14-1}} \qquad \qquad \dots(20)$$

where the sum of the squares was divided by the number of
measurements minus one because the number of measurements was
less than 30 (219). The root mean square error in the cross-
sections is given by e^E. Different values of S were then
tried until the minimum e^E was found. The results are
shown in Table XX.

---

* For the explanation of the Doolittle method the author
  is indebted to Mr. A. Asimakopulos, Lecturer, Department
  of Economics, McGill University.

Table XX

Calculation of the Parameters[*] P,Q and
R for Cobalt Bombarded with 90 Mev. Protons

P	Q	R	S	e^E
0.163	8.39	1.07	0.4712	6.05
0.215	10.69	1.27	0.4680	4.96
0.286	14.31	1.09	0.4630	9.37

[*] Calculated from 14 experimentally determined cross-sections.

The next step was to plot e^E as a function of
S.   The value of S giving the minimum value of e^E was chosen
as 0.468 ± 0.001. For this value of S, $e^E = 5.0$ which
means that the calculated cross-sections agree with the
experimental cross-sections within a factor of 5.0 on the
average. Using the set of parameters just chosen, i.e.
S = 0.468, P = 0.215, Q = 10.69, R = 1.27, calculation of
the cross-sections from equation (14) gave the results shown
in Table XXI for 90 Mev. protons incident on cobalt.

A series of calculations similar to those described
were applied to the experimental data obtained at 60 Mev.
The different values obtained for P, Q and R as a function
of S are shown in Table XXII.

Table XXI

Calculated Cross-Sections for Cobalt Bombarded with 90 Mev. Protons

Nuclide	Observed Cross-Section (mb.)	Calculated Cross-Section (mb.)
Ni^{56}	0.010 ± 0.004	0.066
Co^{56}	$5.6 \quad \pm 2.4$	1.76
Co^{55}	$0.71 \quad \pm 0.06$	0.42
Fe^{52}	0.164 ± 0.012	0.050
Mn^{56}	0.762 ± 0.038	0.611
$Mn^{52,52m}$	$8.0 \quad \pm 1.2$	0.94
Cr^{51}	$2.60 \quad \pm 0.21$	1.3
Cr^{49}	0.038 ± 0.010	0.20
Sc^{48}	0.0030 ± 0.0008	0.046
Sc^{46}	$0.093 \quad \pm 0.010$	0.32
$Sc^{43,44}$	0.0280 ± 0.00015	0.16
Ca^{45}	$0.36 \quad \pm 0.06$	0.088
K^{44}	$0.30 \quad \pm 0.06$	0.012
K^{43}	$0.035 \quad \pm 0.003$	0.048

Table XXII

Calculation of the Parameters[*] P,Q and
R for Cobalt Bombarded with 60 Mev.
Protons

P	Q	R	S	e^E
0.576	27.75	1.27	0.4660	3.49
0.526	25.03	1.37	0.4680	3.20
0.483	22.86	1.36	0.4700	3.39

* Calculated from 11 experimentally observed cross-sections.

The minimum value of e^E was selected as 3.2, which means that the calculated cross-sections reproduce the experimental cross-sections within a factor of 3.2 on the average. The value of S corresponding to this minimum e^E is 0.468 ± 0.001, exactly the same value of S as was obtained for the data at 90 Mev. Using S = 0.468, P = 0.526, Q = 25.03 and R = 1.37, the cross-sections were calculated from equation (14). They are listed in Table XXIII.

The extent of agreement between calculated and experimental cross-sections can be shown graphically as follows: Equation (14) may be written

$$\ln\sigma - PA + Q = -R(Z - SA)^2 \qquad \ldots(21)$$

Equation (21) represents a parabola where the abscissa is $(Z - SA)$ and the ordinate is $\ln\sigma - PA + Q$. Such parabolas are shown in Figures 55 and 56. Although the agreement between

Table XXIII

Calculated Cross-Sections for Cobalt Bombarded with 60 Mev. Protons

Nuclide	Observed Cross-Section (mb.)			Calculated Cross-Section (mb.)
Ni^{56}	1.1	$\pm$	0.7	1.03
$Co^{58,58m}$	214	$\pm$	61	232
Co^{55}	9	$\pm$	2	5.6
Fe^{53}	15	$\pm$	6	2.4
Fe^{52}	0.07	$\pm$	0.05	0.23
Mn^{56}	8	$\pm$	2	11
Mn^{54}	75	$\pm$	10	26
$Mn^{52,52m}$	6.2	$\pm$	1.0	5.5
Sc^{48}	0.008	$\pm$	0.003	0.066
Sc^{46}	0.21	$\pm$	0.03	0.30
Ca^{47}	0.017	$\pm$	0.004	0.003

Figure 55

Agreement Between Calculated and Experimental
Cross-Sections for Cobalt Bombarded with 90
Mev. Protons

⊙   experimental points
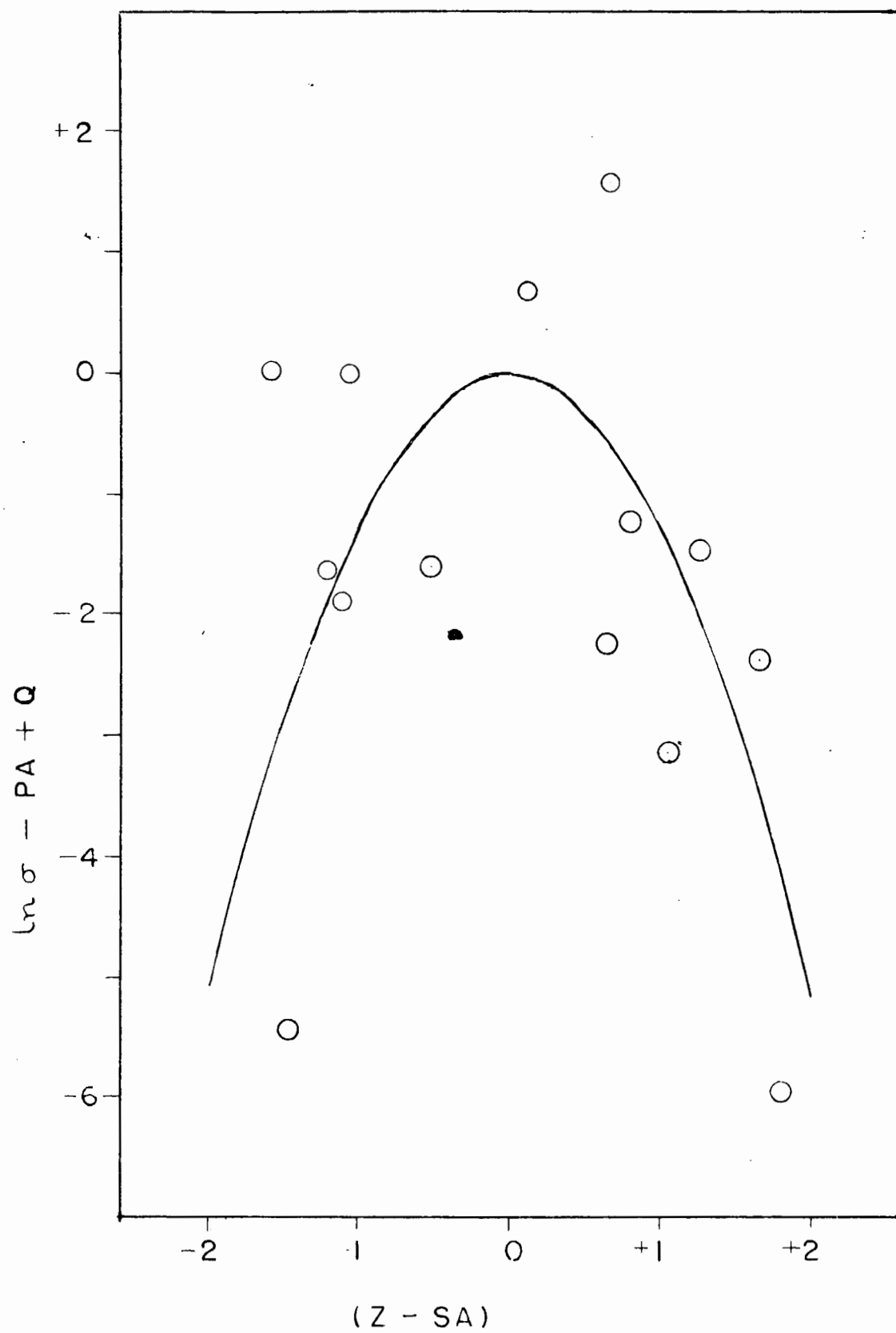
—   Rudstam's equation

FIG. 55

Figure 56

Agreement Between Calculated and Experimental
Cross-Sections for Cobalt Bombarded with 60
Mev. Protons

⊙ experimental points

— Rudstam's equation
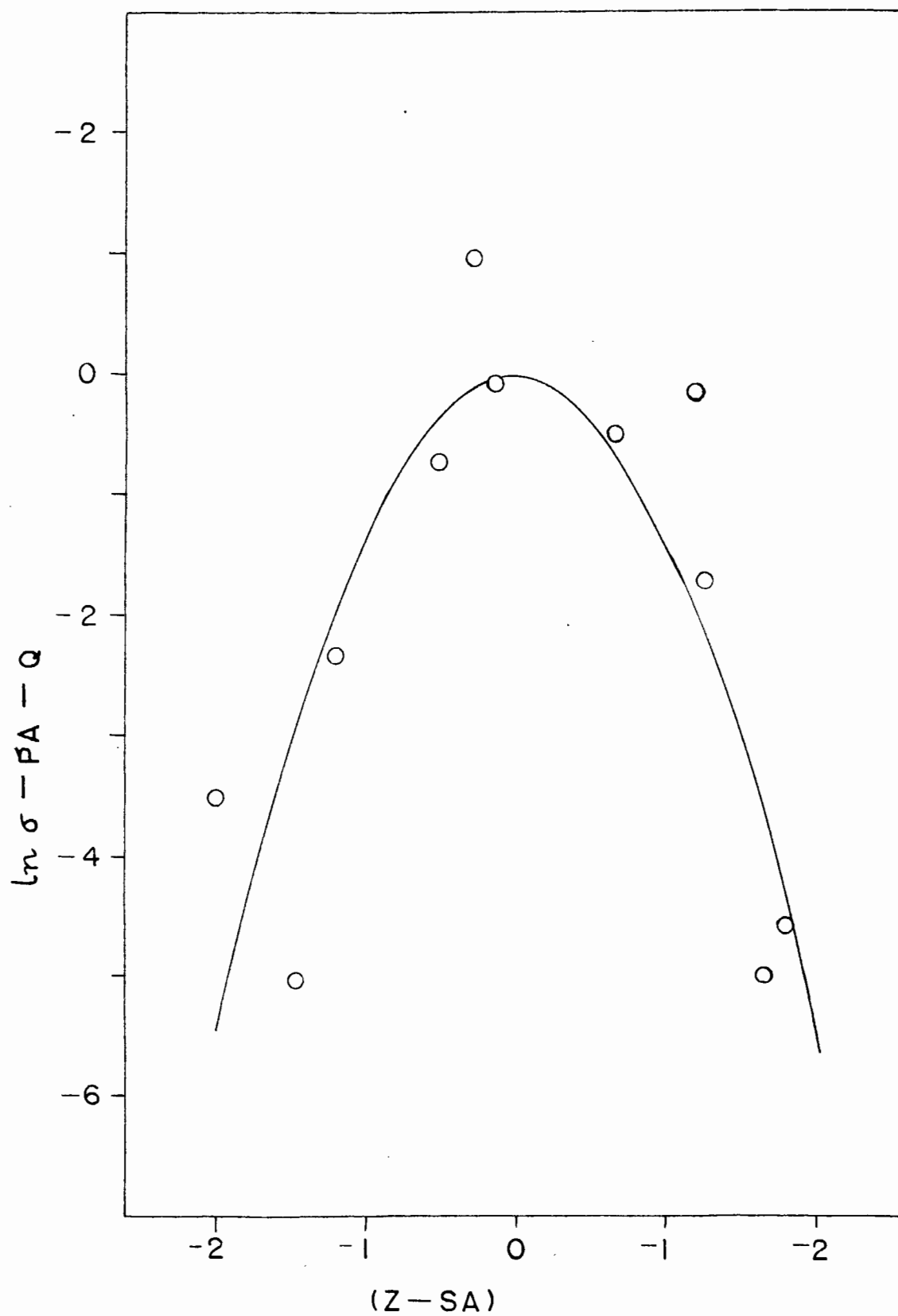
FIG. 56

the calculated and experimental cross-sections is not
as close as in some of the calculations published by
Rudstam (207), the experimental data do exhibit a parabolic
trend.

The purpose in carrying out the above calculations
was to enable the comparison of the cross-section dis-
tributions as denoted by P,Q,R and S with the values of
these parameters obtained in other spallation studies.
Table XXIV is a compilation of the best values of these
parameters for cobalt irradiated with protons.

Rudstam (207) has shown that P is independent of
mass number and decreases with increasing energy of the bom-
barding particle. From Figure 18 in reference (207) P should
be about 0.6 if it is to lie on a smooth curve with Rudstam's
values. However, we found P for 90 Mev. protons incident on
cobalt to be 0.22. There seems to be no ready explanation of
this difference. P for 60 Mev. protons is 0.53 , in closer
agreement.

The function of Q is only to establish the absolute
scale of the cross-sections.

The cross-section formula is based on the assumption,
among others (207), that the charge distribution curve, that
is the independent yield versus the atomic number for isobars,
is a gaussian function of the atomic number. The value of R
represents the width of the charge distribution curve. Rudstam

Table XXIV

The Best Values of the Parameters P,Q,R and S for
Cobalt Bombarded with Protons

Proton Energy (Mev.)	Number of Cross-Sections	P	Q	R	S	e^E	Reference
60	11	0.526	25.03	1.37	0.468	3.20	this work
90	14	0.215	10.69	1.27	0.468	4.96	this work
170	17	0.353	14.06	1.97	0.470	1.48	(207)
360	24	0.232	8.96	1.28	0.468	2.06	(207)

found that R is independent of both mass number of the
target and irradiation energy, and is of the order of
1.5 ± 0.4.

For 90 Mev. protons incident on cobalt, we obtained
a value of R of 1.27, and for 60 Mev. protons a value of 1.37.
Both values are of the same order of magnitude as the values
calculated by Rudstam for cobalt irradiated with 170 Mev.
and 360 Mev. protons (see Table XXIV). The results obtained
in the present investigation thus agree with Rudstam's
findings that the width of the charge distribution curve is
independent both of irradiation energy and of the mass number
of the target.

Instead of the parameter S, Rudstam prefers to
study the trend in a new parameter, U, defined as

$$U = S - \frac{Z}{A} \qquad \qquad \ldots(21)$$

where Z and A refer to the charge and mass of the
hypothetical "compound nucleus". In the present case

$$U = 0.468 - 28/60$$
$$= 0.001$$

for irradiation with both 60 and 90 Mev. protons. According
to Rudstam, the parameter U can be taken as a measure of the
preference of neutron emission. U will be zero if the ratio
of emitted protons: emitted neutrons is the same as the ratio
protons: neutrons in the "compound nucleus" which for Ni^{60}

is 1.14. A positive value of U indicates increased prob-
ability of neutron emission. Since in the present case U
is positive, but small, we may conclude that ratio of
neutron to proton emission is not very much greater than the
value 1.14.

Porges (83) states that two theoretical inferences
may be drawn from excitation functions:

(1) The shape of the excitation excitation functions may
be compared to calculations based on statistical evaporation
theory, and

(2) the experimentally observed total cross-section may
be compared to the theoretical cross-section.

Addition of the experimentally observed cross-
sections gives a minimum value of the total reaction cross-
section, excluding stable nuclides and nuclides for which
the yield was not determined. To a first approximation, the
geometrical cross-section can be calculated from

$$\sigma = \pi R^2 \quad \text{where } R = 1.37 \times 10^{-13} \ A^{1/3} \quad (220)$$

For the case of Co^{59}, such a calculation yields $\sigma = 896$ mb.
The % transparency is equal to $100\left(1 - \dfrac{\text{observed total cross-section}}{\text{geometrical cross-section}}\right)$

The data are shown in Table XXV.

For comparison with the results presented in this
thesis, the maximum % transparency has been calculated from
Table VI for the other studies on the interaction of protons

Table XXV

Experimentally Determined % Transparency
for the Interaction of Protons with Cobalt

Proton Energy (Mev.)	Minimum Total Cross-Section (mb.)	Maximum Transparency (%)	Reference
30	995 - 90	0 - 11	
50	653 - 158	27 - 17	this work
70	332 - 199	63 - 22	
90	249 - 191	72 - 23	
60	401 - 226	55 - 25	(45)
100	312 - 145	65 - 16	
60	812 - 404	9 - 36	
100	425 - 203	53 - 23	(42)
170	223 - 101	75 - 11	

with cobalt. The agreement with the results of the present work is excellent.

The results shown in Table XXV for protons in the 60 Mev. energy range tend to support the work of Sharp, Diamond and Wilkinson (45) rather than the work of Wagner and Wiig (42).

The experimental results support the picture of nuclear transparency proposed by Serber (14) and agree well with determinations of the degree of transparency of nuclear matter observed for targets other than cobalt. Bernardini et al. (74) gave a value of 33% transparency for AgBr emulsions (A = 100) irradiated with 380 Mev. protons. Perry (221) obtained a value of 13% transparency for AgBr emulsions irradiated with 240 Mev. protons. Caretto (220) gave a value of more than 52% transparency in the spallation of yttrium with 240 Mev. protons. De Juren (222) reported 53% for carbon, 41% for copper and 31% for lead, all irradiated with 270 Mev. neutrons. Batzel (47) obtained a value of 30% transparency for the sum of the experimental and extrapolated cross-sections for 340 Mev. protons incident on copper.

Table XXVI is a compilation of ΔE for different elements where

$$\Delta E = \sigma_{max.} \left[p, xn \right] - \sigma_{max.} \left[p, (x-1)n \right]$$

i.e. the difference in proton energy in Mev. between the

maximum yield of a $[p,xn]$ reaction and a $[p,(x-1)n]$ reaction. For example, the difference between the peak yield of the $(p,4n)$ reaction and the $(p,3n)$ reaction for protons incident on cobalt is 13 Mev.

Table XXVI

Proton Energy for Maximum Yields of (p,xn) Reactions

Z	Target	ΔE (Mev.)	Reference
5	B	10	(190)
16	S	11	(190)
28	Co	13	(45)
28	Co	13	this work
29	Cu	13	(30)
41	Nb	15	(224)
55	Cs	15	(56)
82	Pb	10	(225)
83	Bi	11	(73)
90	Th	8	(226)

ΔE changes very little in going from (p,n) to $(p,5n)$ reactions. See, for example reference (223). A smooth curve can be drawn through a graph of Z versus ΔE drawn from the data in Table XXIII. (see Figure 57). From the graph, the experimenter can then estimate within two or three Mev. the proton energy at which a desired reaction will exhibit maximum yield.

Figure 57

Proton Energy for Maximum Yield of
(p,xn) Reactions
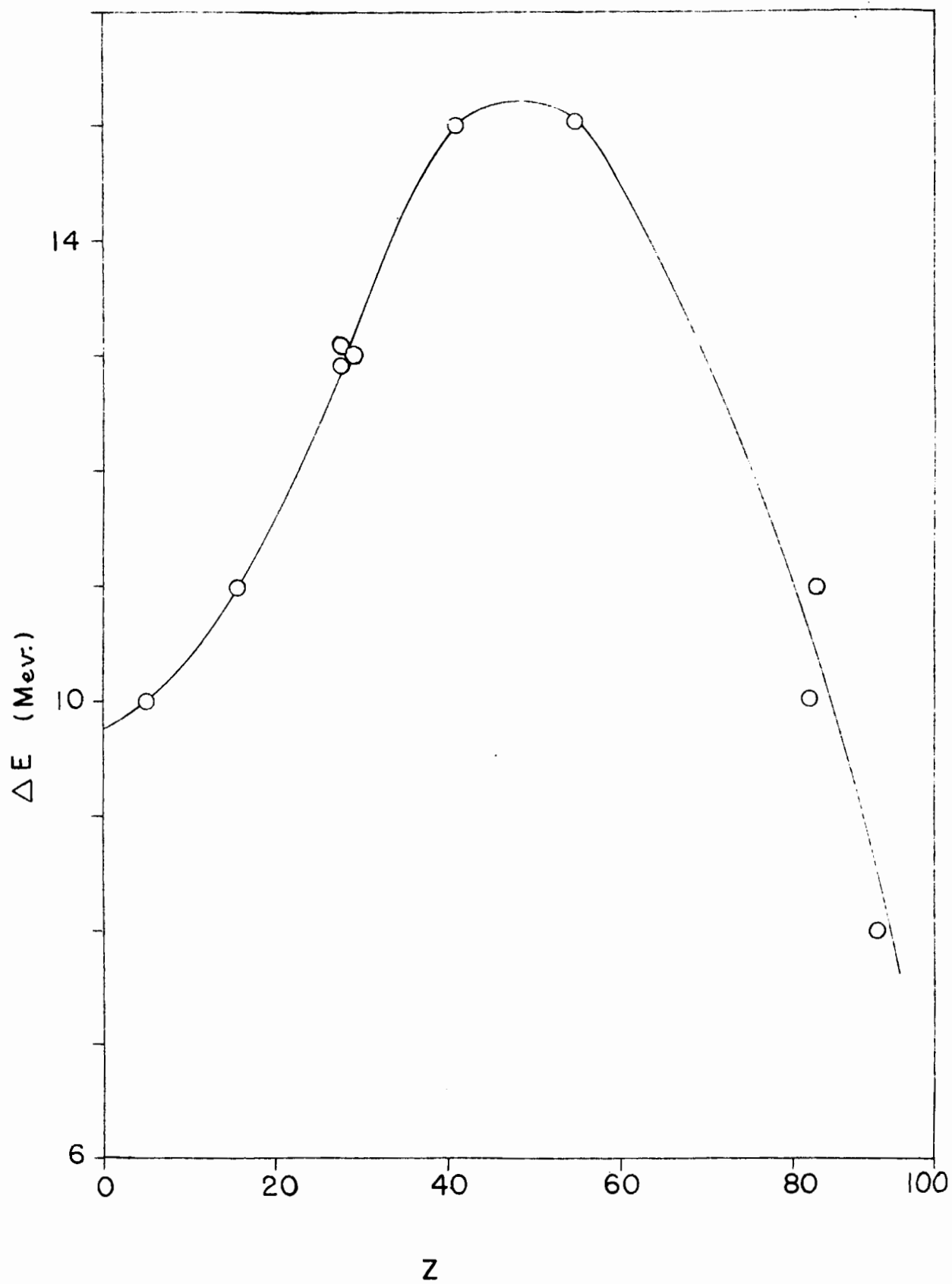
FIG. 57

SUMMARY AND CONTRIBUTION TO KNOWLEDGE

Cobalt has been bombarded with protons of energies up to 100 Mev. in the McGill synchro-cyclotron, and absolute excitation functions have been determined for 26 nuclides formed as spallation products. The half-lifes of Ni^{55} and Ni^{54} have been found to be shorter than 5 minutes or longer than 1 year.

The results have been discussed in the light of previous work. Rudstam's formula for the calculation of cross-sections of medium weight elements has been applied to the experimental results. The calculated cross-sections agree with the experimental values within a factor of 3.2 on the average at 60 Mev., and within a factor of 5.0 on the average at 90 Mev. The ratio of neutron to proton emission was shown to be about 1.2.

The % transparency of cobalt nuclei has been determined experimentally as a function of proton energy. The % transparency observed in other spallation studies of cobalt has been calculated from the reported cross-sections. Excellent agreement was found with the work reported in this thesis.

A graph has been constructed giving the proton energy at which maximum yields of (p,xn) reactions occur for targets of various Z. Use of this graph should enable the experimenter to estimate closely the proton energy at which a desired reaction will exhibit maximum yield.

REFERENCES

1. Rutherford, E. Z. Electrochem. 38:476. 1932.

2. Chadwick, J. Proc. Roy. Soc. London A142:1. 1933.

3. Fermi, E. et al. Proc. Roy. Soc. London A146:483. 1934, and A149:522. 1935.

4. Bohr, N. Nature 137:344. 1936.

5. Graetzer, H.G. and Pollard, E.C. Phys. Rev. 98:1184(A). 1955.

6. Bohr, N. and Wheeler, J.A. Phys. Rev. 56:426. 1939.

7. Lindqvist, T. and Mitchell, A.C.G. Phys. Rev. 95:444. 1954.

8. Konopinski, E.J. and Bethe, H.A. Phys. Rev. 54:130. 1938.

9. Weisskopf, V.F. and Ewing, D.H. Phys. Rev. 57:472. 1940.

10. Friedlander, Miller, Wolfgang, Hudis, and Baker. Phys. Rev. 94:727. 1954.

11. Blatt, J.M. and Weisskopf, V.F. Theoretical Nuclear Physics, p. 371, John Wiley and Sons Inc., N.Y. 1952.

12. Ghoshal, S.N. Phys. Rev. 80:939. 1950.

13. Gugelot, P.C. Phys. Rev. 81:51. 1951.

14. Serber, R. Phys. Rev. 72:1114. 1947.

15. Whitmore, B.G. and Dennis, G.E. Phys. Rev. 84:296. 1951.

16. Graves, E.R. and Rosen, L. Phys. Rev. 89:243. 1953.

17. Gugelot, P.C. Phys. Rev. 93:425. 1954.

18. Brolley, J.E. Jr., Fowler, J.L. and Schlacks, L.K. Phys. Rev. 88:618. 1952.

19. Nabholtz, H., Stoll, P. and Waffler, H. Phys. Rev. 86:1043. 1952.

20. Toms, M.E. and Stevens, W.E. Phys. Rev. 95:1209. 1954.

21. Shapiro, M.   Phys. Rev. 90:171.   1953.

22. Feshbach, H. and Weisskopf, V.   Phys. Rev. 76:1550.   1940.

23. Bradt, H.L. and Tendham, D.J.   Phys. Rev. 72:1117.   1947.

24. Waffler, H.   Helv. Phys. Acta 23:239.   1950.

25. Cunningham, Hopkins, Lindner, Miller, O'Conner, Perlman, Seaborg and Thompson.   Phys. Rev. 72:739.   1947.

26. Chupp, W., McMillan, E.M.   Phys. Rev. 72:873.   1947.

27. Thornton, R. and Senseman, R.W.   Phys. Rev. 72:872.   1952.

28. Cork, McMillan, Peterson and Sewell, quoted in Serber, R. Phys. Rev. 72:1114.   1947.

29. Goldberger, M.L.   Phys. Rev. 74:1269.   1948.

30. Meadows, J.W.   Phys. Rev. 88:143.   1952.

31. Lindner, M. and Perlman, I.   Phys. Rev. 73:1124, 1202. 1948.

32. Hopkins, H.H. Jr., Cunningham, B.B.   Phys. Rev. 73:1406. 1948.

33. Miller, Thompson and Cunningham.   Phys. Rev. 74:347.   1948.

34. Lindner, M. and Perlman, I.   Phys. Rev. 78:449.   1950.

35. Friedlander, G., Hudis, J. and Wolfgang, R.L.   Phys. Rev. 99:263.   1955.

36. Lindner, M.   Phys. Rev. 91:642.   1953.

37. Jones, J.W., Ph.D. Thesis, Dept. of Chemistry, Carnegie Institute of Technology.   1956.

38. Rudstam, S.G.   Phil. Mag. 44:1131.   1953.

39. Heininger, C.G. and Wiig, E.O.   Phys. Rev. 101:1074. 1956.

40. Rudstam, S.G., Stevenson, P.C. and Folger, R.L.   Phys. Rev. 87:358.   1952.

41. Nelson, M.E. and Pool, M.L.   Phys. Rev. 77:682.   1950.

42. Wagner, G.D. and Wiig, E.O. Phys. Rev. 96:1100. 1954.

43. Belmont, E. and Miller, J.M. Phys. Rev. 95:1554. 1954.

44. Wolke, R.L. and Bonner, N.A. Phys. Rev. 102:530. 1956.

45. Sharp, R.D., Diamond, R.M. and Wilkinson, G. Phys. Rev. 101:1493. 1956.

46. Bartell, Helmholtz, Softky and Stewart. Phys. Rev. 80:1006. 1950.

47. Batzel, R.E., Miller, D.R. and Seaborg, G.T. Phys. Rev. 84:671. 1951.

48. Marquez, L. Phys. Rev. 88:225. 1952.

49. Carleson, Acta Chem. Scand. 8: No. 9, 1697. 1954.

50. Coleman, G.H. and Tewes, H.A. Phys. Rev. 99:288. 1955.

51. Vinogradov, A.P. et al. Moscow Conference of Academy of Sciences U.S.S.R. on Peaceful Uses of Atomic Energy. 1955.

52. Worthington, W.J. Jr. M.S. Thesis, University of California Radiation Laboratory UCRL-1627. 1952.

53. Hopkins, H.H. Jr. Phys. Rev. 77:717. 1950.

54. Caretto, A.A. Jr. and Wiig, E.O. Phys. Rev. 103:236. 1956.

55. Kofstad, P.K. Ph.D. Thesis, Univ. of California Radiation Laboratory, UCRL-2265. 1953.

55a. Dropesky, B. Ph.D. Thesis, Dept. of Chemistry, Univ. of Rochester, N.Y. 1952.

56. Fink, R.W. and Wiig, E.O. Phys. Rev. 96:185. 1954.

57. Nervik, W.E. and Seaborg, G. Phys. Rev. 97:1092. 1955.

58. Karraker, D.G. and Templeton, D.H. Phys. Rev. 81:510. 1951.

59. Wolfgang, Baker, Caretto, Cumming, Friedlander and Hudis, Phys. Rev. 103:394. 1956.

60. Miller, J.M. and Friedlander, G. Phys. Rev. 91:485. 1953.

61. Bennett, W.E.   Phys. Rev. 94:997.   1954.

62. Biller, W.F. Thesis, University of California, Radiation
    Laboratory, UCRL-2067.   1953.

63. Murin et al., Conference of the Academy of Sciences
    U.S.S.R. on Peaceful Uses of Atomic Energy.   1955.

64. Sugarman, Duffield, Friedlander and Miller,   Phys. Rev.
    95:1704.   1954.

65. Glass, Carr, Cobble and Seaborg,   Phys. Rev. 98:261(A).
    1955.

66. Perkins, D.H.   Proc. Roy. Soc. London A203:399.   1950.

67. Bartell, F.O. and Softky, S.   Phys. Rev. 84:463.   1951.

68. Dickson, J.M. and Randle, T.C.   Proc. Phys. Soc. London
    A64:902.   1951.

69. Hicks, H.G., Stevenson, P.C. and Nervik, W.E.   Phys. Rev.
    102:1390.   1956.

70. Meadows, J.W. and Holt, R.B.   Phys. Rev. 83:47.   1951.

71. Meadows, J.W. and Holt, R.B.   Phys. Rev. 83:1257.   1951.

72. Bernardini, G., Booth, E.T. and Lindenbaum, S.J.   Phys.
    Rev. 83:669.   1951.

73. Bernardini, G., Booth, E.T. and Lindenbaum, S.J.   Phys.
    Rev. 85:826.   1952.

74. Bernardini, G., Booth, E.T. and Lindenbaum, S.J.   Phys.
    Rev. 88:1017.   1952.

75. Green, A.E. "Nuclear Physics", International Series in
    Pure and Applied Physics.   1955.

76. Fung, Si-Chang and Perlman, I.   Phys. Rev. 87:623.   1952.

77. Segre, E. "Experimental Nuclear Physics II" p. 142.
    John Wiley and Sons Inc.   1953.

78. Eisberg, R.M. and Igo, G.   Phys. Rev. 93:1039.   1954.

79. Cohen, B.L.   Phys. Rev. 98:49.   1955.

80. Batzel, R.E. and Seaborg, G.T.   Phys. Rev. 82:607.   1951.

81. Feld, Fesbach, Goldberger, Goldstein and Weisskopf, U.S. A.E.C. Report NYO-636. 1951. Unpublished.

82. Bleuler, E., Stebbens, A.K. and Tendham, D.J. Phys. Rev. 90:460. 1953.

83. Porges, K.G. Phys. Rev. 101:225. 1956.

84. Maienschein, F. and Meem, J.L. Jr. Phys. Rev. 76:899. 1949.

85. Friedlander, Perlman, Alburger and Sunyar, Phys. Rev. 80:30. 1950.

86. Canada, R. and Mitchell, A.C.G. Phys. Rev. 83:955. 1951.

87. Sheline, R.K. Stoughton, R.W. Phys. Rev. 87:1. 1952.

88. Fink, R.W. Ph.D. Thesis, Univ. of Rochester, N.Y. 1953.

89. Christian, D. and Martin, D.S. Jr. Phys. Rev. 80:1110. 1950.

90. Strauch, K. Phys. Rev. 79:487. 1950.

91. Livingood, J.J. and Seaborg, G.T. Phys. Rev. 60:913. 1941.

92. Cork, J.M., Brice, M.K. and Schmid, L.C. Phys. Rev. 99:703. 1955.

93. Good, W.M., Peaslee, D. and Deutsch, M. Phys. Rev. 69:313. 1946.

94. Cook, C.S. and Tomnovec F.M. Phys. Rev. 104:1407. 1956.

95. Frauenfelder, Levine, Rosoi and Singer, Phys. Rev. 103:353. 1956.

96. Deutsch, M. and Elliot, L.G. Phys. Rev. 65:211. 1944.

97. Craseman, B. and Manley, D.L. Phys. Rev. 98:66. 1955.

98. Alburger, D. and Grace, M. Proc. Phys. Soc. London. A67:280. 1954.

99. Deutsch, M. and Wright, W. Phys. Rev. 77:139. 1950.

100. Grace, M.A., Jones, G.A. and Newton, J.O. Phil. Mag. 8:363. 1956.

101. Burgus, Cowan, Hadley, Hess, Shull, Stevenson and York, Phys. Rev. 95:750. 1954.

102. Cook, C.S. and McDaniels, P.W. Phys. Rev. 62:412. 1942.

103. Elliot, L.G. and Deutsch, M. Phys. Rev. 64:321. 1943.

104. King, Dismuke and Way, Oak Ridge National Laboratory ORNL-1450 Unpublished.

105. Sakai, Dick, Anderson and Kurbatov, Phys. Rev. 95:101. 1954.

106. Darling, B.T., Curtis, B.R. and Cork, J.M. Phys. Rev. 51:1010(A). 1937.

107. Deutsch, M. and Hegran, A. Phys. Rev. 75:1443. 1949.

108. Caird, R.S. and Mitchell, A.C.G. Phys. Rev. 94:412. 1954.

109. Swarthout, J.A. Plutonium Project Report Mon. N-243:4. 1947.

110. Deutsch, Downing, Elliot, Irvine and Roberts, Phys. Rev. 62:3. 1942.

111. Brownell, G.L. and Maletskos, C.J. Phys. Rev. 80:1102. 1950.

112. Bradt, H. et al. Helv. Phys. Acta. 19:222. 1946.

113. Maeder, D. and Preiswerk, P. Phys. Rev. 84:595. 1951.

114. Ridenour, L.N. and Henderson, W.J. Phys. Rev. 52:889. 1937.

115. Rudstam, S.G., Stevenson, P.C. and Folger, R.L. Phys. Rev. 87:358. 1952.

116. Friedlander, G. and Miller, J.M. Phys. Rev. 84:588. 1951.

117. Bartholomew, Hawkings, Merritt and Yaffe, Can. J. Chem. 31:204. 1953.

118. Siegbahn, K. Arkiv Mat. Astron. Fysik 33A: No. 10. 1946.

119. Backofen, E.W. and Herber, R.H. Phys. Rev. 97:743. 1955.

120. Kurbatov, J.D. and Gideon, D. Phys. Rev. 75:328. 1949.

121. Livingood, J.J. and Seaborg, G.T. Phys. Rev. 54:391. 1938.

122. Hemmindinger, A. Phys. Rev. 58:929. 1940.

123. Osborne, R.K. and Deutsch, M. Phys. Rev. 71:467. 1947.

124. Peacock, W.C. and Deutsch, M. Phys. Rev. 69:306. 1946.

125. Keister, G.L. Phys. Rev. 96:855(A). 1954.

126. Nuclear Data, N.B.S. Circular 499. 1950.

127. Burgus, W.H. and Kennedy, J.W. J. Chem. Phys. 18:97. 1950.

128. Koester, L., Z. Naturf. 9A:104. 1954

129. Flammersfield, Von A. and Herr, W. Z. Naturforsch. 7a:649. 1952.

130. Bazorgan, G.A., Irvine, J.W. Jr. and Coryell, C.D. Phys. Rev. 95:781. 1954.

131. Caldwell, D.O. and Stoddart, H.F. Phys. Rev. 81:660(A). 1951.

132. Lyon, W.S. Phys. Rev. 87:1126. 1952.

133. O'Conner, J.J., Pool, M.L. and Kurbatov, J.D. Phys. Rev. 62:413. 1942.

134. Craseman, B. and Easterday, H.T. Phys. Rev. 90:1124. 1953.

135. Wilkinson, J.R. and Sheline, R.K. Phys. Rev. 99:165. 1955.

136. van Lieshout, Greenberg, Koerts and Wu, Phys. Rev. 100:223. 1955.

137. Sheline, R.K. and Wilkinson, J.R.   Phys. Rev. 94:729. 1954.

138. Lyon, W.S.   Phys. Rev. 97:121.   1955.

139. Hayward, R.W. and Hoppes, D.D.   Phys. Rev. 104:183. 1956.

140. Walke, H.   Phys. Rev. 52:777.   1937.

141. Coleman, C.F.   Phys. Rev. 103:647.   1956.

142. Aten, Kool, de Vries and Veenendaal,   Physica 19:1051. 1953.

143. Krisberg, N.L. and Pool, M.L.   Phys. Rev. 75:1693.   1949.

144. Ter-Pogossian, Cook, Porter, Morganstern and Hudis, Phys. Rev. 81:285.   1951.

145. Kubitshek, H.E., Longacre, A. and Goldhaber, M. Phys. Rev. 77:742(A).   1950.

146. Ballon, N.E.   Phys. Rev. 75:1105.   1949.

147. Sharp, R.A. and Diamond, R.M.   Phys. Rev. 96:1713.   1954.

148. O'Kelley, G.D., Lazar, N.H. and Eichler, E.   Phys. Rev. 101:1059.   1956.

149. Walke, H.   Phys. Rev. 57:163.   1940.

150. Andersson, G.   Phil. Mag. 45:621.   1954.

151. Graves, W.E. and Suri, S.K.   Phys. Rev. 101:1368.   1955.

152. Porter, F.T. and Cook, C.S.   Phys. Rev. 81:640.   1951.

153. Miller, A.E. and Deutsch, M.   Phys. Rev. 72:527(A).   1947.

153a. Sorensen, B.N., Dale, B.M. and Kurnatov, J.D.   Phys. Rev. 79:1007.   1950.

154. Nag, B.D. et al.   Ind. J. Phys. 24:479.   1950.

155. Keister, G.L., Schmidt, F.H.   Phys. Rev. 93:140.   1954.

156. Hibdon, C.T., Pool, M.L. and Kurbatov, J.D.   Phys. Rev. 67:289.   1945.

157. Bruner, J.A., Langer, L.M. Phys. Rev. 79:606. 1950.

158. Blue, J.W. and Bleuler, E. Phys. Rev. 100:1324. 1955.

159. Lindqvist, T. and Mitchell, A.C.G. Phys. Rev. 95:1535. 1954.

160. Martin, D.W., Burson, S.B. and Cork, J.M. Phys. Rev. 100:1236(A). 1955.

161. Lidofsky, L.J., Benczer, N. and Fischer, V.K. Phys. Rev. 99:658(A). 1955.

162. Marquez, L. Phys. Rev. 92:1511. 1953.

163. Matthews, D.E. and Pool, M.L. Phys. Rev. 72:163(A). 1947.

164. Walke, H., Thomson, F.C. and Holt, J. Phys. Rev. 57:177. 1940.

165. Ketelle, B.H. Phys. Rev. 80:758. 1950.

166. Cohen, B.L. Phys. Rev. 94:117. 1954.

167. Overstreet, R., Jacobson, L. and Stout, P.R. Phys. Rev. 75:231. 1949.

168. Siegbahn, K. Arkiv Mat. Astron. Fysik 34B:No.4. 1947.

169. Peacock, W.C., Jones, J.W. and Overman, R.T. Plutonium Project Report Mon. N-432:56. 1947.

170. Hollander, Perlman, and Seaborg, Revs. Modern Phys. 25:469. 1953.

171. Green, D. and Richardson, J.R. Phys. Rev. 101:776. 1956.

172. Ticho, H.K. Phys. Rev. 84:847. 1951.

173. Ramsey, M.M., Meem, J.L. Jr., and Mitchell, A.C.G. Phys. Rev. 72:639. 1947.

174. Kline, R.M. and Zaffarano, D.J. Phys. Rev. 96:1620. 1954.

175. Stahelin, P. Phys. Rev. 92:1076. 1953.

176. Friedlander, G. and Kennedy, J.W. Nuclear and Radiation Chemistry. p.266. John Wiley and Sons Inc., N.Y. 1955.

177. Jarvis, G.A. et al. Phys. Rev. 79:929. 1950.

178. Glass, R.A. University of California Radiation
      Laboratory UCRL-2560. 1954.

179. Panofsky, W.K.H. and Phillips, R. Phys. Rev. 74:1732.
      1948.

180. Mileikowsky, C. and Pauli, R.T. Arkiv f. Physik
      4:299. 1952.

181. Cork, B., Johnston, L. and Richman, C. Phys. Rev. 79:71.
      1950.

182. Kelly, E.L. and Segre, E. Phys. Rev. 75:999. 1949.

183. Davison, P.W. Phys. Rev. 75:757. 1949.

184. Wagner, G.D. and Wiig, E.O. J.A.C.S. 74:1101. 1952.

185. Bonner, N.A. and Orr, W.C. Phys. Rev. 76:140. 1949.

186. Warshaw, S.D., Swanson, R.A. and Rosenfeld, A.H.
      Phys. Rev. 95:649(A). 1954.

187. Marquez, L. Phys. Rev. 87:405. 1952.
                              88:225. 1952.

188. Stevenson, P.C. and Folger, R.L. (unpublished)
      quoted in Phys. Rev. 81:953. 1951 and in
                    Phys. Rev. 86:405. 1952.

189. Crandall, Millburn, Pyle and Birnbaum, Phys. Rev. 101:329.
      1956.

190. Hintz, N.M. and Ramsey, N.F. Phys. Rev. 88:19. 1952.

191. Aamodt, R.L., Peterson, V. and Phillips, R. Phys. Rev.
      88:739. 1952.

192. Seliger, H.N. Phys. Rev. 78:491. 1950.

193. Belmont, E. A.E.C. Report NYO-3198. 1952.

194. Perlman, M.L. and Friedlander, G. Phys. Rev. 74:442.
      1948.

195. Siegbahn, K. and Petersson, S.E. Arkiv Mat. Astron. Fysik. 32B:No.5. 1946.

196. Wong, C. Phys. Rev. 95:765. 1954.

197. Solomon, A.K. Phys. Rev. 79:403. 1950.

198. Siegbahn, K. Phys. Rev. 70:127. 1946.

199. Barker, E.C. Phys. Rev. 71:453. 1947.

200. Wiedenbeck, M.L. Phys. Rev. 72:429. 1947.

201. Burcham, W.E., Symonds, J.L. and Young, J.D. Proc. Phys. Soc. London A68:1001. 1956.

202. Rosenfeld, A.H., Swanson, R.A. and Warshaw, S.D. Phys. Rev. 103:413. 1956.

203. Turkevich, A. private communication to Wolfgang and Friedlander, Phys. Rev. 96:190. 1954.

204. Miller, J. private communication to Wolfgang and Friedlander, Phys. Rev. 96:190. 1954.

205. Chackett, Chackett, Reasbeck, Symonds and Warren, Proc. Phys. Soc. London A69:43. 1956.

206. Gilbert, R.S. quoted in Phys. Rev. 102:1390. 1956.

207. Rudstam, S.G. Spallation of Medium Weight Elements. Uppsala, 1956.

208. Chackett, G.A. and Chackett, K.F. Nature 174:232. 1954.

209. Kraus, K.A. and Moore, G.E. J.A.C.S. 75:1460. 1953.

210. Hyde, E.K. Some Notes on Radiochemical Separation Methods. University of California Radiation Laboratory. 1953.

211. Yaffe, L. and Justus, K.M. J.Chem. Soc. Supplement S.341. 1949.

212. Pate, B.D. and Yaffe, L. Can. J. Chem. 33:15. 1955.

213. Langer, L.M. and Price, H.C. Jr. Phys. Rev. 76:641. 1949.

214. Siegbahn, K. Beta- and Gamma-Ray Spectroscopy.
Chapter V. North-Holland Publishing Co. Amsterdam. 1955.

215. Sugarman, N. Campos, M. and Wielgoz, K. Phys. Rev.
101:388. 1956.

216. Rudstam, S.G. Phil. Mag. 46:344. 1955.

217. Bowley, A.L. Elements of Statistics. Charles Scribner's
Sons. 1920. p.452.

218. Klein, L.R. A Textbook of Econometrics. Row, Peterson
and Co. Evanston, Ill., U.S.A. 1953. p.144.

219. Richardson, C.H. An Introduction to Statistical Analysis
Harcourt, Brace and Co. N.Y. 1944. p.452.

220. Caretto, A.A. Jr. Ph.D. Thesis, University of Rochester,
N.Y. 1953.

221. Perry, A.M. Phys. Rev. 85:497. 1952.

222. De Juren, J. Phys. Rev. 80:27. 1950.

223. Bell, R.E. Phys. Rev. 95:651(A). 1954.

224. James, R.A. Phys. Rev. 93:288. 1954.

225. Skarsgard, H.M. Ph.D. Thesis, Radiation Laboratory,
McGill University. 1955.

226. Tewes, H.A. Phys. Rev. 98:25. 1955.